LES Modeling of Flow through Vegetation with Applications to Wildland Fires

A Thesis Submitted to the Faculty of the

Worcester Polytechnic Institute

in partial fulfillment of the requirements for the

Degree of Master of Science

in

Fire Protection Engineering

April 2012

Eric V. Mueller

Eric V. Mueller

Approved:

Professor Albert Simeoni, Advisor

Professor Albert Simeoni, Advisor

William Mell

Dr. William E. Mell, USDA Forest Service, Co-Advisor

A Rangwala

Professor Ali S. Rangwala, WPI, Committee Member

Kathy A. Notarianni

Professor Kathy A. Notarianni, Department Head

Acknowledgements

Abstract

Due to continued outward expansion of industry and community development into the wildland-urban interface (WUI), the threat to life safety and property from wildland fires has become a significant problem. Such fire scenarios can be better understood through the use of computation fluid dynamics based fire-spread models. However, current physical fire models must be specifically adapted to handle the phenomena associated with WUI fires. Only then can they be reliably used as research and decision making tools to help mitigate the problem.

In this research, the current standard in wildland fire modeling for representing the effect on wind flow from a porous vegetative medium is examined. The technique used employs basic correlations for object drag, and its validity with respect to real vegetation has yet to be examined in detail by the scientific community. The modeling of vegetation is studied within the framework of the existing Wildland-Urban Interface Fire Dynamics Simulator (WFDS), and the potential need for continued development is assessed.

Comparisons are made to both experimental and numerical studies. Additionally, the validity of the model is considered at both the scale of an individual tree, as well as that of a whole forest canopy. Results show that as a first approximation the model is able to perform well in the latter case. At the scale of an individual tree, however, the behavior is governed by theoretical constants. The assumption of cylindrical vegetation elements performs slightly better than the commonly used spherical case, but neither adequately captures experimental tendencies. Accurate flow representation for single trees is crucial to modeling the key driving factors of fire behavior (such as combustion and heat transfer) in small scale WUI scenarios. Ultimately, this study illustrates the need for well-designed experiments, specifically to generate empirical constants which will improve the behavior of the simplified theory.

Contents

List of Figures and Tables

Introduction

Due to the combined effects of climate change [1] and the continued expansion of urbanization [2], the problem of fires at the wildland-urban interface (WUI) has become a significant issue both nationally and globally. A 2000 study of United States census data revealed that as high as 39% of all houses in the nation were located in the WUI [3]. While some environments pose greater fire risks, due to local vegetation and weather conditions, studies have predicted that changing climates will shift these tendencies, possibly even increasing the occurrences in currently high-risk areas [4,5]. Owing to the coupled effects of larger fires and an increased number of WUI properties, it has been demonstrated that the WUI fire problem is not diminishing, and demands attention [6]. Not only will an increase in large fires mean greater risks to property and life safety, but it will also inflate the already significant economic burden associated with such events. It was reported that federal expenditures for wildland fire suppression and fuel treatments increased from $1.3 billion annually from 1996 to 2000, to $3.1 billion annually from 2001 to 2005 [7]. As such, it falls upon the scientific community to help find new and innovative ways to help prevent and protect against the threat that such fires pose to both life safety and property. In order to do so, a better understanding of the fundamental behavior of wildland fires must be fostered. Only then, can truly effective methods be developed to combat them.

Computational models are one particular tool through which to study the fundamental behavior of wildland fires [6,8]. Such models can be used to predict parameters such as the rate of spread of a fire, the potential thermal impact to a structure, the production of harmful emissions, or the trajectory of airborne embers. Having access to predicted values for these quantities for wide variety of fire scenarios is important for the planning and management tasks associated with the fire, forestry, and community planning services. Current modeling techniques have been grouped into three categories: empirical, semi-empirical, and physical [9,10]. Empirical models are based on statistical correlations from available data sets. Semi-empirical models combine statistical data with some simple theoretical correlations, such as generalized predictions of heat transfer. Physical models attempt to capture all of the relevant phenomena by solving the conservation equations.

The computational models typically used as operational tools by forestry agencies fall into the semi-empirical category [10]. In the United States the current standards are the FARSITE [11] and BEHAVE models [12]. They are based on the semi-empirical model of Rothermel, with fairly straightforward relationships developed by to estimate the model parameters [13], which have not seen significant change in the last few decades. While these models were developed using a large data set, they have been applied over a wide range of conditions, beyond their technical capacity. The detailed physical models, on the other hand, are technically capable of representing a wide range of environmental and fuel conditions, but they fall short due to the difficulties associated with accurately estimating all of the specific physical parameters required. Additionally, limitations in the understanding of fundamental processes mean that many of the sub-models employed are empirical or involve over-simplifying assumptions which limit the usefulness of the final product. Therefore, significant advances need to be made in the available modeling techniques, either empirical or physical, before the results can be used with confidence in order to guide operational or management decisions.

This research is based upon the idea that by focusing on the improvement of detailed physical models, the benefit can be twofold. First, at the scale of the WUI, a typical scenario might involve several structures and the associated vegetation. This would fall within the range of computational demand which permit the use of detailed physical modeling techniques. Therefore, improving the quality of such models will allow them to become useful tools when completing management, insurance, and community planning related duties. Beyond the apparent benefit of direct physical modeling, such tools can also be used to tune simpler empirical models to specific conditions. Well-tuned empirical models have their own benefit, as they are much less computationally expensive, they can be applied more quickly over larger domains, beyond the small scale WUI. Because they have the potential to be as accurate as a detailed physical model, such techniques may be used as operational tools. It is for these reasons, that focusing on improving the representation of fundamental fire behavior in detailed physical models is important for not only the scientific community, but the wildland fire community at large.

In order to simulate the physical processes involved in a wildland fire, detailed physical models employ a computational fluid dynamics (CFD) approach. Therefore these models directly solve the conservation equations in order to predict the transfer of mass (and species), energy,

and momentum. This research focuses on the conservation of momentum equation, and more specifically the representation of the effect of vegetation elements on fluid flow. Accurate modeling of fluid flow (wind) in a wildland fire scenario is crucial for several different reasons. First, on a small scale, flow within the vegetation, such as in a forest canopy, will directly influence the combustion and heat transfer and therefore the heat release rate. This is especially true because many physical fire models use a mixture model to determine the combustion dynamics [14,15]. Second, on a larger scale, the spread of the fire is strongly influenced by the wind. The flow of hot combustion gases into un-burnt vegetation will increase convective heat transfer, and flame lean caused by wind will increase radiative heat transfer. Both of these will increase drying and pyrolysis, which are directly linked to ignition and flame spread. Third, at the scale of the WUI, where these models will be the most useful, the transport of embers has been shown to be quite significant in assessing the risk to particular structures. Ember transport is directly dependent upon the wind-flow through and around obstacles in the WUI [6]. Last, on the largest scale, the flow of wind above vegetation will influence the plume dynamics and therefore the spread of emissions [16,17,18].

Due to the direct and significant influence of wind on fire behavior, it is important that the CFD models accurately capture the effect of vegetation on flow. This research focuses on the drag force correlation, which is a part of the momentum equation, and only involves cases which do not include combustion (cold flow). It is important to first decouple the wind from any thermal effects, so that the processes being studied are clearly defined. Only then can the sources of uncertainty in a full wildland fire simulation

Chapter 1 of this report details the specific ways in which vegetation may be represented for computational modeling purposes. Previous as well as new correlations are suggested, and general comparisons are made between them. In Chapter 2 CFD simulations of flow through and around a single tree are evaluated. To date, very minimal work has been done to model flow of this nature, making these comparisons a valuable starting point for future research. The chapter is further divided into two sections. In the first, a comparison is made to another simple numerical model as well as to an experiment with a scaled model tree. In the second section, an experiment involving a full-scale tree in a wind tunnel is modeled and the results are compared to the data. Chapter 3 of this report discusses the modeling of flow through and above a full forest canopy. This type of work has been studied in several other cases, and so the work serves as more of a

validation for the particular model being studied in this research. In Chapter 4 conclusions are drawn from the three sections of research. The current state of modeling flow through vegetation is summarized and specific items requiring future research efforts are highlighted. Specific details pertaining to the different sections can be found in the appendices. Appendix E overviews the rationale used for the choice of grid spacing in the various numerical simulations. Appendix F contains cleaned-up versions of the input files used to configure each of the simulations.

Chapter 1 – Model Details

Section 1.1 – (W)FDS Overview

This work focuses specifically on validation and development pertaining to the Wildland-Urban Interface Fire Dynamics Simulator (WFDS). It is an extension of the National Institute of Standards and Technology's (NIST) Fire Dynamics Simulator (FDS) [19]. FDS was first released publicly in 2000 and has continued to see ongoing development efforts, with its 6th official release currently being generated. It was originally created, and has seen the most development, for the problem of modeling compartment fires and stationary outdoor fires. However, starting with the 5th official release, the FDS source code was expanded to contain routines which are aimed at simulating wildland fire scenarios. A user input distribution of vegetation is represented by a series of correlations that model the effect of the solid fuel on the gas phase. This includes representing phenomena such as heat sources and sinks from the solid as well as the mass flow of pyrolysis gases from the solid. Because the solutions for the conservation equations of the gas phase are carried out by the FDS routines, the model will hereafter be referred to as (W)FDS.

(W)FDS uses the large eddy simulation (LES) technique for CFD modeling. LES is one of three main methods for solving fluid flow (which is the essence of CFD modeling) in for turbulent conditions [20]. The simplest approach is to use the Reynolds-averaged Navier-Stokes equations (RANS). This involves a time averaging technique, and therefore does not adequately capture the dynamic nature of typical fire flows. The most complex and detailed approach is direct numerical simulation (DNS), which resolves all scales of the flow. However, due to the different length scales associated with fluid flow, solving the equations with this method is generally prohibitively computationally expensive. LES is an intermediate approach which resolves the large scale flows, and models the small scales. This is done by using a filter approach to separate length scales, and it is usually implicitly linked to the spacing of the computational mesh [20].

The closure model used by (W)FDS for modeling turbulence is the Smagorinsky model, which is the most common model used in LES simulations. An eddy viscosity model is used to

solve the turbulent stress and generate the subgrid-scale eddys [20]. The eddy viscosity model employs either a constant or a dynamic Smagorinsky coefficient. The dynamic approach is considered an improvement in the study of boundary flows as the constant coefficient over-predicts the eddy-viscosity in the near-wall region and inhibits the natural transition to turbulence [21]. It used is in this case due to known difficulties in simulating boundary flows with the constant coefficient model. A more detailed description of the specific solution of the momentum equation can be found in the FDS Technical Reference Guide [22].

Section 2.2 – The Drag Force

In CFD models such as (W)FDS, the effect of the vegetation on the solution of the momentum equation is represented in the form of a body force (F_d), called the drag force [23,24]. As only cold flows are considered in this research, the focus is on the momentum equation and therefore this force. For a single object in a flow, the drag force can be written as

$$F_d = \frac{1}{2} c_d A \rho u^2 \qquad \text{(Eq. 1)}$$

where A is the projected area of the object on a plane perpendicular to the velocity (u), and c_d is a drag coefficient which is dependent on the geometry and surface properties of the particle [25]. For the three previous derivations, the u^2 factor in (Eq. 1) was replaced by $u|u|$, which allows for consideration to be made for the direction of flow. In the case of (W)FDS, the force in the momentum equation must be written in a per-unit-volume form. The model considers vegetation to be a certain number of solid phases consisting of a set of small particles with the same geometry and thermochemical properties. Their properties are then averaged over the volume of a computational cell [26]. Therefore, the contribution to the drag force from all particles within a control volume (computational cell) is considered, and then divided by the volume in question.

If the vegetation particles are assumed to be spherical, with a surface-to-volume ratio σ, and a solid volume fraction β (within a control volume V_b), it follows that [27]

$$\langle F_d \rangle_{V_b} = \frac{1}{V_b} \sum_n \frac{1}{2} c_d A \rho u |u|$$

$$\langle F_d \rangle_{V_b} = \frac{n}{2V_b} c_d \pi r^2 \rho u |u|$$

$$\sigma = \frac{4\pi r^2}{4/3 \pi r^3} = \frac{3}{r}$$

$$\beta = \frac{n * 4/3 \pi r^3}{V_b}$$

$$\langle F_d \rangle_{V_b} = \frac{1}{8} \sigma \beta c_d \rho u |u| \qquad \text{(Eq. 2)}$$

It should be noted that in several publications specific to fire flow modeling in wildland fuels, a factor of $\frac{3}{8}$ was suggested in place of the $\frac{1}{8}$ factor [15,23,27,28]. However, this was determined to stem from a misprint in one particular version of the derivation and does not originate from any empirical study.

In the case of a cylindrical vegetation particle, which (to a first approximation) is an appropriate representation of a pine needle, a simplifying assumption can be made. By considering the length to radius ratio of the cylinder, it can be seen that above a certain value $\sigma = \frac{2}{r}$.
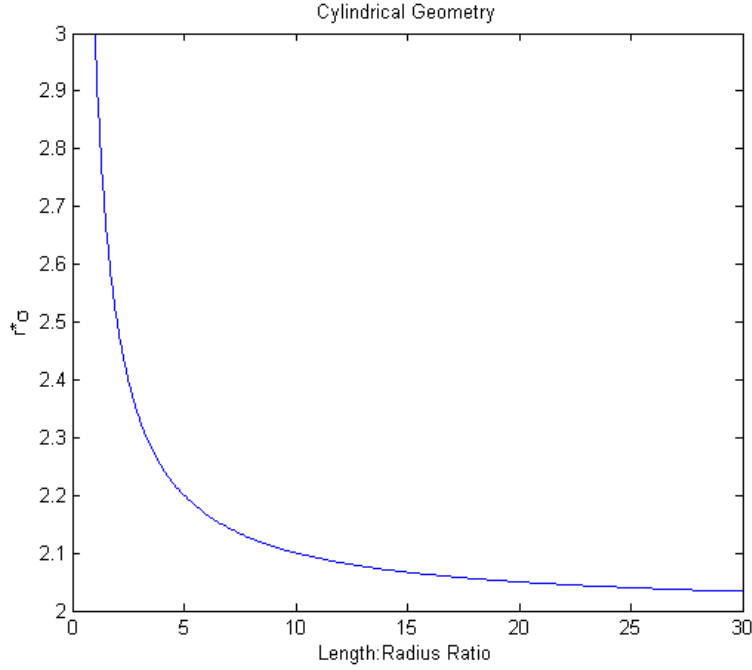
Figure 1.1 – Value of $r\sigma$ with increasing ratio of length to radius

This approximation has been used in the convective heat transfer coefficient in several other studies which represent pine needles as cylindrical elements [23,29]. Using this assumption for flow applications allows the drag force for cylinders to be written

$$\langle F_d \rangle_{V_b} = \frac{1}{V_b} \sum_n \frac{1}{2} c_d A \rho u |u|$$

$$\langle F_d \rangle_{V_b} = \frac{n}{V_b} c_d L r \rho u |u|$$

$$\sigma = \frac{2}{r}$$

$$\beta = \frac{n * 2\pi r^2 L}{V_b}$$

$$\langle F_d \rangle_{V_b} = \frac{1}{4\pi} \sigma \beta c_d \rho u |u| \qquad \text{(Eq. 3)}$$

8

This particular formulation has not been reported to have been used in CFD simulations of wildland fire type flows, and therefore one of the aims of this research is to test its appropriateness.

In the case of a deciduous (flat) leaf with a one-sided surface area A and a thickness T, it follows that

$$\langle F_d \rangle_{V_b} = \frac{1}{V_b} \sum \frac{1}{2} A c_d \rho u |u|$$

$$\sigma = \frac{2 * A}{A * T} = \frac{2}{T}$$

$$\beta = \frac{n * A * T}{V_b}$$

$$\langle F_d \rangle_{V_b} = \frac{n}{2V_b} A c_d \rho u |u|$$

$$\langle F_d \rangle_{V_b} = \frac{1}{4} \sigma \beta c_d \rho u |u|$$

This equation has been used in the past for modeling canopy flows [30]. However, the meteorological convention is not to show the $\frac{1}{2}$ in (Eq. 1) explicitly (it is represented by the choice of c_d) [31], hence

$$\langle F_d \rangle_{V_b} = \frac{1}{2} \sigma \beta c_d \rho u |u| \qquad \text{(Eq. 4)}$$

The $\frac{\sigma \beta}{2}$ factor is often referred to as the leaf area density (LAD). It is considered as a measure of leaf area per unit height per unit ground area (m^{-1}) and is usually notated as a_f [32]. The integral over the entire canopy height is called the leaf area index (LAI). Eq. 4 has been widely used in more recent studies of canopy flow [33,34,32].

Along with geometrically dependent multiplying factor in front of the drag force equation ($\frac{1}{8}$, $\frac{1}{4\pi}$, or $\frac{1}{2}$), the drag coefficient (c_d) also varies between the different choices of vegetation particles. For spheres or cylinders, it is based upon an empirical correlation for each object respectively [25]

9

For Spheres:

$$c_d = \begin{cases} 100 & if\ Re < 0 \\ \left(\dfrac{24}{Re}\right) & if\ 0 < Re \leq 1 \\ \dfrac{24(0.85 + 0.15Re^{0.687})}{Re} & if\ 1 < Re < 1000 \\ 0.44 & if\ Re \geq 1000 \end{cases}$$

For Cylinders:

$$c_d = \begin{cases} \dfrac{10}{Re^{0.8}} & if\ Re \leq 1 \\ \dfrac{10(0.6 + 0.4Re^{0.8})}{Re} & if\ 1 < Re < 1000 \\ 1 & if\ Re \geq 1000 \end{cases}$$

Where:

$$Re = \frac{2ur}{v}$$

Re is the local Reynolds number, and is dependent on the flow and the radius of the particle (r).
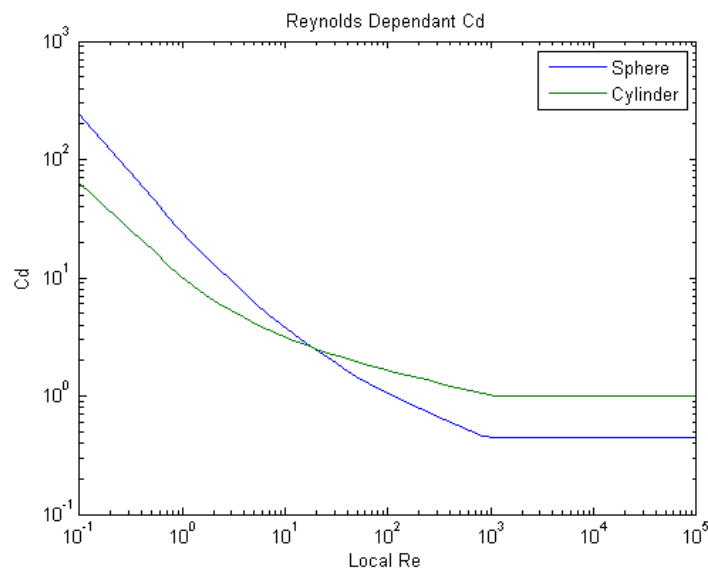
Figure 1.2 – Empirical correlations for the particle drag coefficient

In the case of a flat leaf, there is no established correlation for c_d, so experimentally determined values are generally used. A range of ~0.15-0.37 has been suggested in literature [32] and no dependence on local flow conditions is considered (c_d is constant).

Since the particle surface-to-volume ratio and tree bulk density can theoretically be determined by field measurements (though this presents a whole other challenge), the focus of this study lies in the choice of either (Eq 2.), (Eq. 3), or (Eq. 4).
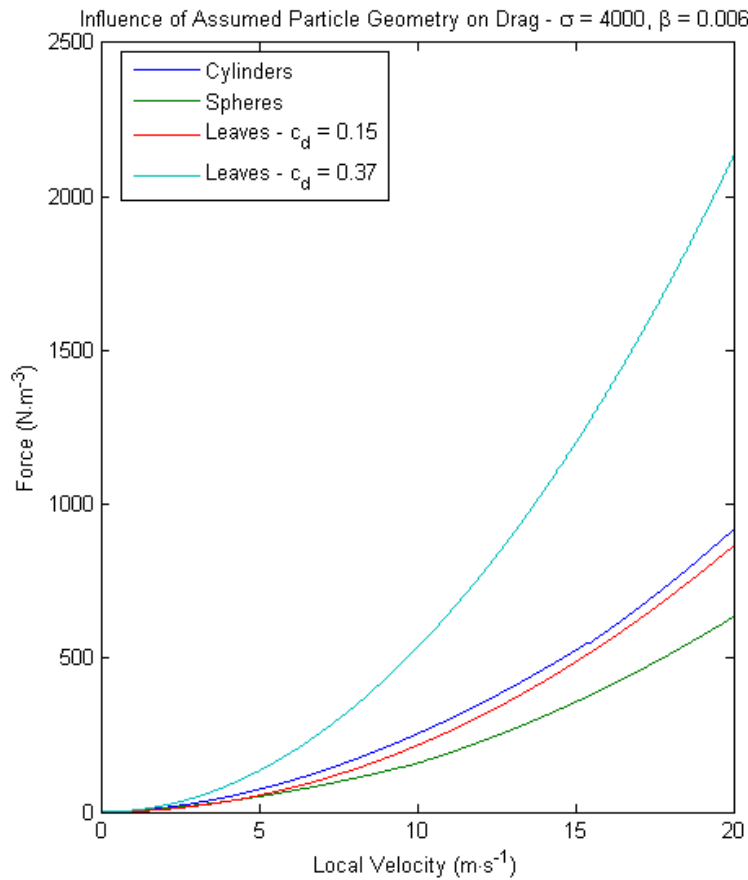
Figure 1.3 – The dependency of drag behavior on the choice of particle geometry for a given, realistic σ and β

It should be noted that in Fig. 1.3, the use of the same σ for different geometries should be considered with caution. That is to say, the measured values of σ will probably be influenced by the assumptions made about particle geometry and may not be the same for the different equations. However, it is possible to find a deciduous tree and a conifer with similar leaf and needle surface-to-volume ratios. It is also important to note that the use of a constant c_d for

leaves results in a different shape to the drag force curve. This can be seen more clearly at low velocities in Fig. 1.4.
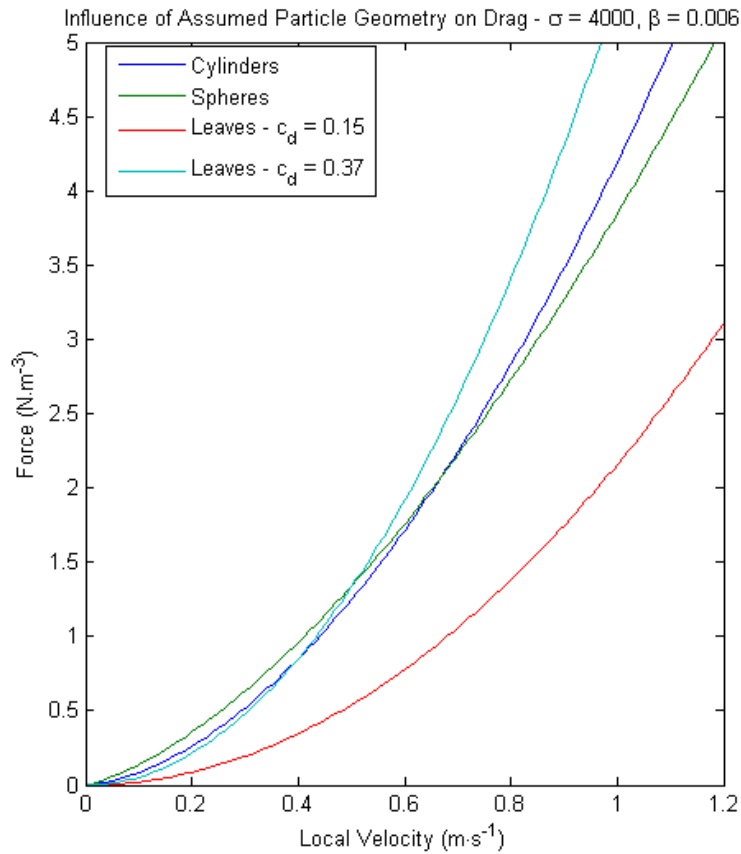
Figure 1.4 – The low-velocity dependence of drag behavior on the choice of particle geometry

It was shown that below a velocity of about 0.7 m·s^{-1} the spheres induce a greater drag force than the cylinders (for the same σ and β), while above this value the opposite is true. Since the velocities of interest in a typical wildland fire scenario will be greater than this value, it is shown that the choice of spherical particles will generate less of an influence on the flow than cylinders.

Chapter 2 – Large Scale Simulation

Section 2.1 – Single Tree Numerical Comparison

2.1.1. Overview

A logical starting point for evaluating the capabilities of (W)FDS to model a flow through and around vegetation was to make a comparison with a paper describing a previously performed numerical study. Comparison to another numerical study, which was in-turn compared to an experimental study, allows an evaluation of not only the (W)FDS model to the experiment, but also between the two different numerical approaches. The model used in the study chosen, conducted by G.Gross, was RANS in nature [35]. Additionally, a very simple configuration was used. A single conical tree was modeled and subjected to an inflow profile. The intent of the study in question was to make simple qualitative comparisons to the experiments of Ruck and Schmitt [36]. In the experiments, a scaled model tree (~30 cm in height) was placed in a wind tunnel. Cases both with and without a stem were considered, and vector fields of the flow were constructed from Laser Doppler Anemometer measurements behind the tree.

a)
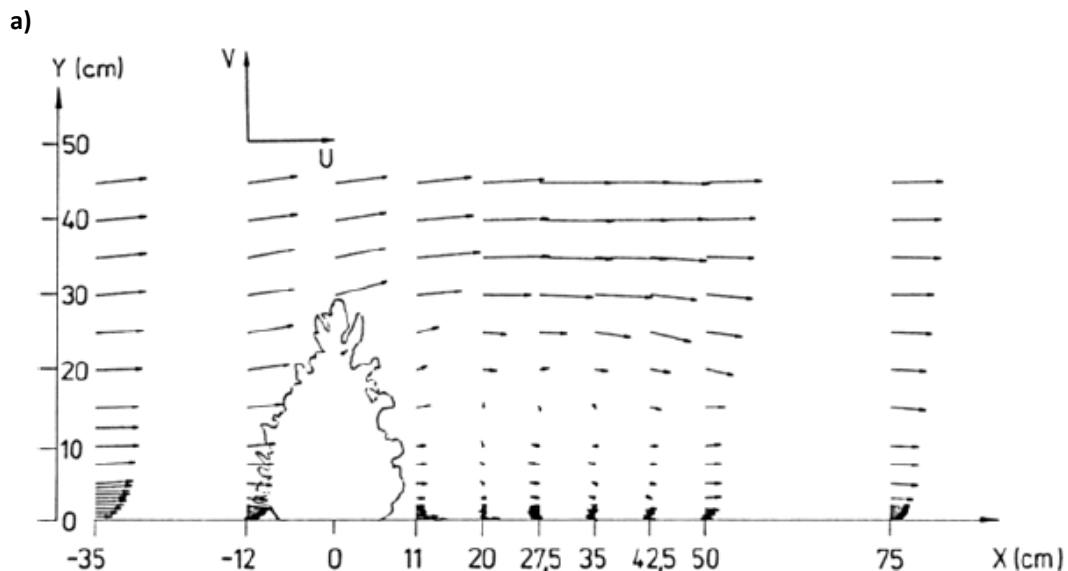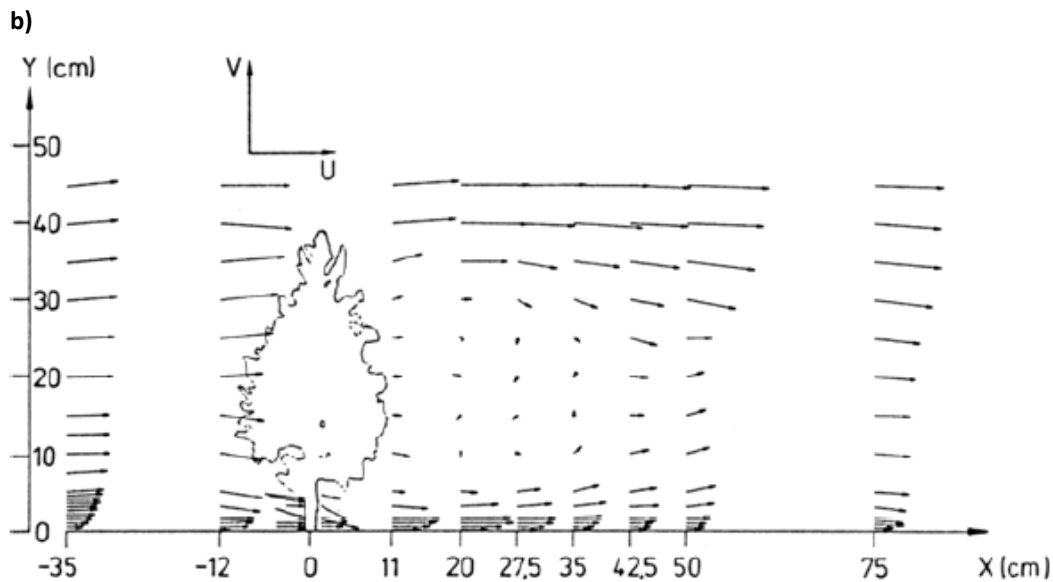
Figure 2.1 – Vector fields of flow behind a model tree: **a)** no stem, and **b)** stem [36]

Unfortunately, very little information was provided about the composition (density, etc.) of the model tree or the configuration of the wind tunnel. Therefore, the RANS numerical comparisons were of a qualitative nature meant to verify the capability of the model to replicate the general characteristics of the flow. Comparisons between (W)FDS and the experiments were of the same nature. When evaluating the two different numerical approaches, assessments must also be qualitative in nature, as driving concepts of the models (the solution of turbulence or not) are fundamentally different. The basic approach was to replicate the numerical conditions used in the RANS study and to compare the results between the two. Observations were then made concerning the experimental results, with similar flow regimes being regarded as a positive outcome for the model.

However, as a first step in evaluating the model, such basic qualitative comparisons do have merit. If the results from (W)FDS show a drastically different effect of the tree on the flow, then it will have been shown that the appropriateness of the overall approach used by (W)FDS (such as the use of LES, the turbulence model, and the general form of the drag equation) needs to be examined in more detail. Only once this has been investigated, can the specific choices of the factors in the drag force be assessed in more detailed studies.

2.1.2. Numerical Details

The parameters of the numerical simulation were chosen to replicate the RANS study as closely as possible. However, due to the differences in approach, some changes had to be made. The domain chosen was 180m x 60m x 40m with a uniform spacing of 0.25m x 0.33m x 0.25m. Details of this choice can be found in Appendix E. The domain was divided into 16 uniform meshes in order to reduce computational costs. In the RANS study, only half of the domain was simulated, as symmetry was assumed and a mirror condition set along the centerline of the tree. In the case of LES, however, the resolution of eddies in the wake region render this assumption invalid, and so the whole domain must be modeled. The upper and lateral (in y) boundary conditions were set as free-slip walls, while the lower boundary was set as a no-slip wall. The inflow plane (x = -20.0 m) was set to follow a logarithmic velocity profile, with the velocity at z = 40 m being set to 1.2 m·s^{-1} ($u(z) = 1.2(\frac{\log(z)}{\log(40)})$). The outflow plane (x = 160 m) was set to the (W)FDS 'OPEN' condition. Details of particular (W)FDS boundary conditions can be found in Appendix A.

In keeping with the RANS study, the tree was centered at the midpoint of the y-axis and at x = 18 m. An additional 20m was added to the domain upstream of the tree in order to assure a smooth profile development before the influence of the tree was seen. In the case of the no stem simulation, the crown width was set to 13 m and the crown height to 16 m. In the case with the stem the crown was moved up by 6 m and the stem was modeled as a cylinder 2 m in diameter.

X = -20 m   X = 18 m   X = 160 m

X = -20m   X = 18m   X = 160m
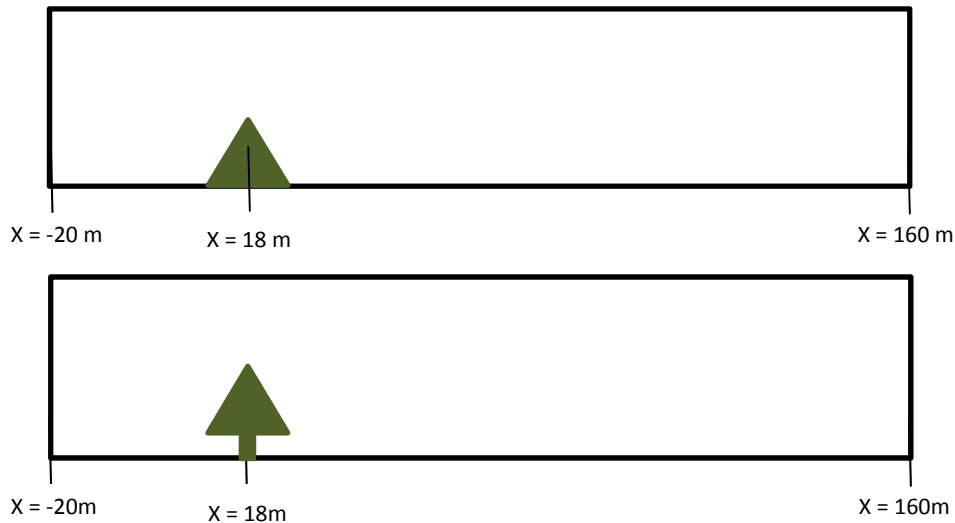
Figure 2.2 – Location of the tree within the computational domain

15

The drag force correlation used in the RANS model was a simplification of the one derived in Chapter 1. The vegetation density and geometry factors were lumped into one term (b), and the drag coefficient was set as a constant

$$F_d = c_d b \rho u |u| \qquad \text{(Eq. 5)}$$

The $c_d b$ term was then considered as one constant, and was varied from 0.1 to 1.0. This approach was mimicked in the (W)FDS simulations. The stem was considered to have the same effect on the flow as the crown vegetation (a porous medium). This approach was originally developed for solving two-dimensional flows, in which flow around a solid obstruction below the tree would not be modeled and the resultant vector field would not be as realistic. However, for current three-dimensional detailed physical models, a solid obstruction would be appropriate.

2.1.3. RANS Simulation Results

The RANS study produced a set of smooth, well behaved results, as can be expected due to the time averaged nature of this approach [20]. For the case of no stem, it was found that the streamwise velocity dropped off in front of the tree, due to the pressure gradient created by the drag force acting at the leading edge of the tree. Within the tree the drag forces dominated and the velocities were reduced. Immediately behind the tree, a small recirculation zone was established close to the ground, while far behind the tree, the velocity gradually returned to the inflow value. The inflow profile itself was re-established at around ~3.2 crown widths from the tree center.
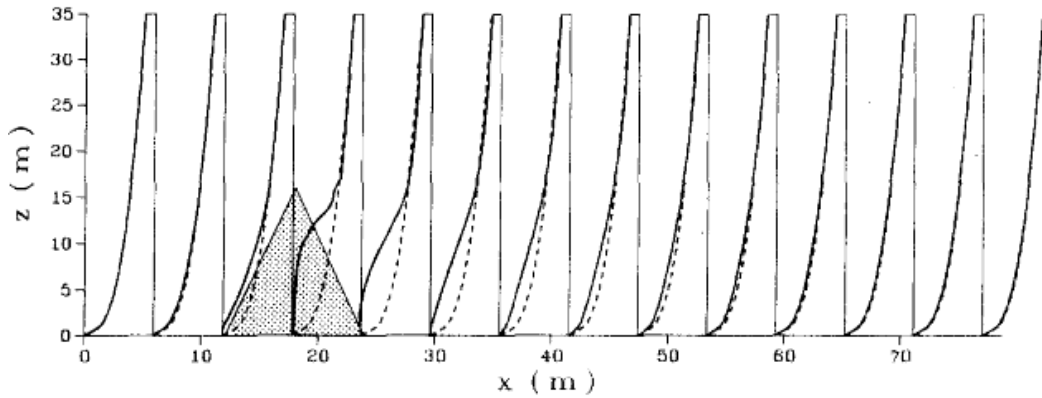
Figure 2.3 – Simulated streamwise velocity along tree centerline, $c_d b = 1.0$ [35]

Both the establishment of a recirculation and the reacquisition of the inflow profile were consistent with experimental observations. This type of behavior can be expected due to the nature of the flow. The velocities above the tree will continue at their inflow values, but those behind the tree will be dramatically reduced. Therefore the fluid in this low flow region will be drawn up into the faster flow, causing the recirculation. However, the size of the simulated eddy was ~10m, or ~1 crown width from the tee center, whereas the eddy in the experimental case extended ~2 crown widths from the tree center. Hence the RANS case under-represented the magnitude of this recirculation.
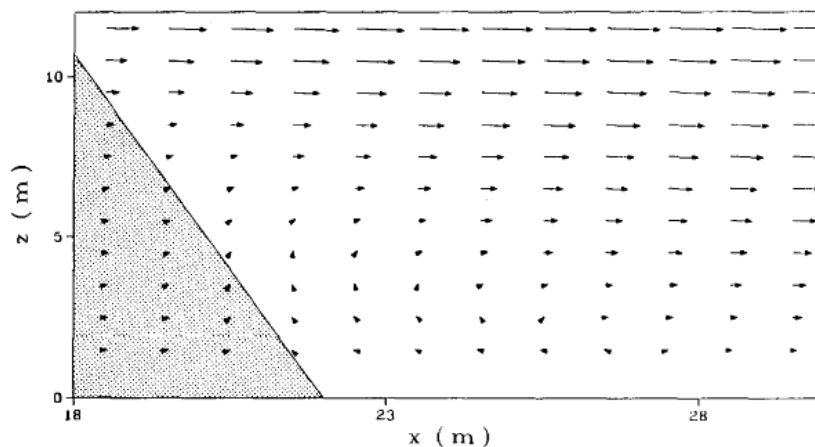
Figure 2.4 – Simulated vector field along tree centerline, $c_d b = 1.0$ [35]

The main point of interest pertaining to the addition of a stem in the tree model was to evaluate the effect it had on the shape of the velocity vector field. Specifically, the relatively un-inhibited flow under the tree changed the shape and location of the recirculation eddy behind the

17

crown. In this case, the flow appeared to be drawn up from under the tree but not down from the top. Additionally, no appreciable eddy was formed.
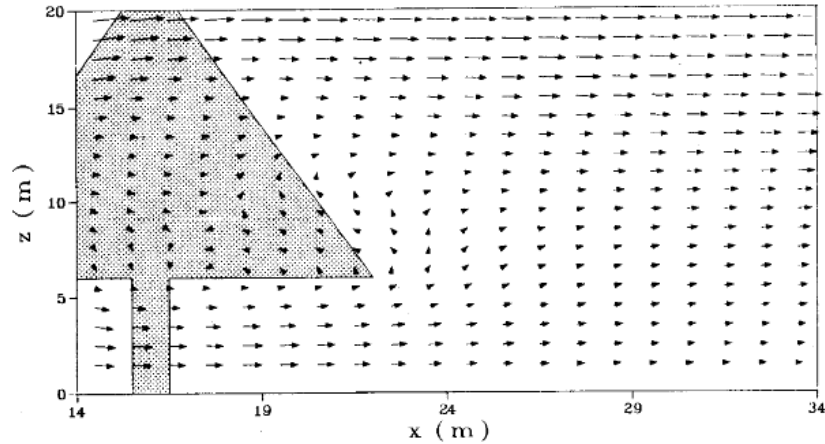
Figure 2.5 – Simulated vector field with tree stem included, $c_d b = 1.0$ [35]

In the experimental results, the eddies formed with and without a stem were of a comparable size (Fig. 2.1). The experimental vector field also showed that, when a stem was included, flow was drawn from both above and below the tree, creating essentially two mirrored eddies. Thus the behavior of the RANS model was shown to deviate from the experiment in both configurations.

2.1.4. (W)FDS Simulation Results

The simulation was run to t = 2500s, with a quasi-steady state being observed by 1000s of simulation time. A FFT analysis was carried out on the fluctuations of instantaneous velocity behind the tree (in the turbulent wake region). This was done in an effort to uncover any dominant frequencies in the turbulence, which would in turn dictate the proper choice for an averaging interval to capture the mean value of the velocity. The analysis was done for each component of the velocity and in all cases a high level of noise was obtained. An example of this noise for the u-velocity component is depicted in Fig. 2.6
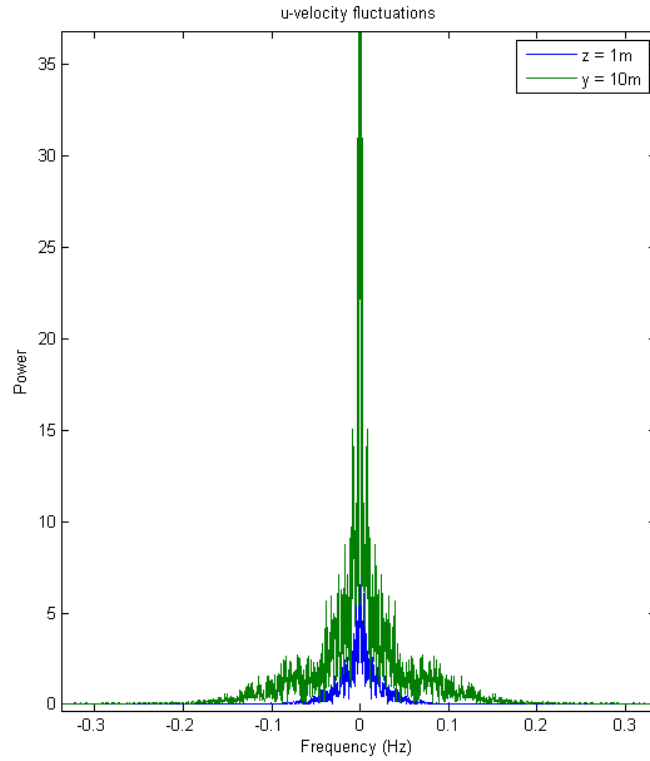
Figure 2.6 – FFT of instantaneous streamwise velocity from 1000-2500s

However, it was decided that averaging on an interval from 1000 to 2500s would be sufficient to capture the average characteristics of the flow, as this would filter out all but the lowest frequency fluctuations ($<6 \cdot 10^{-4}$ Hz). This was confirmed by directly plotting the instantaneous velocity, which demonstrated that if low frequency fluctuations were present, they were not very significant.
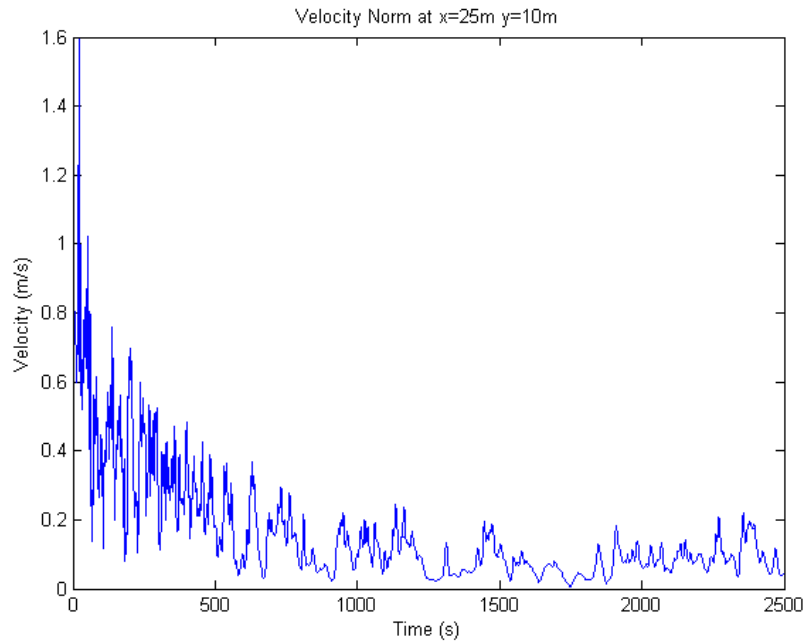
Figure 2.7 – Instantaneous velocity used to determine averaging interval

It was found that with $c_d b = 0.1$ the eddy structure behind the tree was not created, and the velocity within the tree was not decelerated to nearly the same degree as in the corresponding RANS simulation. Both discrepancies were a result of the tree not presenting a significant enough obstruction to the flow.
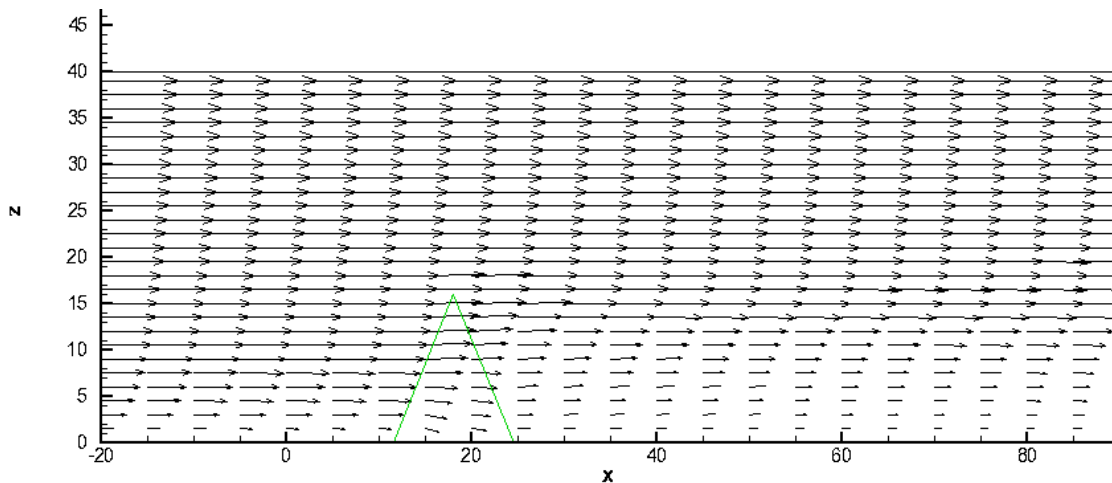
Figure 2.8 – Centerline vector field, $c_d b = 0.1$

20
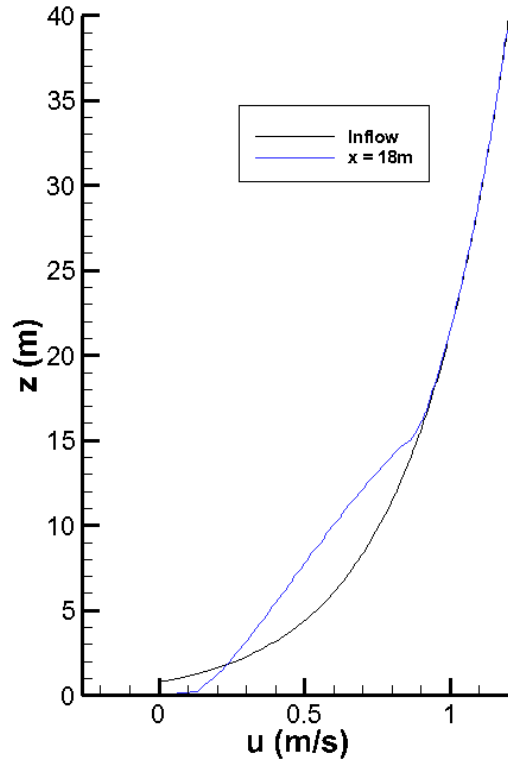
Figure 2.9 – Centerline streamwise velocity within the tree, $c_d b = 0.1$

A sharp discontinuity in the streamwise velocity profile was also observed at the lower boundary, where the velocity was forced to zero by the no-slip model (Fig. 2.9). This was attributed to the fact that the no-slip condition is appropriate only when mesh resolution is on the order of that used for DNS. It was for this reason that wall-models were developed for use in (W)FDS, details of which can be found in Appendix A.

Therefore, two changes were made in the simulations. First, the lower boundary condition was changed to the Werner Wengle wall model. Second, the $c_d b$ factor was increased in a range from 1.0 and 5.0.
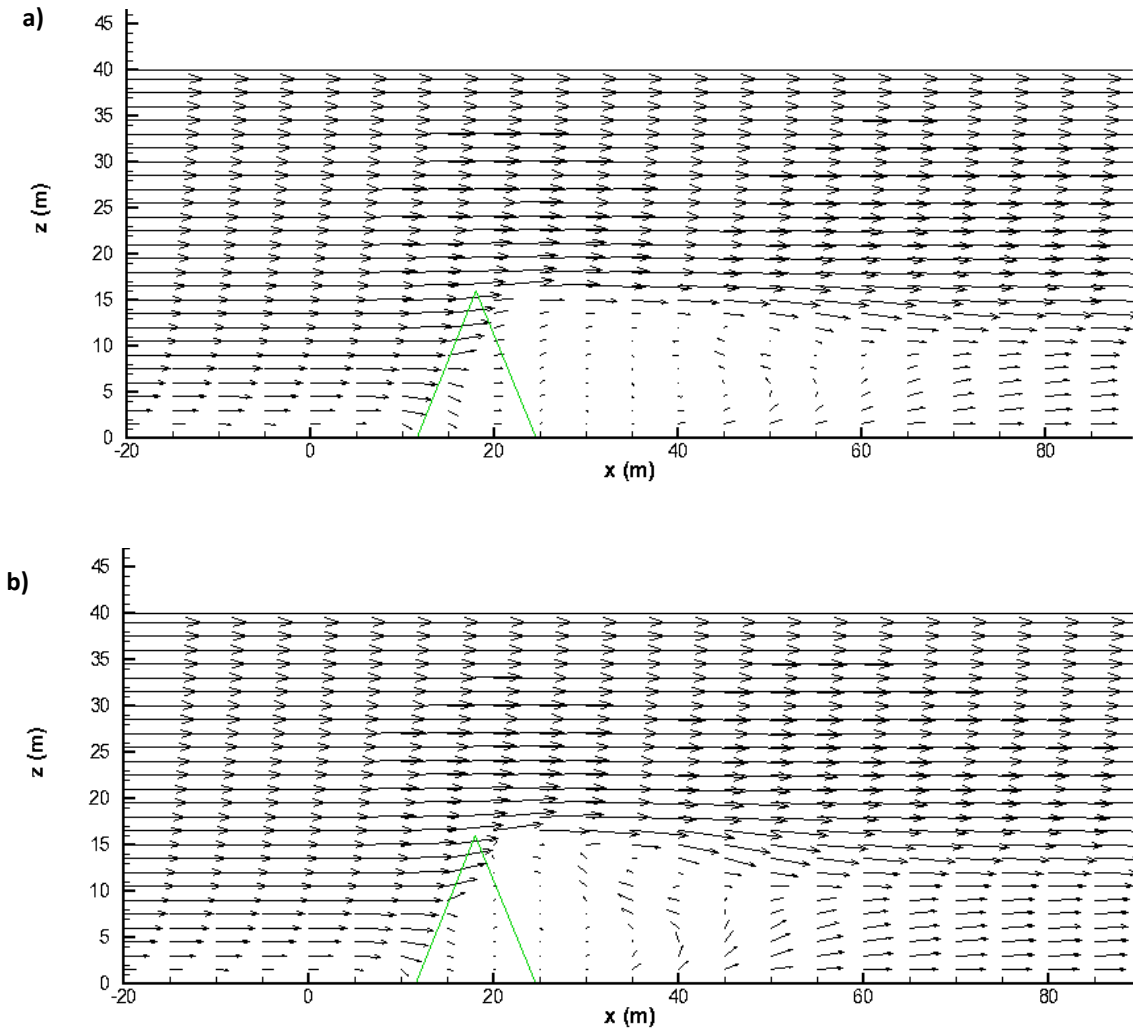
Figure 2.10 – Centerline vector field: **a)** $c_d b = 1.0$, and **b)** $c_d b = 5.0$

A well-formed recirculation zone was seen behind the tree for this range of drag forces. The shape of this eddy was fairly consistent with the experimental results, extending a length of ~2 crown widths from the tree center. Thus, the recirculation was more significant than in the case of the RANS simulation and was more consistent with the experiments. It was also observed that at the upper range of tree density ($c_d b = 5.0$) the direction of the recirculation was driven by a reverse flow of significant magnitude along the top of the eddy. This phenomenon did not appear to be measured experimentally.

For this range of drag forces, the velocities within the tree were also reduced to a degree more consistent with the RANS study, with the denser obstruction ($c_d b = 5.0$) doing a better job of generating velocities close to zero at the tree center, as was shown in the previous study.
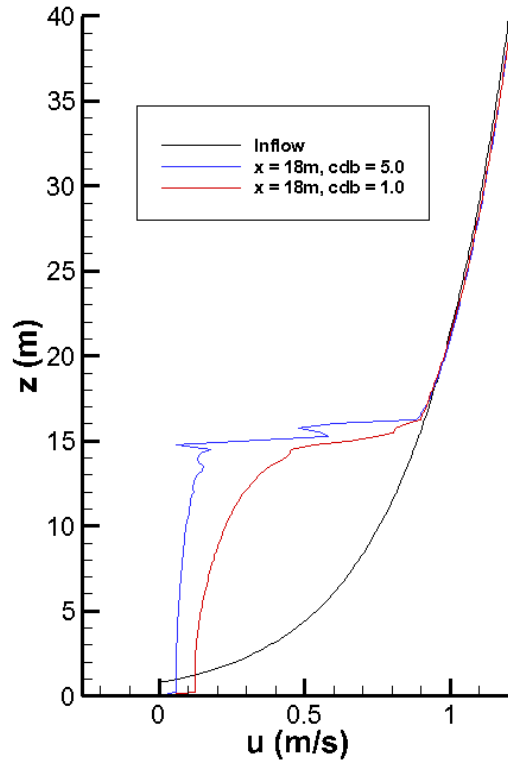
Figure 2.11 – Centerline streamwise velocity within the tree

It was noted that (W)FDS had some trouble resolving the velocity gradient generated at the tip of the tree when it presented a fairly dense obstruction (high $c_d b$) (Fig. 2.11). Depending on the application intended for a particular simulation, an increased mesh resolution around the high of tree crown tops may yield better results.

The case with the stem included was also simulated in (W)FDS. The results suggested the same range of $c_d b$ factors as being appropriate to generate similar flow characteristics to the RANS study and the model experiment.
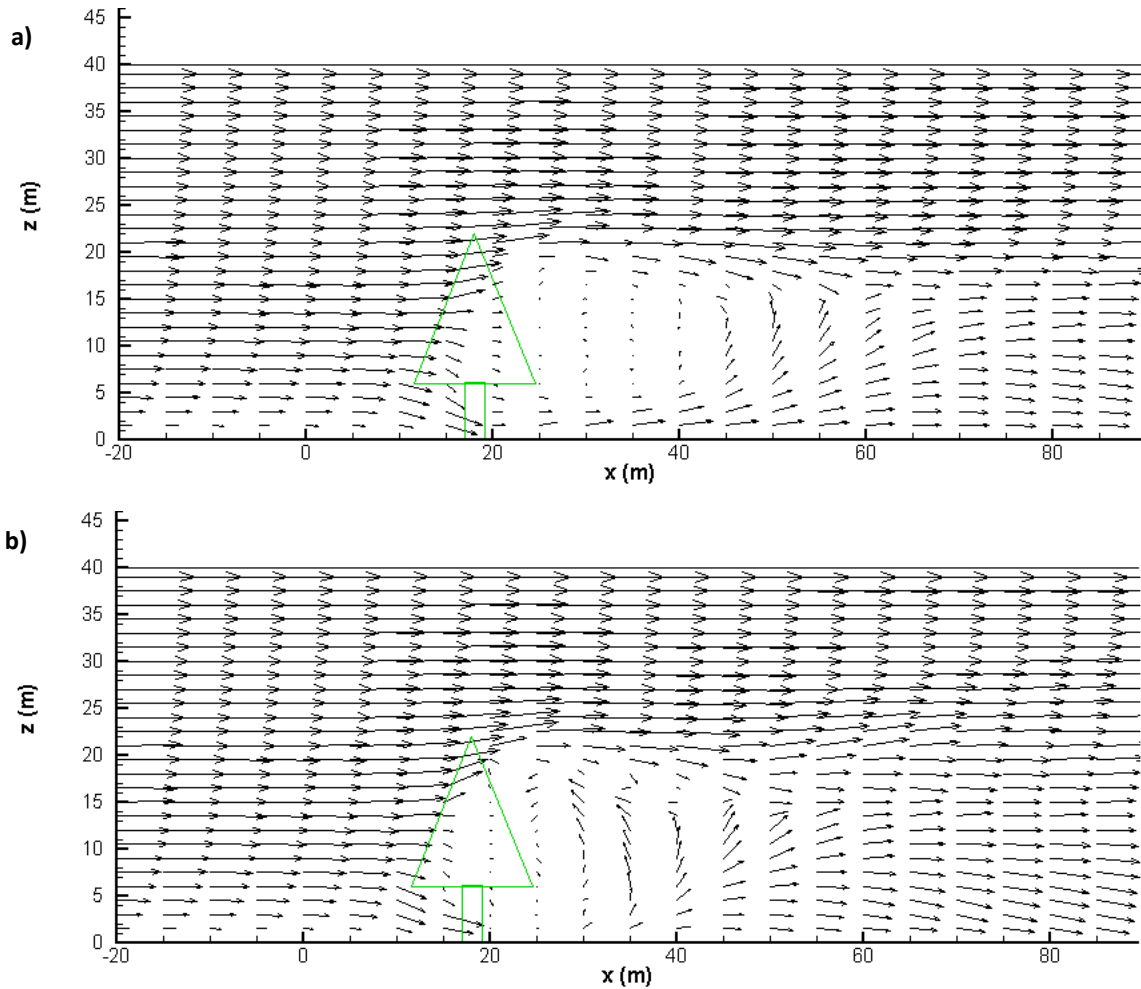
Figure 2.12 – Centerline vector field: **a)** $c_d b = 1.0$, and **b)** $c_d b = 5.0$

The shape of the eddy behind the tree was clearly influenced by the ability for wind to flow easily under the crown. Additionally, the density of the tree had an effect. In case **a)** of Fig. 2.12 the eddy was fairly uniform, with recirculation occurring behind both the top and bottom of the crown. This shape was observed in the experiments of the model tree as well. In case **b)** the flow under the tree appeared to be more significantly drawn into the recirculation region than the flow above the tree. The same strong reversed flow that was seen in the no-stem simulation occurred near the height of the tree top in the $c_d b = 5.0$ case.

One characteristic of the flow which (W)FDS had significant difficulty capturing (in both the stem and no stem configurations) was the far-field recovery of the upstream (inflow) wind profile. While the LES model is inherently turbulent and will not regain the laminar nature of upstream flow (as is suggested by the RANS results), both the experiment and the RANS study

24

suggest that a reasonable boundary layer profile should be obtained around 3-4 crown widths from the tree. In the (W)FDS simulations however, the fairly stable condition reached at ~72m from the tree center (x = 90m in Fig. 2.13) did not recover a boundary layer profile. The wall model was replaced again with the log law (see Appendix A) and a roughness of 1.0, in an effort to help force the return to the boundary layer. The flow took longer to reach a relatively steady condition behind the tree, and it resembled the inflow profile slightly better, but the difference was still significant.
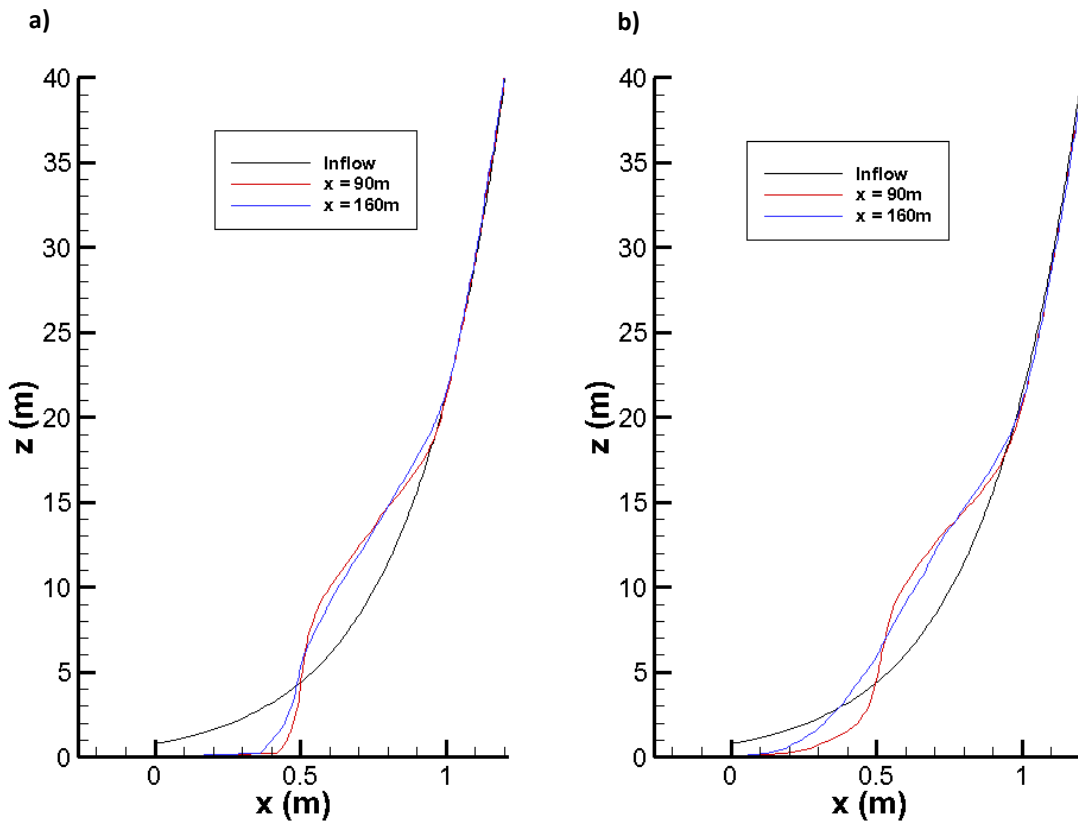
Figure 2.13 – Centerline streamwise velocity for $c_d b = 5.0$ with the **a)** Werner Wengle model, **b)** log law with roughness = 1.0.

It was found that for $c_d b$ values much higher than 5.0 the tree became close to a solid obstruction and the sensitivity to the specified constant was low. For values much lower than 1.0 the tree presented little obstruction to the flow (Fig. 2.7) and the sensitivity was high, putting the 1.0 to 5.0 range at an intermediate level. A more detailed sensitivity analysis can be found in Appendix B.

2.1.5. Conclusions

The results of the LES simulation compare to those of the RANS simulation in a manner consistent with the inherent differences in the numerical approaches. When the tree represented a very little obstruction (low $c_d b$) in the LES case, the intra-tree velocities were not reduced to a significant extent. Decreasing the density of the obstruction drove these velocities towards zero, as was predicted in the RANS model. However, when the tree presented enough of an obstruction for the intra-tree velocities in the LES simulation ($c_d b = 5.0$) to match the RANS simulation ($c_d b = 1.0$), the LES recirculation zone became much more significant than in the RANS case. Due to the inherent inability of the RANS model to capture turbulent dynamics, this was to be expected. The experimental model tree results also showed a more significant recirculation than the RANS model. Therefore, the conclusion is that the adoption of an LES technique for solving such flows is necessary if one wishes to model the details of such flows.

The specifics of the eddy characteristics when formed by a real, full-scale tree need to be examined in greater detail. For example, the faster reverse flows along the top of the eddy, seen in both the stem and no-stem cases, can most likely be attributed to the fact that, for a dense obstruction, the pressure gradient developed by the difference in the fast flow going over the tree and essential lack of flow from within the tree will draw the wake flow back. This is dissimilar to the case of an object such as a cube, where flow along the top will form a small boundary layer and decrease this pressure gradient [20]. However, the validity of the simulations result was questionable, especially because, unlike the uniform numerical tree, the bulk density of a real tree will most likely be reduced near the top and the flexible nature of the tree will allow it to yield to the flow, thus generating a lower pressure gradient.

The recirculation in general is an important characteristic to study in these types of flows. The size of this zone will be significant when studying sparse heterogeneous vegetation in the WUI environment. This, in particular, is the scenario in which the direct resolution of the flow around single trees would be necessary. Depending upon the proximity of two vegetation elements (trees), the recirculation zone from the upstream element could have a significant impact on the flow pattern around the second item. The second element may experience less flow and therefore exhibit different fire characteristics or emit embers over a shorter distance. It should also be noted, as a general statement, that adding a fire will have a significant influence

on the shape and size of this recirculation. The buoyant flow that will be obtained from having a fire within a tree will cause the velocity vectors within the tree to have a larger vertical component. This, in turn, will force the faster flow above the tree in an upward direction as it travels downstream. Additionally, flow immediately behind the tree will be drawn upward. The result will be a larger eddy, with a stronger upward recirculating force near the tree due to the thermal effects.

The issue of the far-field flow behavior is also of particular importance. Inaccuracies associated with the wall model in turbulent wake flow will have minimal effects directly behind the tree where velocities are low. However, as flow converged further down-stream, the boundary condition will have a much more significant impact on the velocity profiles. In the case of a WUI fire scenario, it may be quite important to model the far-field flow accurately. In such a situation, it is likely that there will be more heterogeneity in a vegetation layer and the flow interactions of two objects separated by more than a few crown widths may be important to the overall fire problem.

Comparisons between the simulations and the experiment in Gross' paper must also be considered with caution. Scaling between the two was not carried out with conservations of the relevant non-dimensional parameters. While the scales of the tree and tunnel were changed by a magnitude of ~100x, the velocity and the working fluid were kept the same between experiment and simulation. Therefore, the Reynolds numbers were inconsistent between the two cases, and the simulations were not necessarily representative of the experiments. A general analysis of the model behaviors is still a useful starting point, but future experimental work should be carried out in a manner that will allow a more direct comparison between the two.

The use of a constant $c_d b$ factor also needs to be considered. As a "correct" flow behavior cannot necessarily be identified in this study, and the use of a particle drag coefficient will produce fundamentally different behavior, it is difficult to make a direct comparison. This, however, is the point worth noting. For no choice of σ or β will the flow within the tree will be the same for the two cases (as can be seen in Fig 1.4). The assessment of which drag model will generate a more realistic flow regime for a vegetative obstruction must be conducted in comparison to more detailed experimental data.

Section 2.2 – Wind Tunnel Flow behind a Single, Full-Sized Tree

2.2.1. Experimental Details

In an effort to study how well (W)FDS represents a realistic obstruction to flow in the form of vegetation, simulations of an experimental data-set were conducted. Through the efforts of the National Institute of Standards and Technology (NIST), in conjunction with the Building Research Institute (BRI) in Japan, flow measurements were taken behind a conifer. These results were provided courtesy of Dr. Sam Manzello of NIST and Dr. Yoshihiko Hayashi of BRI. The aim of the experiment was not only to capture the effect of the tree on a known flow-field, but also to capture contribution to this effect from different elements of the tree (namely those which would be consumed in a fire and those which would not). This was accomplished by conducting four distinct sets of experiments. The first consisted of taking velocity measurements within the BRI wind tunnel without any tree in place in order to characterize the flow in the tunnel. The second consisted of taking velocity measurements with the tree in the tunnel, the third with the needles removed, and the fourth with the needles and branches less than 6 mm in diameter removed. Measurements were taken for each of these cases at tunnel velocities of 1, 3, 6, and 9 $m \cdot s^{-1}$, making a total of 16 experiments.

Experiment	Description
Case1	No Tree – Wind Tunnel Characterization
Case2	Full Tree
Case3	Needles Removed
Case4	Branches <6 mm in Diameter Removed

Table 2.1 – Overview of the different vegetation test conditions

The BRI tunnel consisted of an enclosed segment in which the flow was developed and laminarized to produce a uniform distribution. The flow then enters a channel with an open top, and the tree was placed at the interface between the two segments, as can be seen in Fig. 2.12.

28
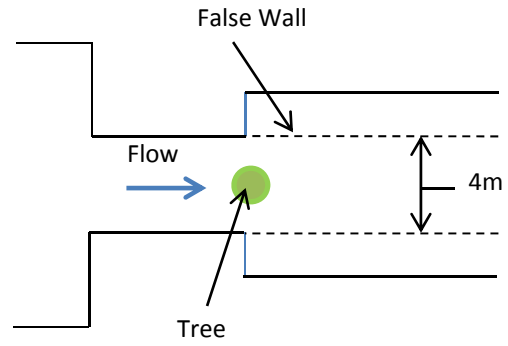
Figure 2.14 – Location of the tree within the wind tunnel. The cross-section measured 4m x 4m.

Measurements were taken by an array of hot wire anemometers, which was systematically placed in each of the locations shown in Fig. 2.15. For reference, the location of the origin was selected as the base of the center of the tree. As the measurements were taken close to the tree, the issues associated with regaining the boundary layer flow (discussed in the previous section) were considered not to have a significant effect on the simulation results.
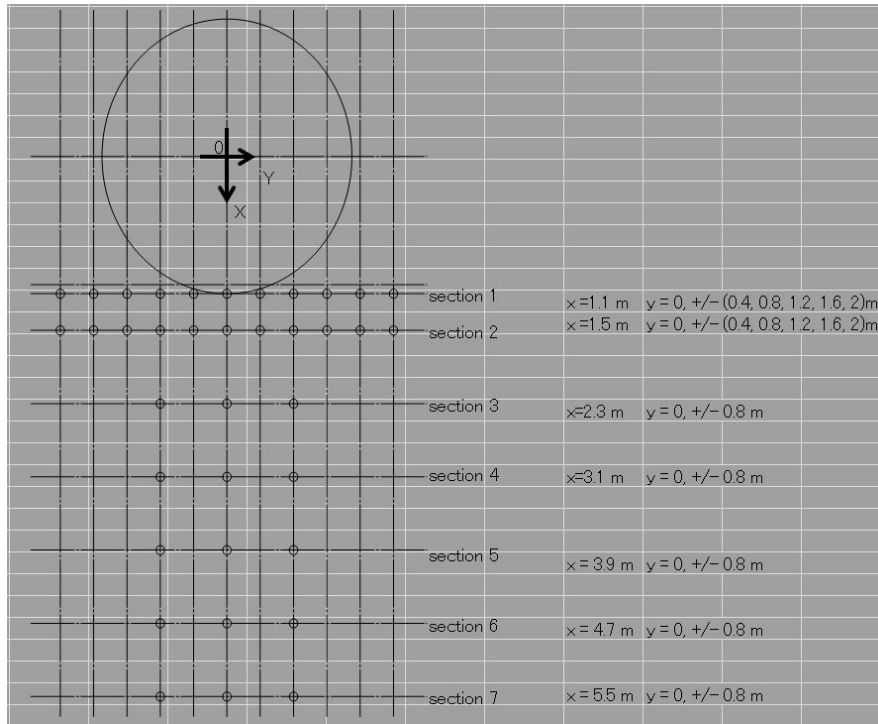
Figure 2.15 – Location of anemometer tower behind the tree

The tower consisted of 20 anemometers at even intervals from 0.2 m to 4.0 m in height. The anemometers were one-dimensional and oriented to capture flow in the streamwise direction (along the x-axis). Data was collected for 60 seconds at a frequency of 10 Hz. Unfortunately, the response time of the anemometers was not well documented, nor was the resolution. However, data from the low velocity tests (1 m·s^{-1}) showed a clear stepping in measurements which suggested a resolution of ~0.007 m·s^{-1}. This can be seen in Fig. 2.16, as the velocity measurements are measured in a stepping fashion, with 0.007 m·s^{-1} being the consistent magnitude of the step. A brief error analysis of the experimental measurements can be found in Appendix C.
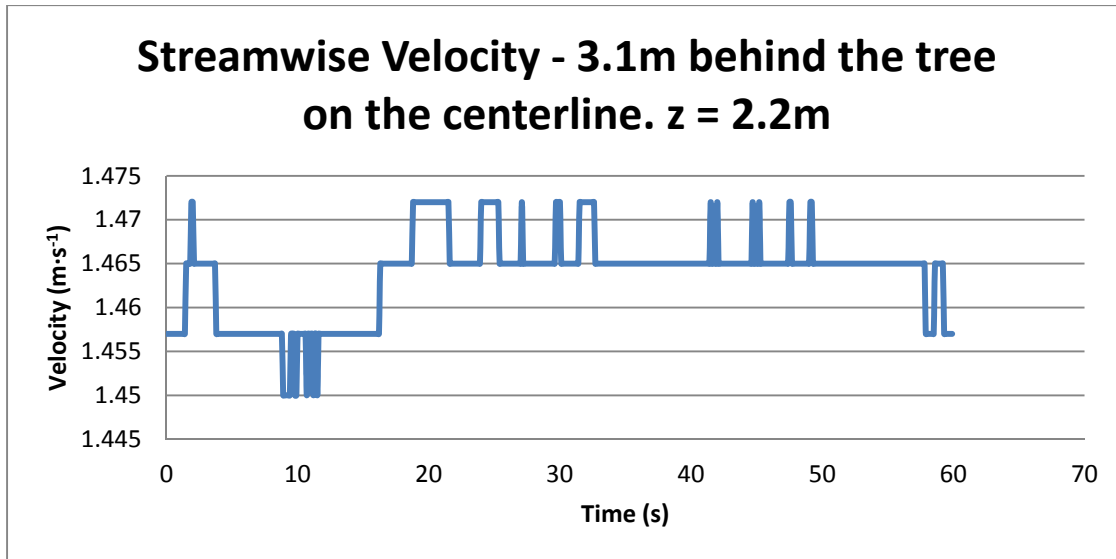
Figure 2.16 – Example of 0.007 m·s^{-1} resolution of anemometer

Various properties of the tree were measured by the team from NIST and the BRI and were reported as shown in Table 2.2.

Property	Reported Value
Tree height	4.9 m
Crown width	3.22 m
Surface-to-volume ratio of needles	5714 m^{-1}
Mass of needles	16.9 kg
Mass of branches <3mm in diameter	2.0 kg
Mass of branches <6mm in diameter	1.3 kg

Table 2.2 – Measured Vegetation properties from the BRI/NIST experiment

2.2.2. Numerical Details

The numerical simulations attempted to replicate the experimental properties of the tree as closely as possible. However, certain simplifying assumptions had to be made due to a lack of detailed information. The tree crown was assumed to be a symmetrical cone seated on the floor of the tunnel (the height of the crown base was assumed to be 0.0 m). The density of all vegetation elements was assumed to be 514.0 kg/m^3 [23]. The needles and small branches were assumed to be uniformly distributed throughout the cone volume with bulk densities corresponding to their respective masses. At first it was considered that the branches less than 3

31

mm in diameter and less than 6 mm in diameter were considered to have the same surface-to-volume ratio as the needles, as this approach had been taken before [23]. However, if one were to consider these branches to be small cylinders that obey the rule of $\sigma = \frac{2}{r}$ then a unique surface-to-volume ratio could be calculated. For the 3 mm branches it was calculated as $\sigma = \frac{2}{0.0015} \cong$ $1333 \; m \cdot s^{-1}$ and for the 6 mm branches it was calculated as $\sigma = \frac{2}{0.003} \cong 667 \; m \cdot s^{-1}$. The assumptions pertaining to density and bulk density distribution have all been used in previous (W)FDS simulations involving conifers [23].

The simulation was carried out on a 12m x 7.2 m x 6m computational domain, with a uniform grid of 0.05 m x 0.1 m x 0.1 m spacing. Details of this choice can be found in Appendix E. Solid boundaries were used to construct a channel for the flow representative of the actual tunnel configuration. All solid boundaries employed the standard Werner Wengle wall model employed by (W)FDS, and the boundary conditions at the maximum X and Z boundaries were defined as the (W)FDS 'OPEN' (details can be found in Appendix A). A uniform inlet velocity was defined at the upstream end of the closed channel in order to drive the flow. The geometrical arrangement of the numerical domain used the same 4m x 4m cross-sectional area, and is shown in Figure 2.17.
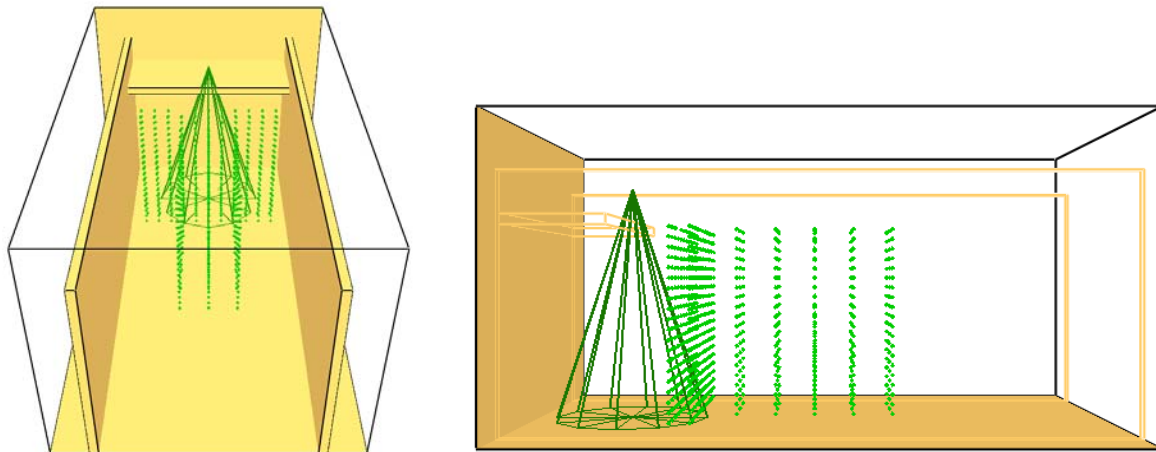
Figure 2.17 – Geometry of the numerical domain. The cone represents the outline of the tree and the green dots mark the various locations in which the experimental anemometers were positioned

The drag force correlation used in these simulations was of the dynamic form which is intended to be used in (W)FDS. It uses σ and β to represent the vegetation as a number of individual particles within each grid cell, and it utilizes the Reynolds dependent drag coefficient discussed previously. These simulations first assumed a cylindrical shape to the pine needles (Eq. 3). Not only does this make intuitive sense, though pine needles are not ideal cylinders, but it is also the assumption that was used to determine the experimentally measured surface-to-volume ratio. Simulations were also conducted to the drag correlation for spheres (Eq. 2) in order to assess the sensitivity of (W)FDS to the chosen formulation, as well as the general consequence of the use of this assumption in previous studies [23,27].

2.2.3. Simulation Results

Comparisons were made between experimental and simulated velocities behind the tree. The first step was to convert the time-varying experimental velocities into a form which allowed for easy comparison. Given that the information was collected in a quasi-uniform arrangement, it was possible to convert the data to be read by Smokeview (the (W)FDS visualization tool) as though it were the output of a simulation. This was done by writing the data to binary files written in the form of a Smokeview slice file [19], and reading them into a manufactured numerical domain. The manufactured domain had to utilize two different meshes with grid intervals that corresponded to the two different densities of anemometer locations shown in Fig. 2.13. This data conversion was carried out at all of the locations, for each tunnel velocity, in each of the four scenarios. Examples of the experimental data visualization are shown in Fig. 2.18.
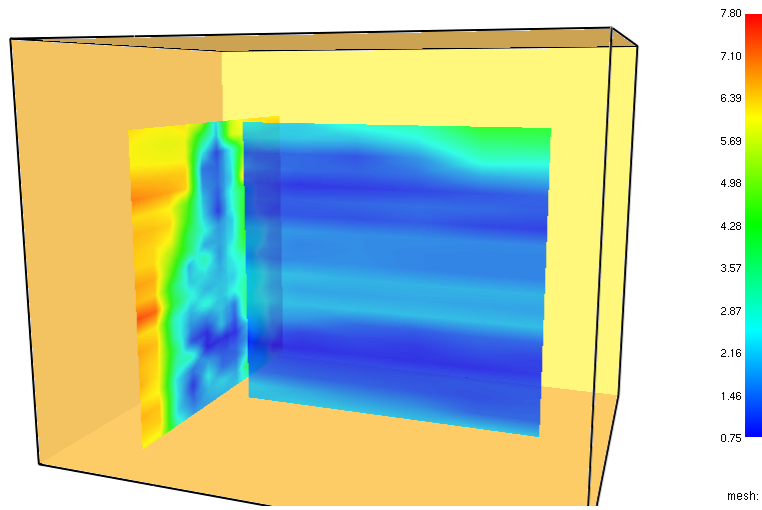
Figure 2.18 – Experimental velocity data for Case2 with a 6 m·s^{-1} tunnel velocity. The x-oriented slice (on the left) corresponds to the array of anemometers placed immediately behind the tree (x = 1.1 m in Fig. x). Units are in m·s^{-1}

Due to the unknown response time of the anemometers, it made more sense for this study to examine the average flow behind the tree, than to try to make an assessment of (W)FDS capability to replicate turbulent statistics. Because the flow had been well established before the start of experimental data collection and the relative fluctuations in the flow were small and high frequency, averages were taken over the entire 60s sampling period. In the case of the numerical simulations, it was found that quasi-steady flow conditions were established behind the tree by 40s of simulation time, so the flow was averaged over the from 40s to 100s.

In order to better understand the significance of the downstream velocities, it was necessary to consider the case where no tree was placed in the tunnel (Case1). This allows one to characterize the flow in the tunnel, so that the changes generated by adding the obstruction can be properly understood. The Case1 velocities from the experiment are shown in Fig. 2.19, and those from the numerical simulations in Fig. 2.20.
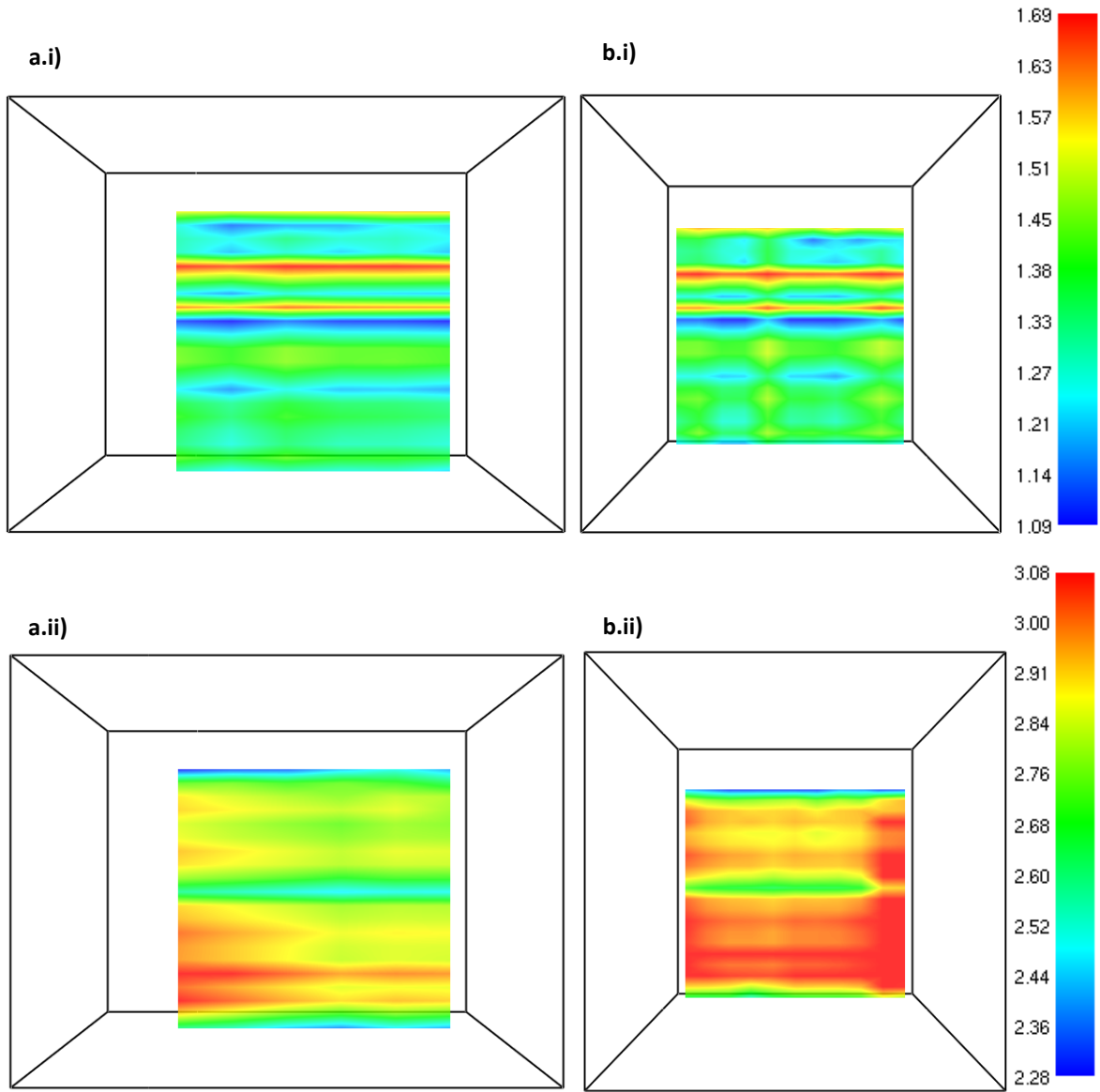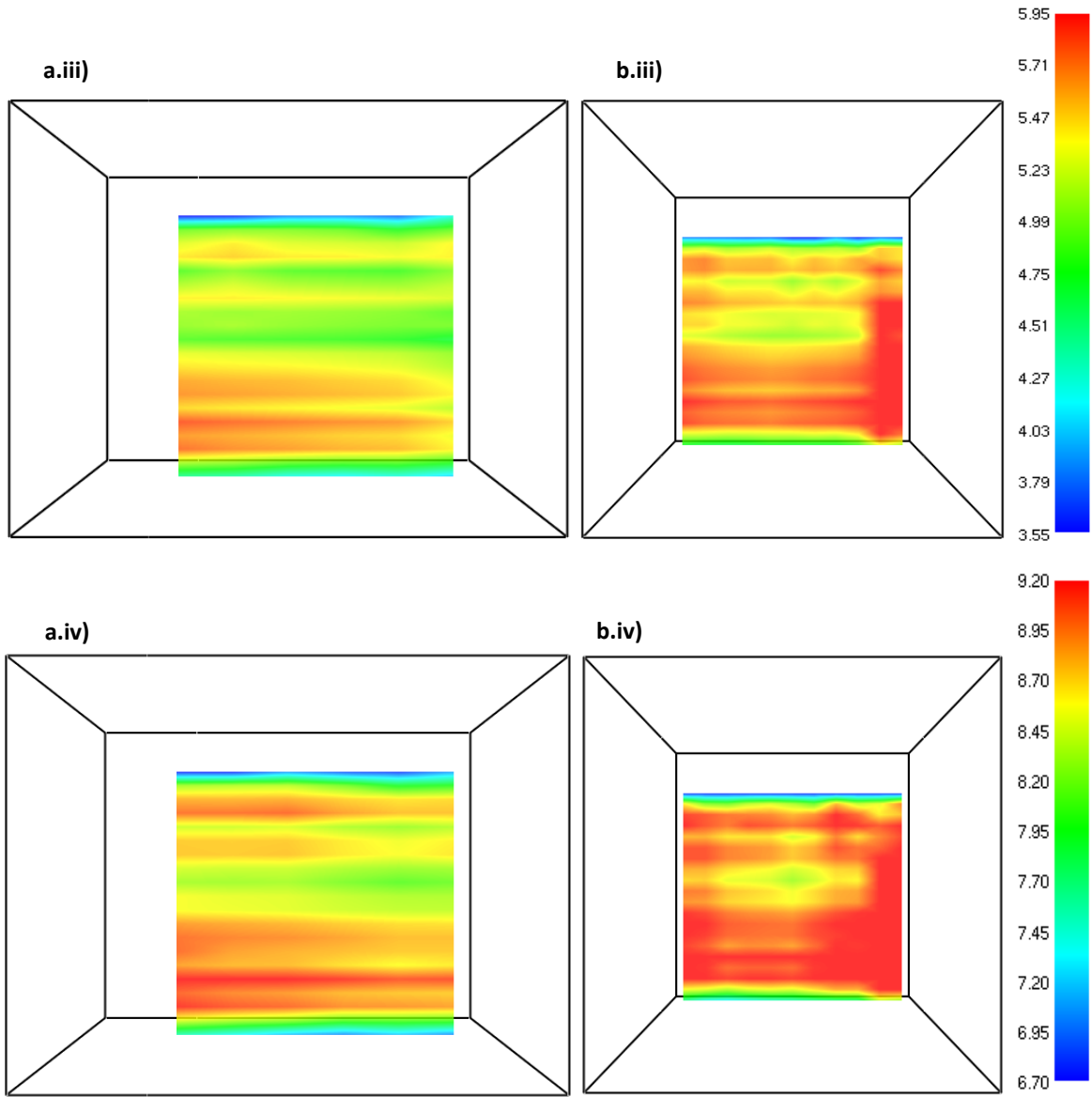
Figure 2.19 – Experimental streamwise velocity: **a)** along the centerline of the tunnel from x = 1.5m to 5.5m, and **b)** in a cross-section at x = 1.1m. Shown for characteristic tunnel velocities of **i)** 1 m·s⁻¹, **ii)** 3 m·s⁻¹, **iii)** 6 m·s⁻¹, and **iv)** 9 m·s⁻¹. Units are in m·s⁻¹.
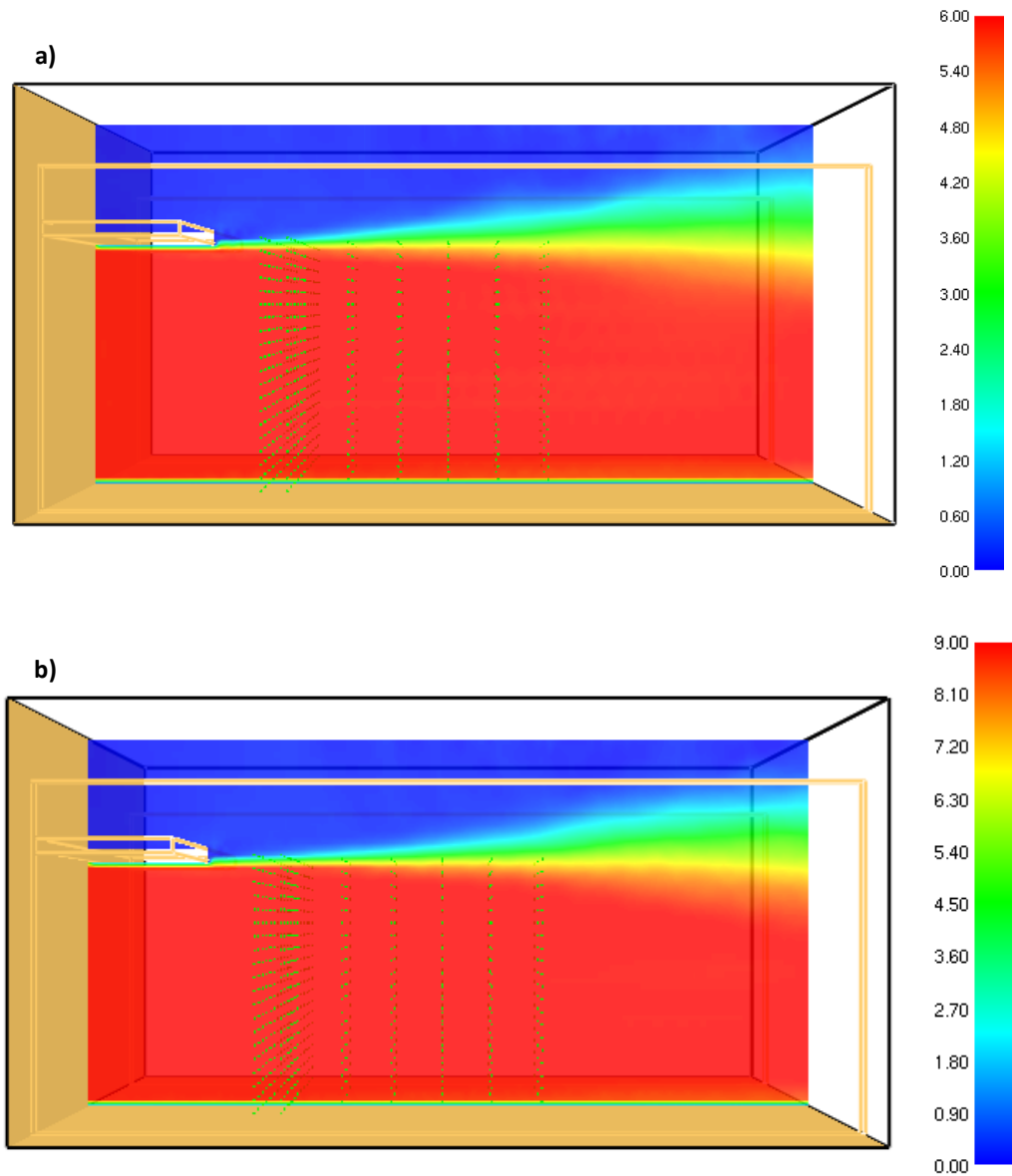
Figure 2.20 – Examples of simulated streamwise velocity (m·s^{-1}) along the centerline of the tunnel for **a)** 6 m·s^{-1} and **b)** 9 m·s^{-1} flow

It was observed that (W)FDS did a good job of representing a uniform flow through the tunnel, without a dependence on tunnel velocity magnitude. However, the experimental case (Fig. 2.17) shows a non-uniformity of the flow which is dependent on the magnitude of the velocity. Of particular note was a "hot-spot" of faster velocities measured along the y = 2.0 m wall. This is resolved in greater detail in Appendix C. These issues with the experimental flow are something

that can be expected, due to the difficulties associated with developing a uniform flow across such a large area.

In order to minimize the influence of non-uniformities in the tunnel flow when comparing the simulations with the experiments, a normalization was carried out. The velocities from Case1 (no tree) were averaged over 60s, and the measured (or simulated) instantaneous velocity in any other Case was divided by the average Case1 velocity at the same point in space. The effect was a percent measurement which quantified the influence that the tree had on the un-obstructed tunnel velocity.
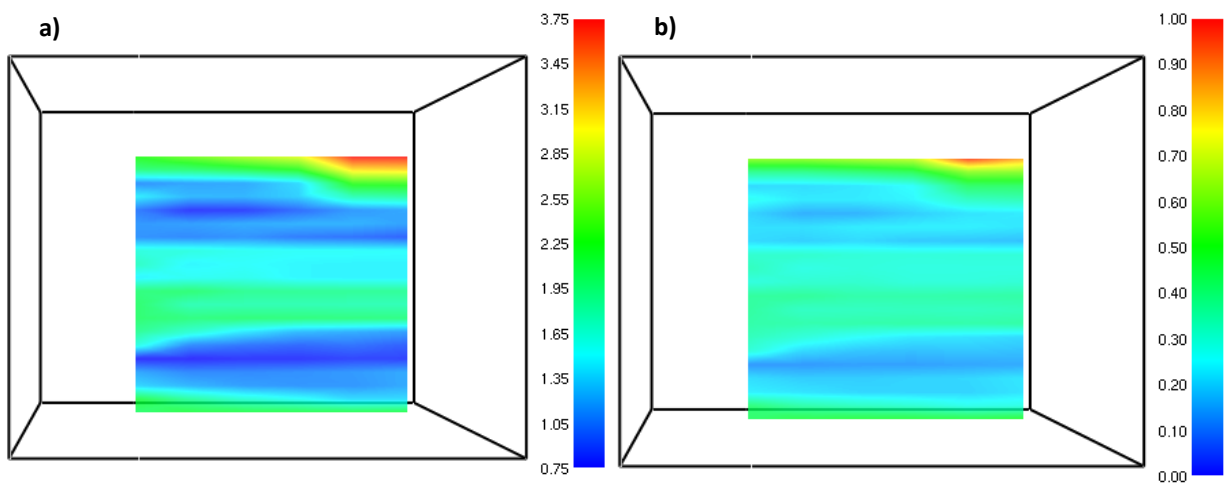
Figure 2.21 – An example of experimental **a)** raw velocities, and **b)** normalized velocities for Case2, at 6 m·s^{-1} tunnel flow. Slices are along the tunnel centerline from 1.5 m to 5.5 m behind the tree

Comparisons between the simulations and the experiments revealed several facts worth noting. First, the change in tunnel velocity has an effect on both experimental and numerical results. However, the trends are not equivalent. The experimental data shows an increasing influence of the tree on the normalized velocities for increasing prescribed tunnel velocities.
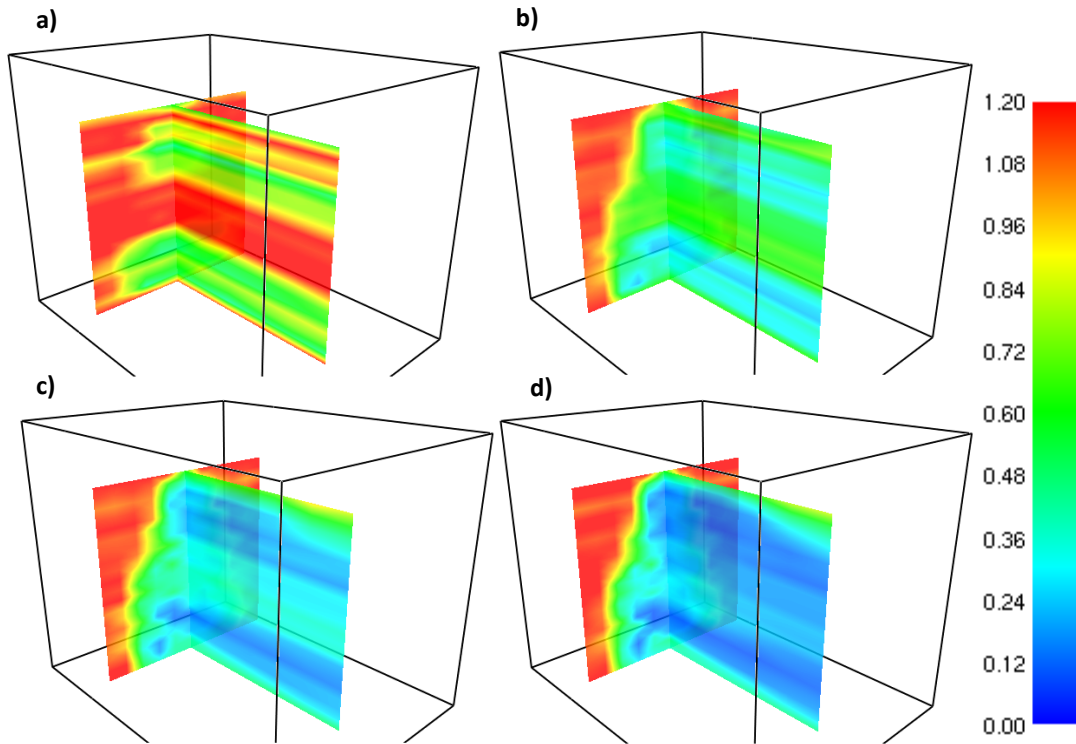
Figure 2.22 – Experimental changing influence of tree for **a)** 1m·s⁻¹, **b)** 3 m·s⁻¹, **c)** 6m·s⁻¹, and **d)**, 9m·s⁻¹ prescribed tunnel velocity

The ability of (W)FDS to match this tendency was evaluated by taking vertical profiles of velocity behind the tree at x = 1.5m and on the centerline y = 0.0m (this is the location of the intersection of the two slices shown in Fig. 2.22)
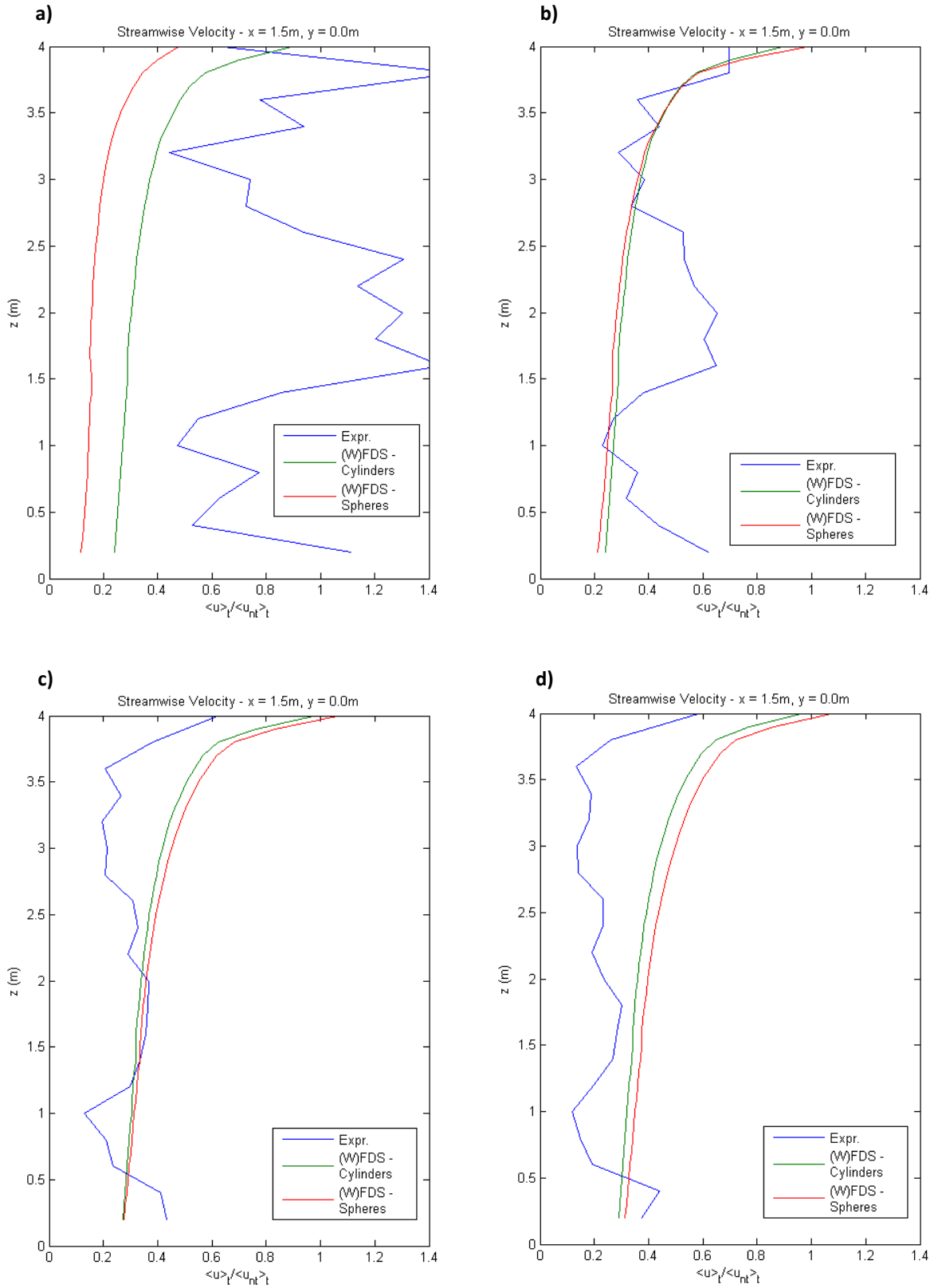
Figure 2.23 – Vertical profile of normalized streamwise velocity directly behind the tree for **a)** 1m·s⁻¹, **b)** 3 m·s⁻¹, **c)** 6m·s⁻¹, and **d)**, 9m·s⁻¹ prescribed tunnel velocity

40

The plots show that, in the case of modeling the vegetation as cylinders, a small increase in the normalized numerical velocities behind the tree is observed as the tunnel velocity increases. This is the opposite trend of the experimental data, which shows a noticeably stronger influence as the tunnel velocity increases from 1 m·s^{-1} to 3 m·s^{-1}. However, the experimental influence of the tree on the flow at the centerline seems to tend towards velocity-independence as the tunnel velocity increases past 6m·s^{-1}. The numerical simulations do not appear to be reaching a steady-state. Additionally, the spheres perform more poorly, exhibiting a greater sensitivity to tunnel velocity. The different behavior between the two formulations of the drag force matches the trend discussed in Chapter 1, with the spheres exhibiting greater influence at very low velocities, but a lower influence when velocities exceed ~1 m·s^{-1}.

Vertical slices of normalized streamwise velocity were also modeled at the same downstream location (x = 1.5m) but at an offset of y = -0.8m from the centerline.
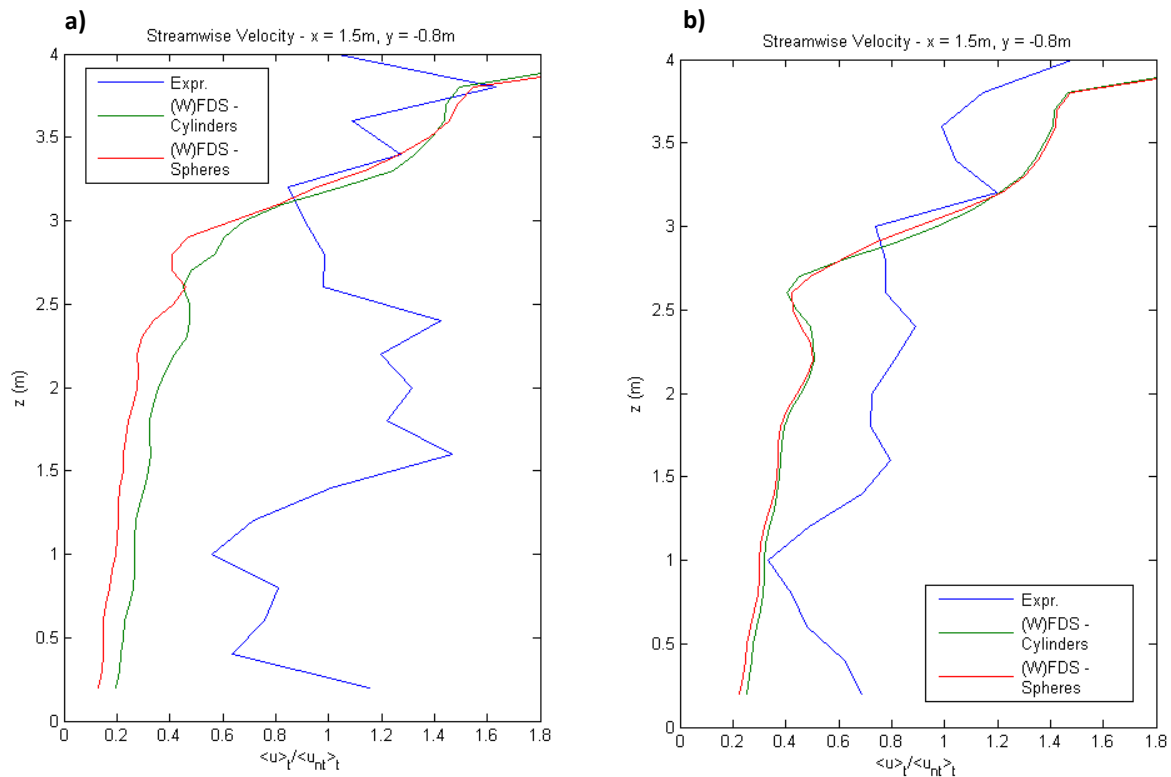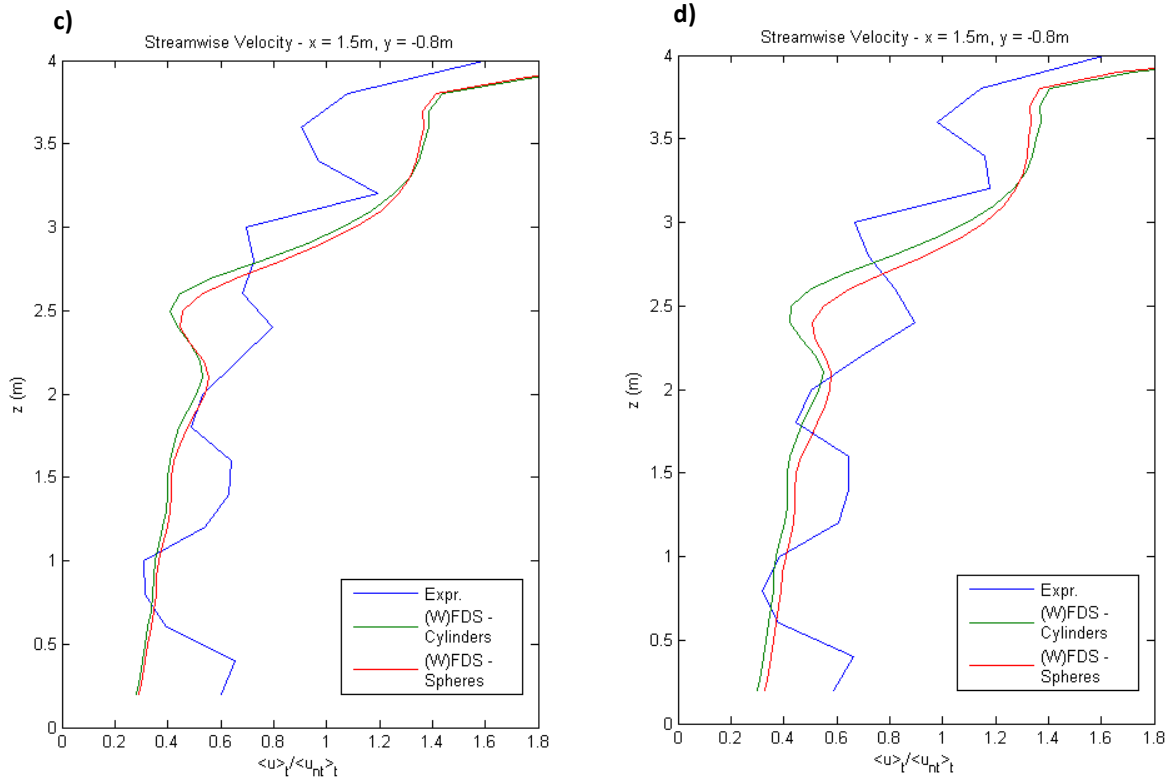
Figure 2.24 – Vertical profile of normalized streamwise velocity at an off-center location behind the tree for **a)** 1m·s^{-1}, **b)** 3 m·s^{-1}, **c)** 6m·s^{-1}, and **d)**, 9m·s^{-1} prescribed tunnel velocity

This analysis revealed the same trend as at the location directly behind the tree center. The experimental data shows an increasing influence of the tree with higher tunnel velocities, but tends towards a constant profile at the highest tunnel velocities. The experimental data shows a consistent decrease in tree influence as the tunnel velocity increases.

The trend at both y-locations of the numerical simulation can attributed to the empirical correlations for c_d. The value is local-Reynolds dependent, and decreases in magnitude with an increase in Reynolds number. Thus, while the total drag force will be higher at higher velocities (as u^2), the influence relative to u will decrease. The trend at both y-locations for the experimental situation can be explained by the inherently non-rigid nature of vegetation. As velocity increases, deformations in branch location will reduce the projected frontal area of the tree, referred to as streamlining. This will have a reducing effect on the total drag of the tree [37], but the local changes will be radially dependent. Along most of its width, the depth will increase as the tree streamlines. This will increase effect of drag seen behind the tree in all locations but those at the very edges, where the effect will decrease. Only behind the outermost edges of the tree will the drag effects decrease.
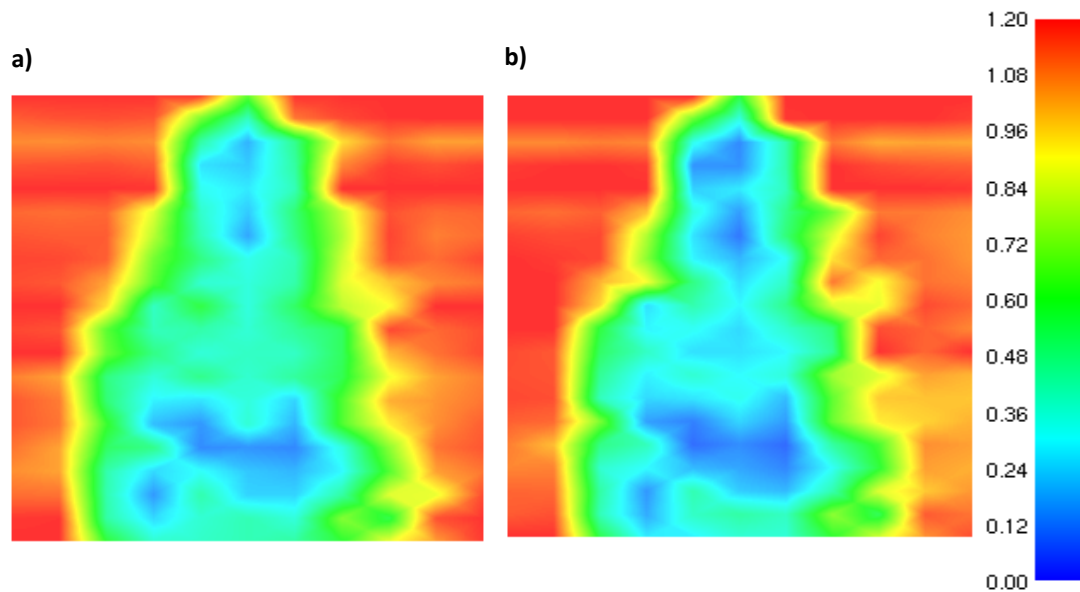
Figure 2.25 – Influence of the tree on a plane perpendicular to the flow direction at x = 1.1 m from the tree center for **a)** 6 m·s⁻¹, **b)** 9 m·s⁻¹ prescribed tunnel velocity

The influence of the distribution of vegetation throughout the tree crown should also be considered. In reality, the specific distribution will never be accurately represented. Therefore, it is important to establish that (W)FDS can generate the appropriate overall shape of the flow, and it appears to be capable of this. The numerical profiles generated in Fig. 2.23. and Fig 2.24 exhibit a fairly smooth shape with mean values that do not deviate significantly from the experimental curves. Sources of some discrepancies can be traced to simplifications made in the description of the numerical tree.

The lower simulated velocities consistently seen close to the ground, as in Fig. 2.23 for example, can be attributed to the fact that the simulated tree sat directly on the ground, and the base was its widest point of the frontal area. The experimental tree however, as shown in Fig 2.14, appeared to be on some type of stand, and its widest point was actually a small distance above the crown base. Therefore, faster velocities will be permitted along the ground in the experimental case. Another discrepancy can be seen in Fig. 2.23, 2.24 and very clearly in Fig. 2.22. This was the fact that, experimentally, there was a region of greater flow measured near the center of the tree. This can be attributed to non-uniformities in the distribution of vegetation within the real tree. The numerical tree, which was considered to contain a uniform density

distribution, would not capture this faster flow, and that can be seen by observing the smooth nature of the curves in Fig. 2.23 and Fig 2.24

Additionally, the sudden increase in velocity simulated in the off-center profiles (Fig 2.4), at ~2.5 m above the ground, is a product of the interface between the tree and the free stream. Not only is this discontinuity not highly resolved in the simulation (similar to the effect at the top of the tree in Chapter 2), but in a real tree there will be a more gradual reduction in vegetation at the outside of the tree combined with an allowance for branch motion. The result would be a smoother transition from intra- to extra-tree flow.

The simulation of Case3, using the method described previously, showed that a new approach for distributing vegetation density should be considered. In this study, the numerical simulations of Case3 involved removing the representation of pine needles from the domain. This only left the branches <6 mm in diameter, as no information had been provided regarding the trunk or large branches. In the simulations, for both cylinders and spheres, the branches <6 mm presented almost no obstacle to the flow. However, experimentally there was still a measurable effect even after the removal of the needles.
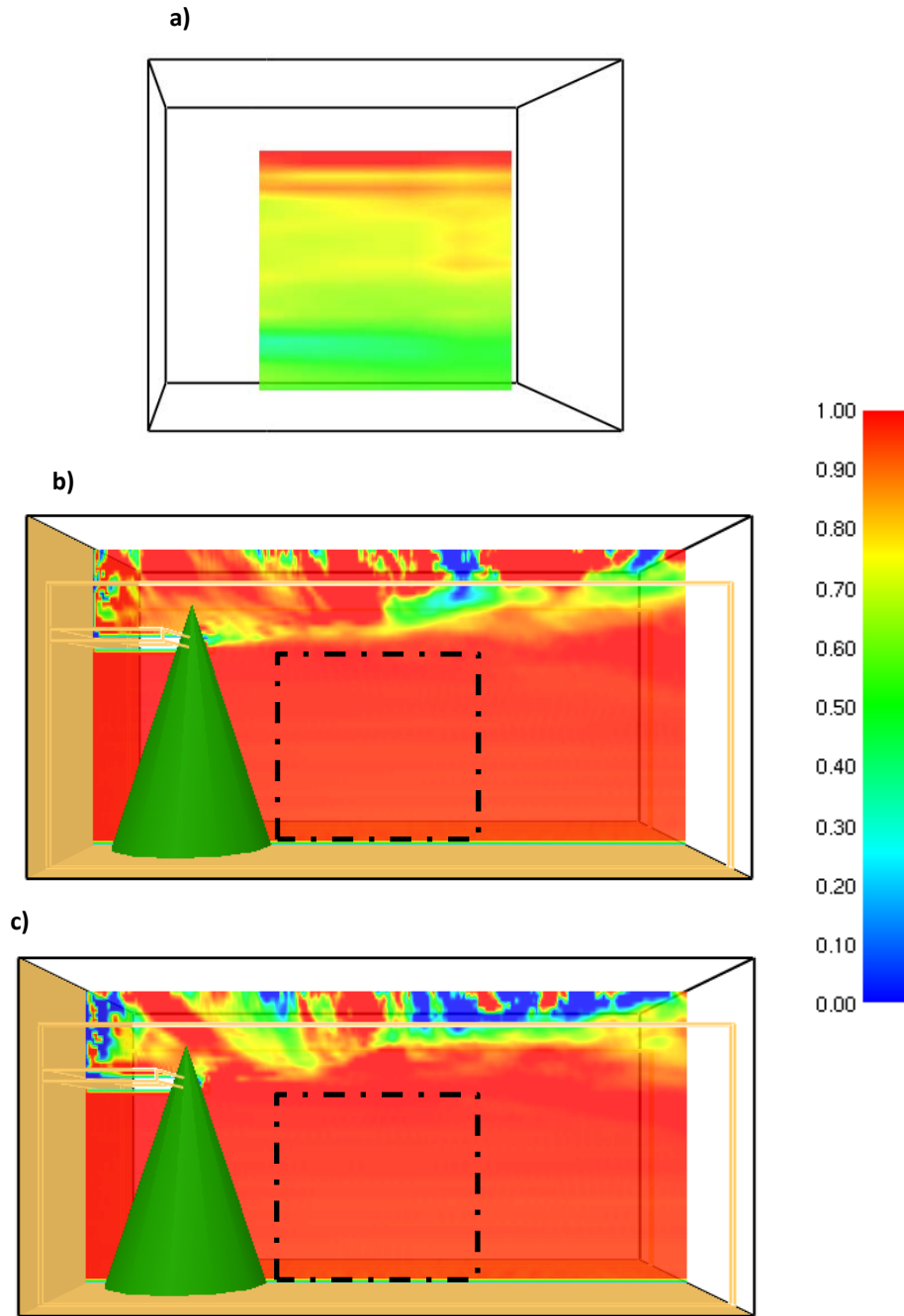
Figure 2.26 – Case3 normalized centerline velocities for the **a)** experimental, **b)** cylinder, and **c)** sphere simulations. Tunnel velocity is 6 m·s⁻¹

The visualization of Case4 further helped demonstrate that the small branches had an effect, and that velocities measured in Case3 were not only influenced by the large branches and trunk. The difference in the velocities observed between the two cases quantified the influence of the branches <6 mm owing to the fact that presence of these small branches was the only

characteristic of the tree which changed. Velocities measured ~0.5 m off of the centerline (out of the influence of the trunk) were shown to increase by ~50% following the removal of the small branches, thus demonstrating their significant influence on the flow (Fig. 2.27).
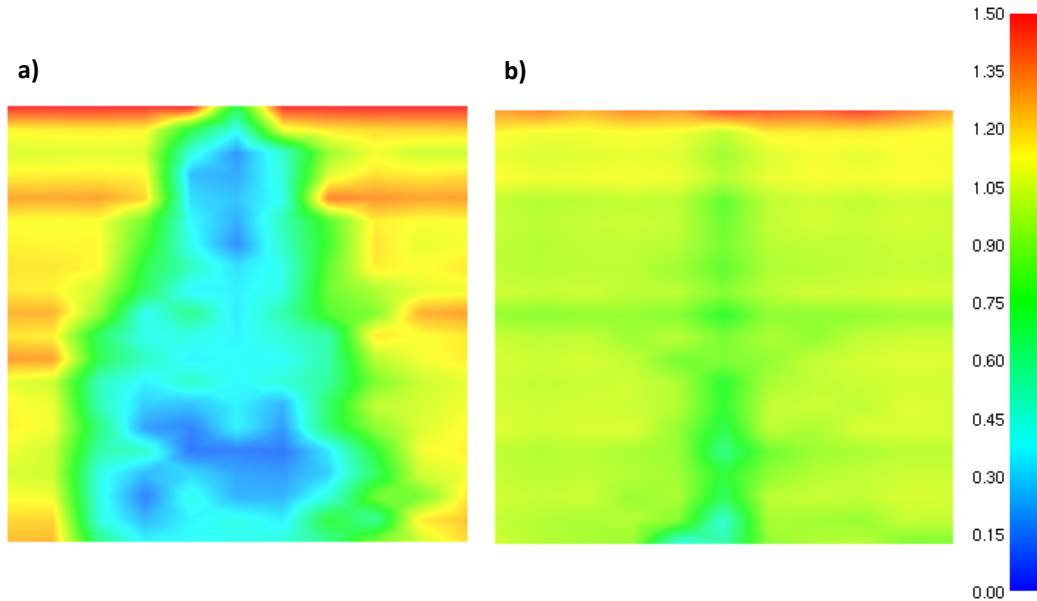
Figure 2.27 – Influence of the small branches on a plane perpendicular to the flow direction at x = 1.1 m from the tree center for **a)** Case3 and **b)** Case4, 6 m·s^{-1} prescribed tunnel velocity

Taking a further step, the simulation of Case4 was not conducted. As no vegetation >6 mm was considered in the numerical simulations, removal of branches <6 mm equated to the free-stream flow regime and the simulations would be identical to Case1. However, this fact is worth pointing out due to the fact that Fig. 2.25 reveals that, while it may have been small, the influence of the trunk and large branches was measurable. Velocities on the centerline, 1.1 m behind the tree, were reduced to ~75% of their free-stream value. More than this, the Case4 experiments revealed that capturing the effect of the trunk was secondary to that of the small branches, as its influence was markedly less.

2.2.4. Total Drag Force

Another method was implemented to assess the representation of vegetation in (W)FDS using the individual fuel element method and the two factors discussed above. This involved

comparing the total drag force imposed upon the tree. Several studies have been conducted on measuring the total drag experienced by a tree, especially as it relates to storm damage and wind-throw [38]. One such study, conducted in 1973, calculated the total drag coefficient for several different tree species at a number of wind speeds [39]. The coefficients were calculated using the still-air projected frontal area, so that the decrease in area does not have to be measured to make these values valid. It was noted that the drag coefficients decreased with velocity, following a similar trend across most tree species.
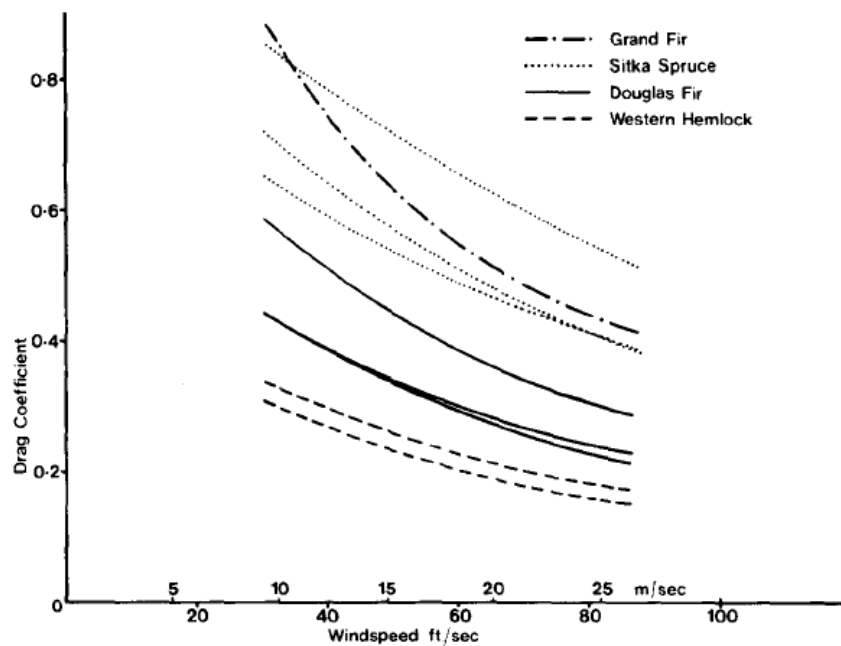
Figure 2.28 – Measured drag coefficient for different conifer species [39]

This information can be used with (Eq. 1) to calculate the expected drag force on a tree. In the NIST/BRI experiment, the tree studied had a projected frontal area of ~6.44 m^2, which was in the same order of the sizes of trees measured in Fig. 2.28. A tunnel velocity of 9 m·s^{-1} was considered, as this was the closest to the range presented in Fig 2.28. This velocity, for a spruce tree, should produce a drag coefficient of ~0.8. Therefore, a total drag of ~250 N can be predicted for this tree.

In order to calculate the total drag on the simulated tree, some small adjustments were made to the (W)FDS code. At each time step, the drag caused by the x-component of the velocity (as this is the only component of the drag force which was measured experimentally) was

summed for all computational cells and written to a data file. These values were then multiplied by the volume of one computational cell in order to get the total drag in the x-direction. Additionally, the capability to visualize slice files of the drag force was written into the code, which had not previously existed.
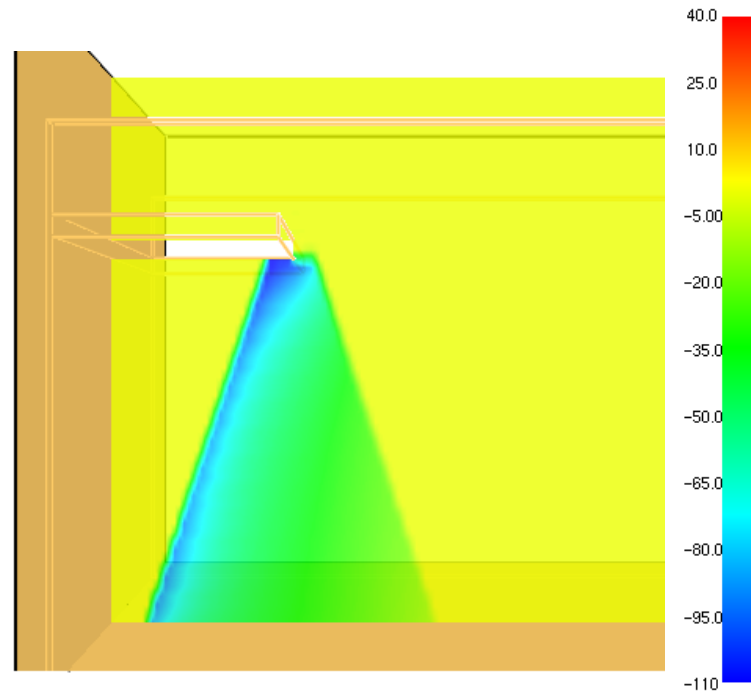
Figure 2.29 – Visualization of the distribution of the streamwise component of the drag force per unit-area along the tree centerline for Case2, 9 m·s^{-1} prescribed velocity

Interestingly, the predicted total drag forces for both simulation cases were significantly higher than expected. A total value of 737 N was predicted for the cylinder formulation, while 674 N was predicted for the spheres. It is difficult to pinpoint the cause of this discrepancy, especially as the method used to determine the expected total force was an approximation which assumed that the density of the tree from the NIST/BRI study was comparable to the fir trees used in the 1973 drag force study [39]. What can be concluded is that, while the simulations seem to be able to represent the mean flow behind the tree, the distribution of the drag within the tree might not be well described. This relates to the issue of streamlining. The coefficient suggested for a tree of this type was generated from experimental data, thus in a situation where tree motion played a role. In the numerical case, the tree is not able to deform in such way as to reduce its total drag, thus the total force experienced will be higher. This possibility needs to be study in greater detail,

48

but it has been shown that the current drag force model in (W)FDS is not likely to be valid when assessing the total force

2.2.5. Conclusions

Several important conclusions can be drawn from this study. The first of which is that the use of drag equation derived for cylinders seemed to produce more reasonable results than with spheres. This is demonstrated by the fact that, within the range of velocities considered, the drag force showed a rather mild dependence on velocity. This was more consistent with the experimental trend than the more velocity-sensitive behavior of the sphere drag. The cause of this can be traced back to the shape of the basic drag coefficient curves shown in Fig. 1.2. The sphere curve is steeper than the cylinder curve. Therefore, drag forces due to cylinders will be less sensitive relative to the free stream velocity than those of the spheres, as changes in local velocity will result in a less dramatic change in the cylinder c_d. The general conclusion is that the cylindrical formulation, while still in need of development, can be recommended over the spherical one as a first approximation.

In the case of both drag force formulations, the predictions tend to be more accurate at higher velocities. One interpretation of this is that the theoretical correlations are over-representing the drag force for a tree in essentially still air, but when the velocities increase and the tree deforms, the representations are more consistent. As the effect of trees on higher velocities (where a 30% change in velocity, for example, might mean a fluctuation of 3 m·s^{-1}) are of greater interest to the wildland fire problem, the poor behavior of the simulations at low velocities is of less concern. This is especially true for dealing with the problem of ember transport, in which a low winds will not be expected to carry embers far, but in high winds the proper modeling of the flow fields will have a dramatic effect on the estimation of long range transport.

The most significant conclusion related to modeling of the influences of the tree at higher velocities is the importance of tree motion. One of the factors that makes CFD modeling with vegetation so different from typical scenarios studied is the tendency of the obstruction to yield to the force of the flow. Both the profiles in Fig. 2.23 and Fig. 2.24, as well as the slices in Fig.

2.25 display evidence of the tendency of the tree to streamline in the presence of higher wind speeds. The resultant effect is a greater influence on the flow behind the main bulk of the tree and a lower influence at the edges, as the branches are pushed inward. The effect appeared to tend to velocity independence behind the tree center around the 6 m·s^{-1} tunnel velocity, but this did not appear to be the case very close to the tree edges, as a distinct difference was noticed in overall tree silhouette between 6 m·s^{-1} and 9 m·s^{-1}. The streamlining phenomenon has been noted in literature, and it has even been suggested that the streamlining will level out (velocity independence) at around 30 m·s^{-1}, though this has not been well tested [38]. This behavior is important to note due to the fact that the numerical simulations do not represent it whatsoever. In fact, at all locations behind the simulated trees a decrease in the relative influence on the flow is seen for higher velocities. This is due to the Reynolds dependence of the drag coefficient, as was noted earlier. One of the next big steps going forward will be to attempt to simulate this behavior. By obtaining more experimental measurements for a wider range of velocities, it may be possible to generate an empirical velocity and radially dependent scaling factor that will adjust the drag forces in such a way as to represent streamlining.

The other area which demands future improvement was highlighted by the results of the Case3 and Case4 comparisons. The significant under-representation of the drag effect from small branches is of particular concern. If these elements are to be modeled separately in terms of fuel consumption, it is important that they be well represented in the flow. The needles will tend to burn more rapidly and there will be a period where the effect of the tree on the flow will be largely due to the slower burning small branch elements. Additionally, these elements will contribute to ember generation, and if the tree no longer represents an obstruction while this is occurring, the ember trajectories will be highly inaccurate. Because the assumption that these larger elements are ideal cylinders does not seem to yield a good representation, more work needs to be conducted to quantify their influence on the drag. This may involve either changing the drag correlation to consider the roughness of the branches, or finding a new approach altogether, as the size of these elements may prohibit the multiphase modeling assumption of a distribution of small particles.

Less important than the small branches, but still worth considering, is the issue of the trunk. It was shown that of all the elements of the tree considered, the trunk and small branches had the least appreciable influence on the flow. This will be true to different degrees for different

species (depending on the relative trunk size), and so it may still be important to model. Most important, would be the case where the array of remaining trunks behind the fire front would still impose a significant influence on the driving velocities into a head fire (such as in a dense forest). The most logical way to represent these elements would be to model solid cylindrical obstructions and adjust them in size to match the measured influence from experiments such as Case4. Combined with the representation of needles and small branches, both including empirical streamlining adjustments, a much more complete and realistic representation of a tree could be generated.

Chapter 3 – Large Scale Simulation

Section 3.1 - Canopy Flow

3.1.1. Overview

The simulation of flow within and around a single tree is important, especially in the case of evaluating a WUI scenario where sparse, inhomogeneous vegetation may be used as defense against fire spread. However, for some larger scale applications, it makes more sense to consider an entire forest canopy as a single homogeneous layer. This method aims to model the flow through the vegetation layer as well as the shear that is created by drag along the top of the forest canopy. The large coherent eddies which are produced by this flow are the main mechanism responsible for the scalar dispersion in forest canopies and are often studied, especially in relation to the natural exchanges of heat, water vapor, CO_2 [40], and even pollen [41]. However, this characteristic flow will also influence the dynamics of a fire, and thus is important to model accurately in this specific context.

When an atmospheric boundary layer is incident on a forest canopy edge, several regimes of the flow have been identified by Belcher et al. [42]:

i) The impact region: An increase in pressure is seen in air parcels entering the canopy decelerate. The resultant pressure gradient causes deceleration to occur upwind of the canopy edge as well. Conservation of momentum means that the deceleration in streamwise flow causes an upward motion over the canopy.

ii) The adjustment region: At the upwind canopy edge, and within the canopy itself, the streamwise flow is decelerated by the canopy drag. Conservation of momentum causes an upward flow out of the canopy due to streamwise deceleration, while canopy shear generates downward flow.

iii) The canopy interior: The flow reaches equilibrium with the canopy. The streamwise velocity profile has been found to match certain empirical correlations in this range, exhibiting an inflection point at the canopy top.

iv) The canopy shear layer: At the top of the canopy, a shear layer develops which is responsible for creating the large coherent eddy structures that drive the exchanges of mass, momentum, and energy between the forest and the atmosphere.

v) The roughness-change region: The canopy shear causes the generation of an inertial boundary layer above the canopy.
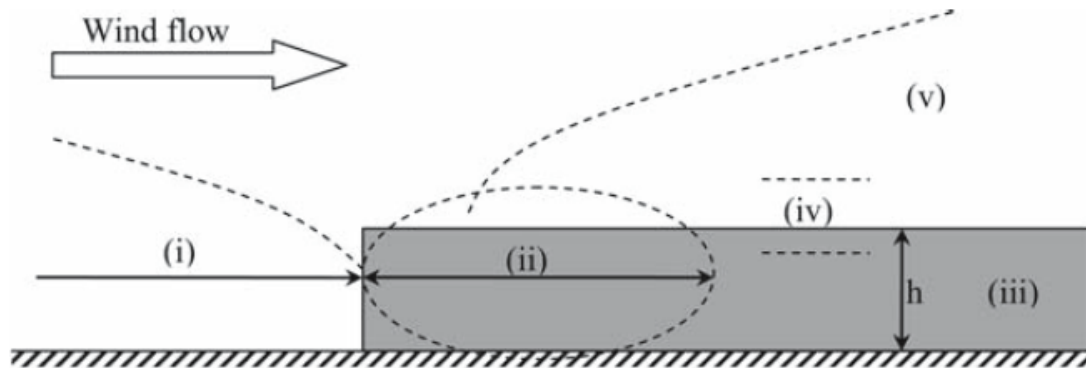
Figure 3.1 – The different regions associated with canopy flow [34]

The ability of LES models to recreate this type of flow has been studied several times before [34,32]. However, it is worthwhile to conduct such a study with (W)FDS, not only because it has yet to be reported in literature, but also because the (W)FDS approach differs in the method of turbulence modeling from the others tested. While (W)FDS employs the Smagorinsky model described in Chapter 1, models such as those of Su et al. and Pimont et al. solve separate conservation equations for the subgrid-scale turbulent kinetic energy (SGS TKE) [32,43].

3.1.2. Numerical Details

The initial intent in running this numerical simulation was to keep the prescription of specific numerical parameters (boundary conditions, initial conditions, etc.) as consistent as possible with those used in other LES simulations of canopy flow. Thus, comparisons of the simulation results will highlight the differences in the details of the various modeling approaches. In this particular study, the comparison focused on validation work conducted for FIRETEC/HIGRAD [32]. This is an LES-like model in that resolves eddy motions larger than twice the grid spacing and models subgrid-scale motion. It was designed to simulate large-scale fire scenarios. HIGRAD solves for compressible flow in the lower atmosphere, and is linked to FIRETEC which uses a multi-phase representation in order to solve mass, energy, and momentum exchange with the solid fuel. The report referenced here focused only on the FIRETEC portion of the code. It takes a common approach used in LES canopy modeling, which is to solve for the Reynolds stress tensor by solving a conservation equation for subgrid-scale turbulent kinetic energy (SGS TKE). The model goes one step further, however, and solves for SGS TKE at three distinct length scales. These are intended to capture eddies at the scale of the canopy, medium vegetation (branches etc.), and the smallest vegetation elements (needles etc.), respectively [32,44].

In the particular validation study conducted for FIRETEC, two scenarios of basic, cold-flow were considered. The first involved a continuous forest canopy and was compared to the field measurements within and above a deciduous forest [45]. The second involved a canopy with an inhomogeneity, intended to be representative of a fuel break. These results were compared to wind tunnel data for a similar configuration in a model forest [46]. For the scope of this research only the case of the continuous canopy was considered.

The (W)FDS domain was set to be 200m x 150m x 216m with a uniform grid spacing of 2m x 2.08m x 0.9m. Details of this choice can be found in Appendix E. It was divided into 16 identical meshes of 50m x 37.5m x 216m. This domain was comparable to the FIRETEC simulation, except that it presented a higher resolution in the z-direction (the FIRETEC mesh was stretched vertically from 1.8m at ground level to 40m at the domain top). The higher resolution was utilized in order to ensure that the vertical profiles of velocity and turbulent statistics would be well resolved within the canopy. Due to this high resolution, height of the domain (216m) was set at about 1/3 of that used in the FIRETEC case. As only flow structures up to twice the canopy height (36m) are typically measured experimentally (as in this case) and,

therefore, the behavior of (W)FDS could not be evaluated above this, the smaller domain height was considered acceptable.

The forest canopy was set to a height (z_h) of 18m. The drag force representation in the momentum equation was set to be the same for both models, and took the form of the flat leaf representation (Eq .4). The drag coefficient was set to 0.25, which falls within the accepted range discussed in Chapter 1. The leaf area density (a_f) was prescribed as a particular height varying profile, indicative of the forest from which experimental measurements originated [32]. The density was invariant in the x- and y-directions.
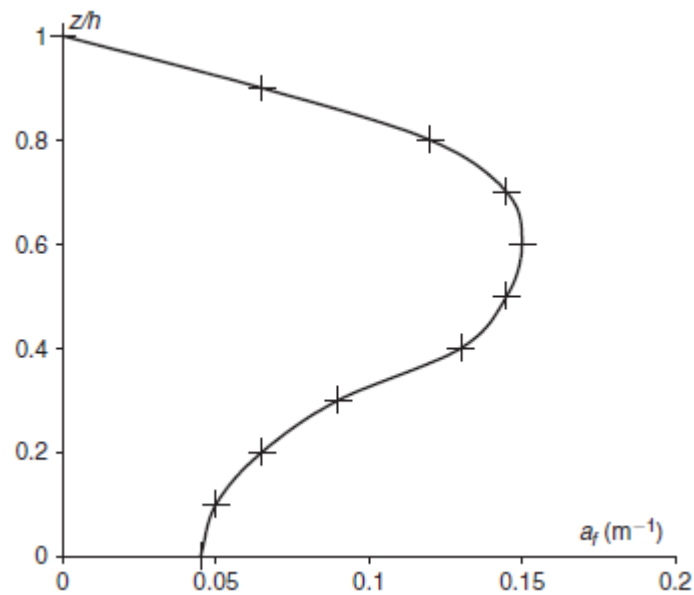
Figure 3.2 – Leaf area density profile [32]

In the FIRETEC and similar LES simulations of canopy flow, the adopted approach involved setting periodic lateral boundary conditions. The rationale is that a flow through a homogenous layer of vegetation with periodic boundary conditions will reach a quasi-steady state that is indicative of the stable canopy interior. This is the equivalent of modeling a scenario far enough into the forest that edge effects are no longer relevant. The velocity field is typically initialized with a form of an atmospheric profile (exponential or logarithmic), and is then maintained high above the canopy by setting a constant flow (or driving force) at the top of the domain. For this specific case, the initial velocity profile was set to $u(z) = u_{2h} \frac{\log z}{\log 2h}$, with u_{2h} set to 2.75 m·s⁻¹. The lower boundary condition was not considered to have a significant due to

the continuous presence of vegetation. In (W)FDS it was left as the standard Werner Wengel wall model.

Unfortunately, when attempting to replicate this scenario in (W)FDS some complications were encountered. Due to the size of the computational domain considered in this case, it was necessary to split the calculation across a number of meshes (and therefore processors). It was discovered that due to small velocity errors created at the mesh interfaces (a bi-product of the (W)FDS pressure solver [19]) and the presence of periodic boundaries, turbulence was spontaneously generated in cases without any vegetation present. By setting the VELOCITY_TOLERANCE parameter in (W)FDS, it is possible to force multiple iterations of the pressure solver in order to limit the velocity errors. However, this increases computational time, and as turbulence was still being generated in cases with a VELOCITY_TOLERANCE of $1 \cdot 10^{-5}$ m·s^{-1}. It was determined that more work needed to be done to investigate this issue before going forward with simulating a canopy flow in this manner. Details of this investigation can be found in Appendix D.

However, another approach was taken in order that the ability of (W)FDS to simulate canopy flow might still be evaluated. The initial velocity profile was of the form of an atmospheric profile developed over open terrain. Therefore, this profile was prescribed as constant at one end of the domain. It was allowed to develop over 50 m before coming into contact with the upwind edge of the canopy. The canopy flow was then modeled for an additional 1000 m downwind. The setup (Fig 3.3) resembles that of wind tunnel studies [47], and allows to comparisons to be made to the different regimes of canopy flow described earlier in this chapter. The grid spacing was kept the same as described before, but now the domain was divided over 84 uniform meshes of 50m x 37.5 x 108m. The removal of periodic boundary conditions means that the small velocity errors developed at mesh boundaries did not grow to have a significant influence on the overall flow. Full details of the differences between the (W)FDS and FIRETEC simulations can be found in Appendix D.
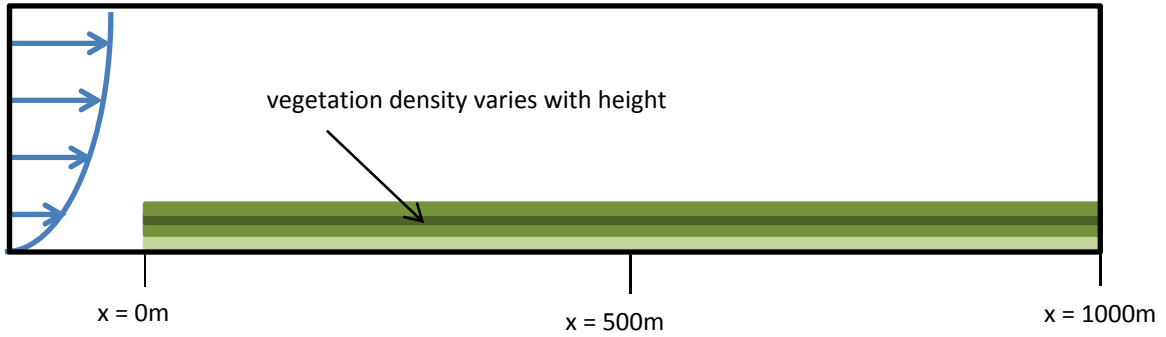
Figure 3.3 – Domain developed in for simulation with (W)FDS

3.1.3. Simulation Results

The simulation was observed to obtain quasi-steady flow characteristics after 2000s of simulation time. This was evaluated by comparing average velocities over the interval 2000-4000 s and 3000-5000 s. Reported results were averaged over the interval from 3000-6000s. The streamwise velocities were found to converge to experimental measurements within the canopy, as shown in Fig 3.4.
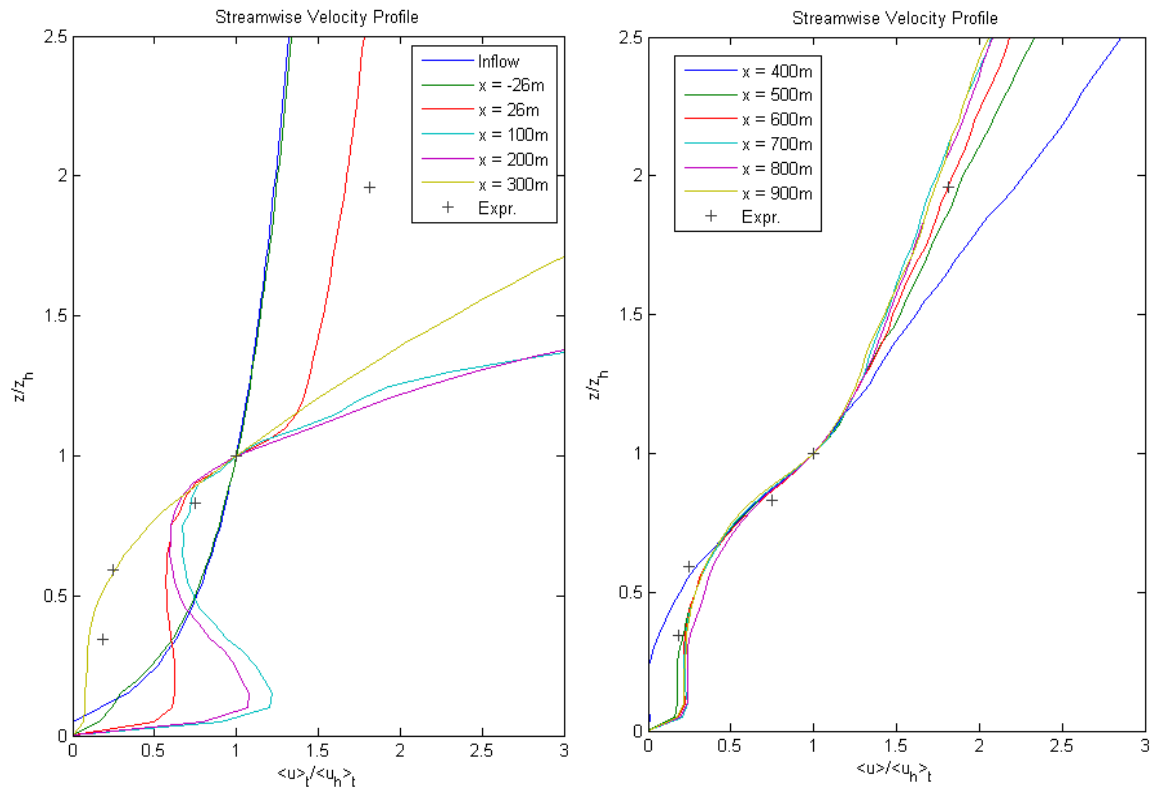
Figure 3.4 – Development of velocity profiles along the length of the domain. Values are normalized to the canopy height (z_h)

The velocity flow upwind of the canopy edge (x = -26m) exhibited the anticipated deceleration indicative of the impact region (i) due to the pressure gradient developed within the canopy. As the flow entered the canopy, a deceleration was seen in the upper half, as was anticipated in the adjustment region (ii). In the lower half of the canopy, however, an acceleration was seen. This was due to the lower density of vegetation near the 'forest floor' and the conservation of momentum, and such behavior has been noted before [34,47]. The magnitude of this acceleration will be somewhat dependent on the choice of wall model, as noted in Chapter 2, but will not have a significant effect on the overall profiles, especially when the stable condition is reached (see Appendix D). However, an appropriate choice of wall model for a forest floor does require a more detailed investigation. Further into the canopy (between 400m and 500m) the essentially steady canopy interior (iii) flow is obtained. It is also noted that (W)FDS successfully captures the inflection point which has been reported in the mean velocity profile at the canopy top [32].

Several characteristic turbulent statistics are also examined. The simulated average turbulent kinetic energy $k = \langle \frac{1}{2}(u'^2 + v'^2 + w'^2) \rangle_t$, momentum flux $\langle u'w' \rangle_t$, and standard deviations $\sqrt{\langle u_i'^2 \rangle_t}$ all converged more rapidly than the mean velocities. They matched fairly well to experimental measurements.
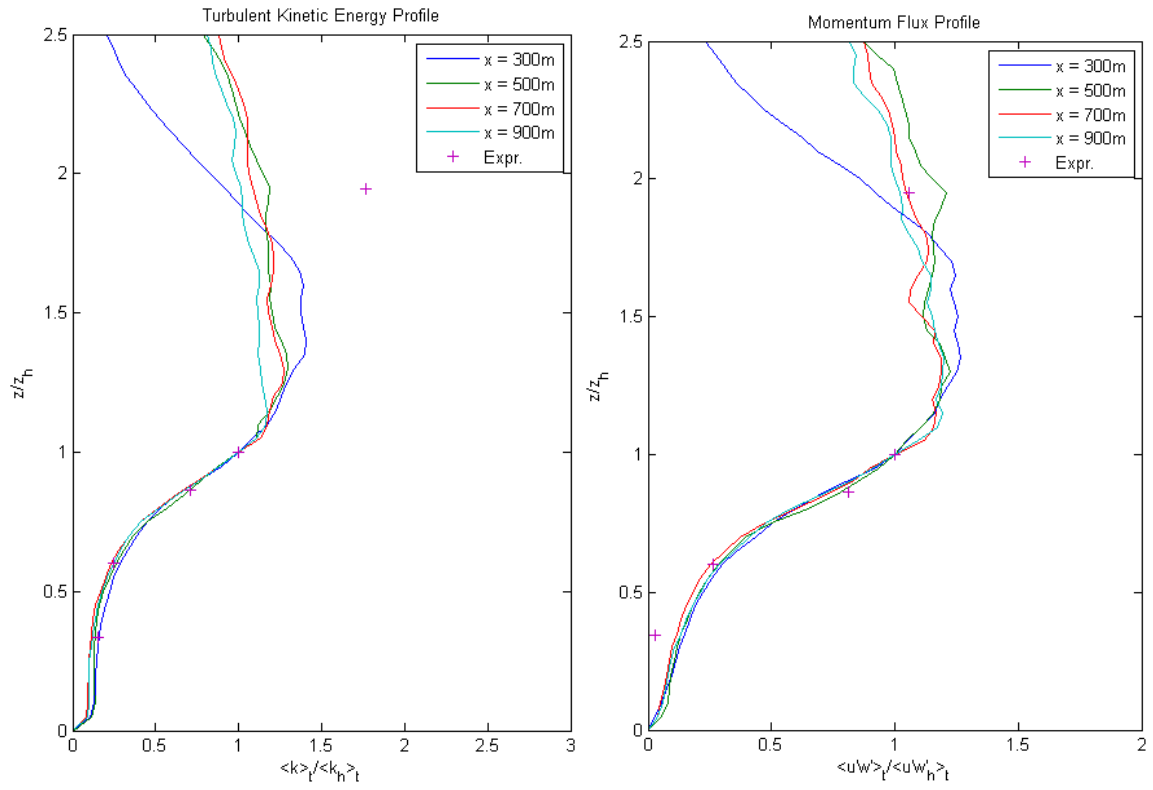
Figure 3.5 – Development of **a)** turbulent kinetic energy, and **b)** momentum flux along the length of the domain. Profiles are normalized to the respective values the canopy height (z_h)
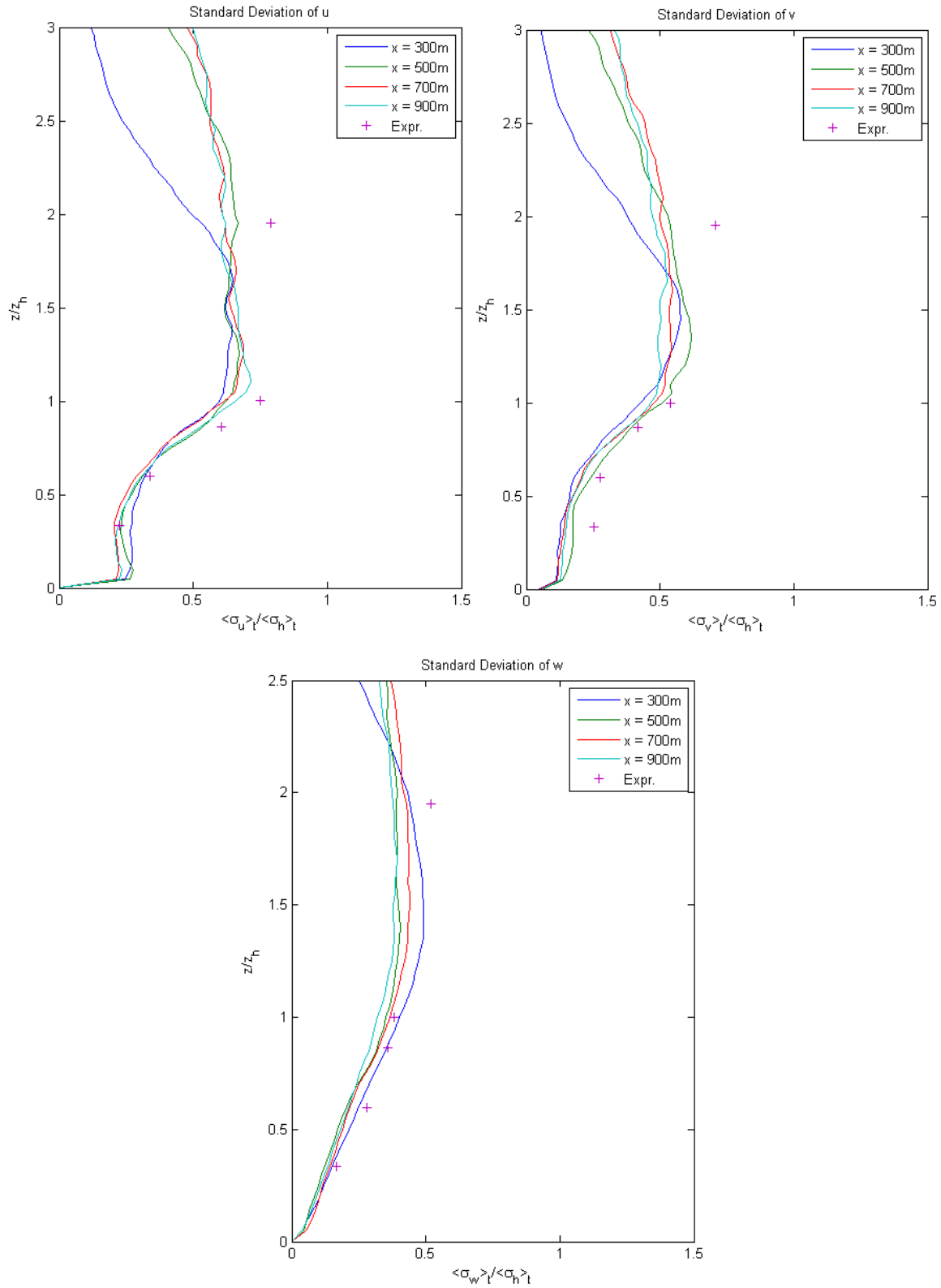
Figure 3.6 – Development of velocity standard deviations. Values are normalized to σ_h at the canopy height (z_h), where $\sigma_h = \sqrt{\langle 2k \rangle_t}$

It was observed that the numerical model had the greatest difficulty in matching the experimental data at $2z_h$. While the mean velocity profile tended to show a reasonable value at this height (Fig 3.4), the measures of turbulence showed consistently lower values than expected (Fig 3.5 and 3.6). However, this difficulty was also noticed in the FIRETEC results.
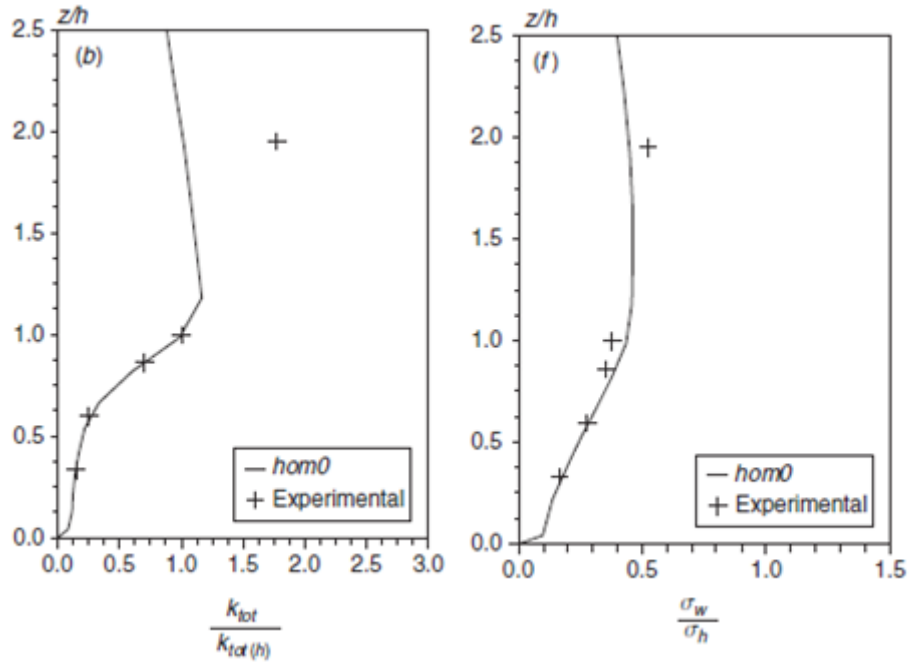
Figure 3.7 – Examples of some turbulent statistics as generated by FIRETEC [32]

The examples shown in Fig 3.7, as well as the others which may be found in Appendix D, suggest that this issue was not related to the models, so much as it was related to the inputs chosen. The velocity profile (specifically the value specified at z_h) and the drag coefficient were both selected arbitrarily in an effort to obtain convergent results, rather than being based on experimental values. Therefore, it is possible that these values were not representative of the real forest. Additionally, it was found that when the velocity and the drag coefficient were adjusted, the results within the forest were not highly sensitive, while those above the forest were [32].

60

z/h

2.5
(b)

2.0

+

1.5

1.0

0.5

0.0
0.0 0.5 1.0 1.5 2.0 2.5 3.0

— hom0
··· hom1
-- hom2
-· hom3
+ Experimental

$$\frac{k_{tot}}{k_{tot(h)}}$$
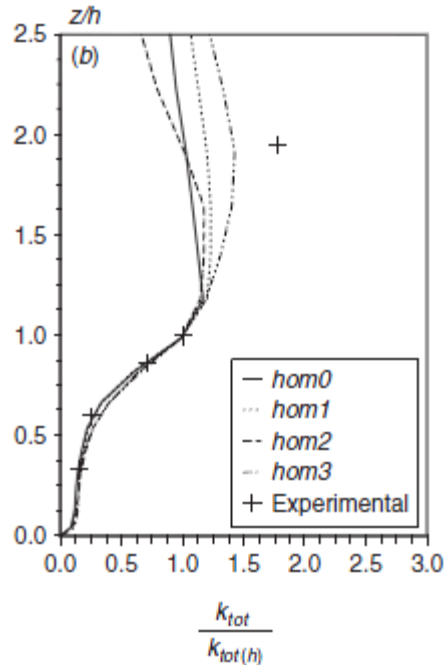
Figure 3.8 – An example of the above-canopy sensitivity to drag and velocity input choices [32]

Therefore, it is reasonable to suggest that a combination of velocity and shear inducing drag forces (c_d) may be found which will generate a larger shear layer and therefore increase the turbulent statistics above the forest canopy.

3.1.4. Conclusions

The most significant conclusion from this study is that (W)FDS does appear to be fully capable of replicating the characteristics of a canopy flow. This stands to reason, as not only in this case was a drag coefficient pre-determined which would yield good results, but when considering a large dense canopy, local tree movements do not have the same effect. The flow regimes around individual trees are not resolved, but this does not affect the results as the bulk influence of the canopy will remain the same, especially beyond a depth of a few canopy heights.

While expected trends for both mean streamwise velocity and turbulent measures were generally achieved, there were several points which need further investigation. Foremost, the streamwise velocity did not develop into a steady profile until beyond 400m from the canopy edge. This is a larger value than the suggested $10z_h$ [34]. Linked to this was the issue of the under-prediction of turbulence at $2z_h$. The first issue which must be addressed is the accuracy of

the experimental measurements. In the case of the depth required to obtain a stable profile, there exists a minimal amount of experimental work to back this assertion, and it is generally based upon one wind tunnel study as opposed to a real forest [46]. Additionally, little information is given on the experimental measurements above the canopy in the real forest, and so it would be worthwhile to confirm these measurements in the future. Assuming, however, that the measurements are all accurate, these two problems in the simulation are also linked to the choice of the velocity profile and the canopy drag. As was discussed previously, these values were selected to obtain good results, but it was found that the sensitivity of the stabilized profile within the canopy was not high with respect to these choices. As such, slightly adjusting the input values (specifically the canopy drag) may create a situation in which the same quasi-steady profiles are obtained within the profile, but at a depth closer to $10z_h$. The increased generation of shear from higher drag may also increase turbulence above the canopy, though the steamwise velocity may have to be increased in order maintain the bulk value of the flow. This modification is currently being evaluated as these issues with the simulation results are not insignificant. The distance for flow stabilization is important for modeling the winds which have a direct influence on the fire behavior. Likewise, while a high accuracy of the flow modeling at twice the canopy height may not seem very important for fire modeling within the canopy, this problem might have implications for emissions modeling.

The next logical step in this line of investigation is to examine the ability of (W)FDS to simulate flows through a discontinuous forest, such as the wind-tunnel fuel-break experiment examined by several other LES models. Typically periodic boundary conditions are used in order to obtain a fully developed canopy interior flow at either end of the domain. Therefore, the issues associated with periodic boundary conditions in (W)FDS will have to examined in more detail. Alternatively, the fully developed profiles of velocity and turbulent statistics generated in this research could be applied at an inflow boundary, to simulate a point far within a forest canopy. In either case, this will be a very important next step owing to the fact that simulations of WUI fires will not involve continuous forest layers, and so the influence of an inhomogeneity must be well represented.

Conclusions and Future Work

The research effort undertaken can be grouped into two main categories. The first was a general assessment of the types of fundamental drag force correlations which have been previously suggested, and an analysis of their applicability to real flow scenarios. The second was a study of the ability of CFD models (specifically (W)FDS) to generate realistic flows within and around vegetation at multiple scales. This separation of focuses allows a clear understanding of the improvements that need to be made in the fundamental way vegetation is represented and the improvements that need to be made in the general modeling tools. To a first approximation however, promising results were found in both focus areas of the research.

With respect to the fundamental drag forces, the choice of representing vegetation as an array of solid particles was shown to be significantly influenced by two factors. The first was the choice of the geometry of said particles. Spheres have been the classical choice when using this formulation to model wildland fire flows, however, a correlation for cylinders was suggested in Chapter 1. It was shown that for moderate to high winds (>1 m·s^{-1}) the spheres will present a lesser obstruction to the flow. This was confirmed in the simulations run in Chapter 2. Also confirmed in these simulations was the higher sensitivity of the sphere drag to free-stream velocities. Both correlations performed well at generating mean flows representative of the real tree considered in Chapter 2. However, the more velocity sensitive nature of the spheres resulted in less accurate predictions (though not drastically so) and so the cylinder correlation was recommended for future work.

The second influencing factor on the drag generated from a particle array was its assumed rigidity. In Chapter 2, it was demonstrated that the flow regime created by a single tree was directly dependent on the free-stream velocity. This was due to the streamlining capacity of vegetation. Experimental results showed that, for higher velocities, the influence of the vegetation increased behind the tree and decreased at the edges as the branches were pushed back and inward. The rigid array of particles represented by the drag force correlations inherently neglected this effect. The omission of this phenomenon combined with the local Reynolds dependence of the drag coefficient manifested in a slight decrease in the influence behind the simulated tree, as opposed to an increase.

The choice of a constant drag coefficient model was also examined. It was shown to generate fundamentally different drag forces, as can be expected. It was also shown to perform well when generating a recirculation region behind a tree. This behavior has been indicated as being realistic in experiments involving model trees, but still needs to be assessed for full trees. The use of LES was shown to generate a more significant recirculation than previous RANS simulations, which had better agreement with experimental results.

With respect to the larger ability of CFD-based physical models to employ these basic correlations and represent realistic flows, there were several issues uncovered. The first was the dependency on the general description of vegetataion. At the scale of an individual tree, it was shown that the inputs specified for representing small branches, large branches, and the trunk were all important factors which are usually thought to be minimal, but need to be considered more thoroughly. Experimentally the small branches were shown to have an appreciable effect on the flow which will be important to model, especially in modeling ember transport. The trunk was shown to have less of an influence, but should still be considered for the representation of sections of the WUI or a canopy in which small vegetation has already burned. Modeling of small branches can take the same basic form as used for the needles (but perhaps with different geometrical considerations), while the trunk can easily be modeled as a solid obstruction in CFD models (though for large scale canopy flow one trunk may not be resolvable in the mesh, and they will have to be represented as a sparse array of large particles). Therefore, the issues here were related to the manner in which these elements were input into the model, and not with the fundamental representation of drag.

At the scale of a canopy, the dependency on inputs was related to the velocity and the drag coefficient. Poor matches to experimental data of turbulence above the canopy were a product of these two driving quantities. As the drag coefficient used in these simulations was not based on any specific correlation, but rather was selected from a range of suggested values, the simulation results will be dependent on the choice that is made for the factor. Given an appropriate choice, it was shown that LES models (even with different turbulence sub-models) were capable of generating flow characteristics which were an accurate representation of real canopy flow.

Specific issues related to (W)FDS were also uncovered. Most significant were the troubles related to representing far-field wake flow. In Chapter 2 it was demonstrated that the model has some trouble with forming a good boundary layer flow far behind a single tree. It is still unclear whether this is due to issues associated with the wall model or whether it has to do with the inherently turbulent nature of LES flow (which may be over-predicted in this region). The cause must be determined in future work as the flow close to the ground behind a tree demands a higher level of accuracy. One of the most important phenomena in a wildland fire scenario, and one which is of particular interest to model accurately, is the transition from a ground fire to a crown fire [48]. This occurrence represents a critical condition for which the behavior of the fire drastically changes in way that makes it much more difficult to contain or manage. Therefore, the flow conditions at ground level must be reasonable in order to model the behavior of such a fire and its possible transition to crowning.

The need for future work is quite clear. This need can be divided into two components. The first is to make improvements to the significant gaps in the simulation of cold-flow scenarios through vegetation. This is likewise comprised of two needs. First is the small-scale modeling of individual trees. Improvements here are primarily motivated by the possibility of generating an empirical improvement to the drag force correlation. By specifying a scaling factor which is dependent on branch location and local velocity, it may be possible to represent the observed streamlining effects. Capturing the dynamic flow effects at this scale is very important if CFD models are to be used for any small scale WUI applications. The second component is continued large scale experimentation to confirm canopy flow scenarios. If (W)FDS is shown to perform well in a similar type of configuration as the one discussed in Chapter 3, then confidence in the model at this scale will be greatly improved. Once this work has been accomplished, the next step will be fire flows. With the influence of the solid phase on the flow being modeled with more confidence, then the influence of thermal flow driving forces can be studied in a manner that will allow a decoupling of the two respective influences on the flow.

These driving motivations for future work have one common factor, and that is the need for more experimentation at both scales. This is perhaps most significant conclusion from the combined body of work represented here. When considering the individual tree scale, only a handful of experiments have been conducted on flow through vegetation. The results tend to

report only basic mean flow characteristics, and most significantly, fall short when it comes to characterizing the geometry and density of the vegetation being studied so that meaningful comparisons can be made [36]. At the canopy scale, there have also been a few experimental studies, but once again the only very basic characteristics of the flow are reported on [45]. For both the tree and the canopy scale, a number of scaled-down wind tunnel tests have been conducted. However, in the references found for this study there was a certain disregard for proper scaling techniques. For one, studies were conducted where the characteristic length scale of the tree, and correspondingly the canopy, have been scaled, but the length scale of the branches and needle or leaf elements is not adjusted in an equivalent manner [47]. When considering a vegetative obstruction as an array of particles, as is done in (W)FDS, both the scale of the array matters for large scale wake formulation, as well as the scale of the particles as this will drive the local drag coefficient. Another questionable approach taken with modeling a canopy or tree is that the velocities were not scaled appropriately. In order to conserve a characteristic parameter, such as the Reynolds number, when measuring flow around a scaled down object, the velocity must be increased correspondingly (or the fluid properties changed). However, several scale experiments conducted for flow through vegetation used velocities in the range of 1-2 m·s^{-1}. These numbers are an appropriate order of magnitude for full-scale flow (though on the low side), and therefore cannot be considered reasonable in a scaled situation. This is especially true when considering the fact that scaling down a real tree in a velocity of 2 m·s^{-1}, for example, a reduction in size 1/10th will require an increase in velocity by a factor of 10 (20 m·s^{-1} in the wind tunnel). There is significant need, and a good opportunity to be found, for conducting carefully designed scale experimentation. This is especially true because the controlled, characterized conditions in a wind tunnel are desirable, but not usually accessible at the size of a full-scale tree.

The potential of CFD-based detailed models to simulate flow through and around vegetation is clearly presented, and the results at a first approximation are positive. At the same time, the shortcomings and opportunities for improvement are evident as well. This work has demonstrated not only the need, but the possibility for improving the representation of such flows. If detailed physical models are to be used to simulate representative fire scenarios, this flow behavior must be modeled with confidence. Therefore, it is important that this work

continue. However, it will also be important to determine the point at which the benefits obtained from improving this part of the model are outweighed by the work necessary to implement them.

References

[1] Gillett, N.P., Weaver, A.J. (2004) "Detecting the effect of climate change on Canadian forest fires." *Geophysical Research Letters*. 31.

[2] Hammer, R.B., Radeloff, V.C., Fried, J.S., Stewart, S.I. (2007) "Wildland-urban interface housing growth during the 1990s in California, Oregon, and Washington." *International Journal of Wildland Fire*. 16, pp. 255-265.

[3] Radeloff, V.C., Hammer, R.B., Stewart, S.I., Fried, J.S., Holcomb, S.S., McKeefry, J.F. (2005) "The wildland-urban interface in the United States." *Ecological Applications*. 15, pp. 799-805.

[4] Brown, T.J., Hall, B.L., Westerling, A.L. (2004) "The impact of twenty-first century climate change on wildland fire danger in the western United States: an applications perspective." *Climatic Change*. 62, pp. 365-388.

[5] Westerling, A.L., Bryant, B.P. (2008) "Climate change and wildfire in California." *Climatic Change*. 87, pp. S231-S249.

[6] Mell, W.E., Manzello, S.L., Maranghides, A., Butry, D., Rehm, R. (2010) "The wildland-urban interface fire problem - current approaches and research needs." *Ineternational Journal of Wildland Fire*. 19, pp. 238-251.

[7] GAO, , "Wildland fire management: lack of clear goals or strategy hinders federal agencies' effort to contain the costs of fighting fires. Report to Congressional Requesters," US Government Accountability Office, GAO-07-665, June 2007.

[8] Morvan, D. (2011) "Physical phenomena and length scales governing the behaviour of wildfires: a case for physical modelling." *Fire Technology*. 47, pp. 437-460.

[9] Weber, R.O. (1991) "Modelling fire spread through fuel beds." *Prog Energy and Combustion Science*. 17, pp. 67-82.

[10] Pastor, E., Zarate, L., Planas, E., Arnaldos, J. (2003) "Mathematical models and calculation systems for the study of wildland fire behaviour." *Prog. in Energy and Comb. Sco.* 29, pp. 139-153.

[11] Finney, M.A. , "FARSITE: Fire area simulator: Model development and evaluation," USDA, Forest Service, Rocky Mountain Research Station, Ogden, UT, Research Paper RMRS-RP-4, 1998.

[12] Andrews, P. L., Chase, C. H. , "BEHAVE: Fire behavior prediction and fuel modeling system-BURN subsystem, Part 2," USDA, Forest Service, General Technical Report INT-260, 1989.

[13] Rothermel, R. (1972) "A mathematical model for predicting fire spread in wildland fuels." *Technical Report, USDA Forest Service Research*.

[14] Morvan, D., Porterie, B., Larini, M., Loraud, J.C. (1998) "Numerical simulation of turbulent diffusion flame in crossflow." *Combust. Sci. and Tech.* 140, pp. 93-122.

[15] Mell, W., Jenkins, M.A., Gould, J., Cheney, P. (2007) "A physics-based approach to modelling grassland fires."

International Journal of Wildland Fire. 16, pp. 1-22.

[16] McKenzie, D., O'Neil, S.M., Larkin, N.K., Norheim, R.A. (2006) "Integrating models to perdict regional haze from wildland fire." *Ecological Modelling*. 199, pp. 278-288.

[17] Potter, B.E., Charney J.J., Heilman, W.E., Bian, X. , "Advances in fire convection dynamics," in *Advancing the fundamental sciences: proceedings of the Forest Service national earth sciences conference, PNW-GTR-689*, San Diego, CA, 2007.

[18] Sigler, J.M., Lee, X., Munger, W. (2003) "Emission and long-range transport of gaseous mercury from a large scale canadian boreal forest fire." *Environmental Science and Technology*. 37, pp. 4343-4347.

[19] McGratten K., McDermott, R., Hostikka, S., Floyd, J. , "Fire Dynamics Simulator (Version 5) User Guide," National Institute of Standards and Technology, 2010. [Online]. http://fds-smv.googlecode.com/svn/trunk/FDS/trunk/Manuals/All_PDF_Files/FDS_User_Guide.pdf

[20] Chung, T.J. , *Computational Fluid Dynamics*. Cambridge: Cabridge University Press, 2002.

[21] Leveque, E., Toschi, F., Shao, L., J.P. Bertoglio (2007) "Shear-improved Smagorinsky model for large-eddy simulation of wall-bounded turbulent flows." *J. Fluid Mech.* 570, pp. 491-502.

[22] McGratten, K., et al. , "Fire Dynamics Simulator (Version 5) - Technical Reference Guide," National Institute of Standards and Technology, 2010.

[23] Mell W., Maranghides, A., McDermott, R., Manzello, Samuel L. (2009) "Numerical simulation and experiments of burning douglas fir trees." *Combustion and Flame*. 156, pp. 2023-2041.

[24] Grishin, A.M. , "Mathematical modeling of forest fires and new methods of fighting them," Publishing House of the Tomsk State University, Tomsk, Russia, 1997.

[25] Incropera, F.P., DeWitt, D.P., *Fundamentals of heat and mass transfer, 6th ed.* Hoboken, NJ: Wiley, 2007.

[26] Larini, M., Giroud, F., Porterie, B., Loraud, J.C. (1998) "A multiphase formulation for fire propagation in heterogeneous combustible media." *International Journal of Heat and Mass Transfer*. 41, pp. pp. 881-897.

[27] Morvan, D. (2001) "Modeling of fire spread through a forest fuel bed using a multiphase formulation." *Combustion and Flame*. 127, pp. 1981-1994.

[28] Morvan, D., Dupuy, J.L. (2004) "Modeling the propagation of a wildfire through a mediterranean shrub using a multiphase formulation." *Combustion and Flame*. 138, pp. 199-210.

[29] Porterie, B., Morvan, D., Larini, M., Loraud, J.C. (1998) "Wildfire propagation: a two-dimensional multiphase approach." *Combust. Explo. Shock Waves*. 34, pp. 139-150.

[30] Raupach, M.R., Coppin, P.A., Legg, B.J. (1986) "Experiments on scalar dispersion within a model plant canopy - Part 1: The turbulence structure." *Boundary-Layer Meteorology*. 35, pp. 21-52.

[31] Raupach, M.R., Thom, A.S. (1981) "Turbulence in and above plant canopies." *Annual Review of Fluid Mechanics*. 13, pp. 97-129.

[32] Pimont, F., Dupuy, J.L., Linn, R., Dupont, S. (2009) "Validation of FIRETEC wind-flows over a canopy and fuel-break." *International Journal of Wildland Fire*. 18, pp. 775-790.

[33] Shaw, R.H., Schumann, U. (1992) "Large-eddy simulation of turbulent flow above and within a forest." *Boundary-Layer Meteorology*. 61, pp. 47-64.

[34] Dupont, S., Brunet, Y. (2008) "Edge flow and canopy structure: A large-eddy simulation study." *Boundary-Layer Meteorology*. 126, pp. 51-71.

[35] Gross, G. (1987) "A numerical study of the air flow within and around a single tree." *Boundary-Layer Meteorology*. 40, pp. 311-327.

[36] Ruck, B., Schmitt, F. (1986) "Das stroemungsfeld der einzelbaumumstroemung." *Forstw. Cbl.* 105, pp. 178-196.

[37] Rudnicki, M., Mitchell, S.J., Novak, M.D. (2004) "Wind tunnel measurements of crown streamlining and drag relationships for three conifer species." *Canadian Journal of Forest Research*. 24 , pp. 666-676.

[38] Cullen, Scott (2005) "Trees and wind: A practical consideration of the drag equation velocity exponent for urban tree risk management." *Journal of Arborculture*. 31, pp. 101-113.

[39] Mayhead, G.J. (1973) "Some drag coefficients for british forest trees derived from wind tunnel studies." *Agricultural Meteorology*. 12, pp. 123-130.

[40] Poggi, D., Katul, G., Albertson, J. (2006) "Scalar dispersion within a model canopy: Measurements and three-dimensional lagrangian models." *Advances in Water Resources*. 29, pp. 326-335.

[41] Dupont, S., Brunet, Y., Jarosz, N. (2006) "Eulerian modelling of pollen dispersal over heterogeneous vegetation canopies." *Agricultural and Forest Meteorology*. 141, pp. 82-104.

[42] Belcher, S.E., Jerram, N., Hunt, J.C.R. (2003) "Adjustment of a turbulent boundary layer to a canopy of roughess elements." *Journal of Fluid Mechanics*. 488, pp. 369-398.

[43] Su, H.B., Shaw, R.H., Paw U, K.T., Moeng, C.H., Sullivan, P.P. (1998) "Turbulent statistics of neutrally stratified flow within and above a sparse forest from large-eddy simulation and field observations." *Boundary-Layer Meteorology*. 88, pp. 363-397.

[44] Linn, R.R., Harlow, F.H. (1998) "FIRETEC: a transport description for wildfire behavior," in *AMS Second Symposium of Fire and Forest Meteorology*.

[45] Shaw, R.H., Den Hartog, G., Neumann, H.H. (1988) "Influence of foliar density and thermal stability on profiles of Reynolds stress and turbulence intesisty in a deciduous forest." *Boundary-Layer Meteorology*. 45, pp. 391-409.

[46] Raupach, M.R., Bradley, E.F., Ghadiri, H. , "A wind tunnel investigation into aerodynamic effect of forest clearing on the neseting of Abbott's Booby on Christmas Island," CSIRO Marine and Atmospheric Research, Centre for Environmental Mechanics, Canberra, Australia, Technical Report T12, 1987.

[47] Hsi, G., Nath, J.H. (1970) "Wind drag within simulated forest canopies." *Journal of Applied Meteorology*. 9, pp. 592-602.

[48] Cruz, M.G., Butler, B.W., Alexander, M.E., Forthofer, J.M., Wakimoto, R.H. (2006) "Predicting the ignition of crown fuels above a spreading fire: Part I: Model idealization." *International Journal of Wildland Fires*. 15, pp. 47-50.

[49] Sagaut, P. , *Large Eddy Simulation for Incompressible Flows*.: Springer, 2001.

[50] Pope, S.B. , *Turbulent Flows*.: Cambridge, 2000.

Appendix A

Details of the Built-In (W)FDS Boundary Conditions [19,22]

The 'OPEN' Condition

For outflow, the condition is set by taking a user specified external dynamic pressure ($\tilde{P}_{ext}$), which is set to zero by default. The pressure head at the boundary is then given as

$$\mathcal{H} = \frac{\tilde{P}_{ext}}{\rho_\infty} + \frac{|\boldsymbol{u}|^2}{2}$$

For inflow, the condition is set by taking considering a fluid element on a streamline from point 1 outside the domain to point 2 on the inflow boundary

$$\tilde{P}_1 + \frac{1}{2}\rho_1|\boldsymbol{u_1}|^2 = \tilde{P}_2 + \frac{1}{2}\rho_2|\boldsymbol{u_2}|^2$$

And taking $\tilde{P}_{ext}$ as specified and $|\boldsymbol{u_1}|^2$ to be the initial velocity (as defined by the user)

$$\mathcal{H}_2 = \frac{\tilde{P}_{ext}}{\rho_2} + \frac{1}{2}|\boldsymbol{u_1}|^2 \frac{\rho_1}{\rho_2}$$

Wall Model

Due to the inability of the model to resolve the gradient of the streamwise velocity normal to the wall, there is difficulty in solving for the viscous stress in this region ($\bar{\tau}_{xy}\big|_{z=0} = \bar{\tau}_{wall}$). Using the following scaling definitions

$$u^* \equiv \sqrt{\bar{\tau}_{wall}/\rho}$$

$$u^+ \equiv u/u^*$$

$$z^+ \equiv z/l$$

$$l = \mu/(\rho u^*)$$

The Werner Wengle model [49] (the default solid wall condition in (W)FDS) is then written

$$u^+ = z^+ \quad for \quad z^+ \leq 11.81$$

$$u^+ = A(z^+)^B \quad for \quad z^+ > 11.81$$

Where $A = 8.3$ and $A = 1/7$

In (W)FDS, the first off-wall velocity is being solved for. Since this is defined at the cell face

$$z = \frac{\delta z}{2}$$
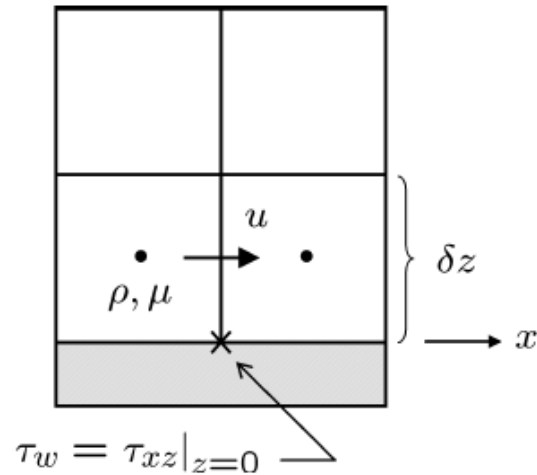
Figure A.1. – The application of the (W)FDS wall model [22]

If the wall is prescribed with a 'ROUGHNESS', then the Pope log law [50] is used

$$u^+ = \frac{1}{\kappa} \ln \left(\frac{z}{z_0} \right) + \tilde{B}$$

Where $\kappa = 0.41, \tilde{B} = 7.44$, and z_0 is user defined (in meters).

In the case of a 'NO_SLIP' surface, the tangential velocity component is forced to 0, (this is the default for DNS, as the boundary layer can be resolved). In the case of a 'FREE_SLIP' surface, the tangential velocity is not influenced by the wall.

Appendix B

Drag Force Sensitivity

A sensitivity analysis of the effect of changing the $c_d b$ factor on the flow shape around the tree was conducted. Because the u-velocity represents the dominant direction of the flow, a study of just this component was indicative of the sensitivity in general.
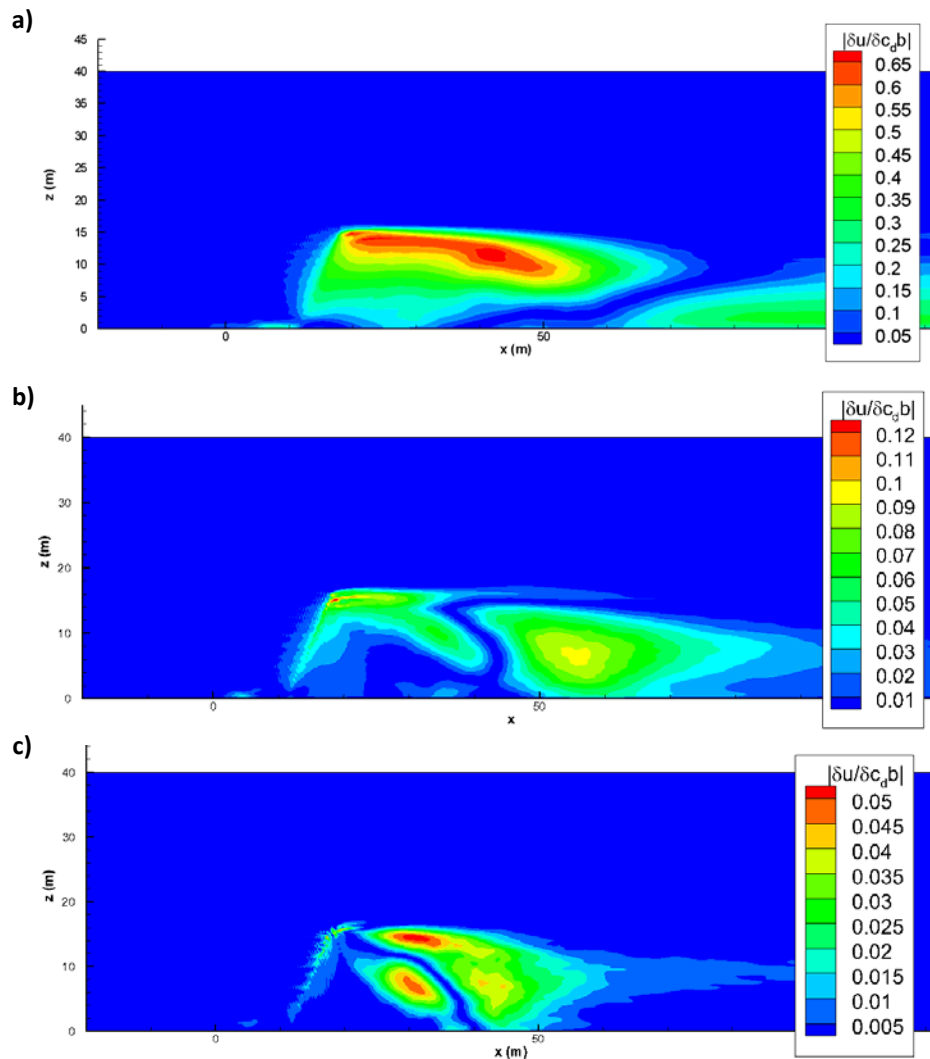

Figure B.1. – Sensitivity of streamwise velocity for a $\Delta c_d b$ of **a)** 0.1 to 1.0, **b)** 1.0 to 5.0, **c)** 5.0 to 10.0

It was found that velocities were more sensitive to changes in the $c_d b$ factor for the lower range of chosen values (0.1 to 1.0). The decreased sensitivity at higher factors indicates that the tree is tending towards a solid obstruction.

Appendix C

Additional Results from the BRI/NIST Study
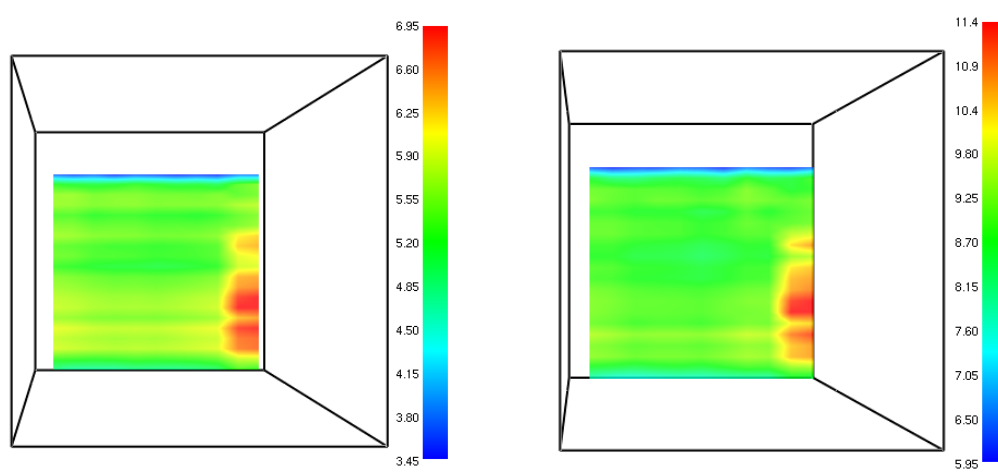
Figure C.1. – Area of faster velocity observed along the y=2.0m wall in the no tree tunnel experiment. Slices shown are located at x = 1.1m for (Left) 6 m·s^{-1} and (Right) 9 m·s^{-1} prescribed velocity

NIST/BRI Experimental Uncertainties

Uncertainties associated with the experimental measurements provided by the NIST/BRI study were assessed. As it was determined that the hotwire anemometers had an intrinsic error of ±0.0035m·s^{-1}, the propagation of errors formula was applied to obtain the error present in the averaged normalized velocities.

In general

$$\sigma_f{}^2 = \Sigma \left(\frac{\partial f}{\partial x_i} \sigma_{x_i}\right)^2$$

With

$$f = \bar{u}_{norm} = \frac{1}{n}\Sigma \frac{u_i}{\bar{u}_{no-tree}}$$

and

$$\sigma_{u_i} = \sigma_{\bar{u}_{no-tree}} = 0.0035 \text{ m} \cdot \text{s}^{-1}$$

$$\sigma_{\bar{u}_{norm}} = \sqrt{\left(\frac{\sigma_{u_i}}{\bar{u}_{no-tree}}\right)^2 + \left(\frac{\overline{u_i}\sigma_{u_i}}{-\bar{u}_{no-tree}^2}\right)^2} \quad \text{(Eq. B.1)}$$

This formula can then be applied to the experimental data. The resultant error in the normalized profiles was relatively small. The highest errors were found to be in the range of $\sigma_{\bar{u}_{norm}} = 0.006$
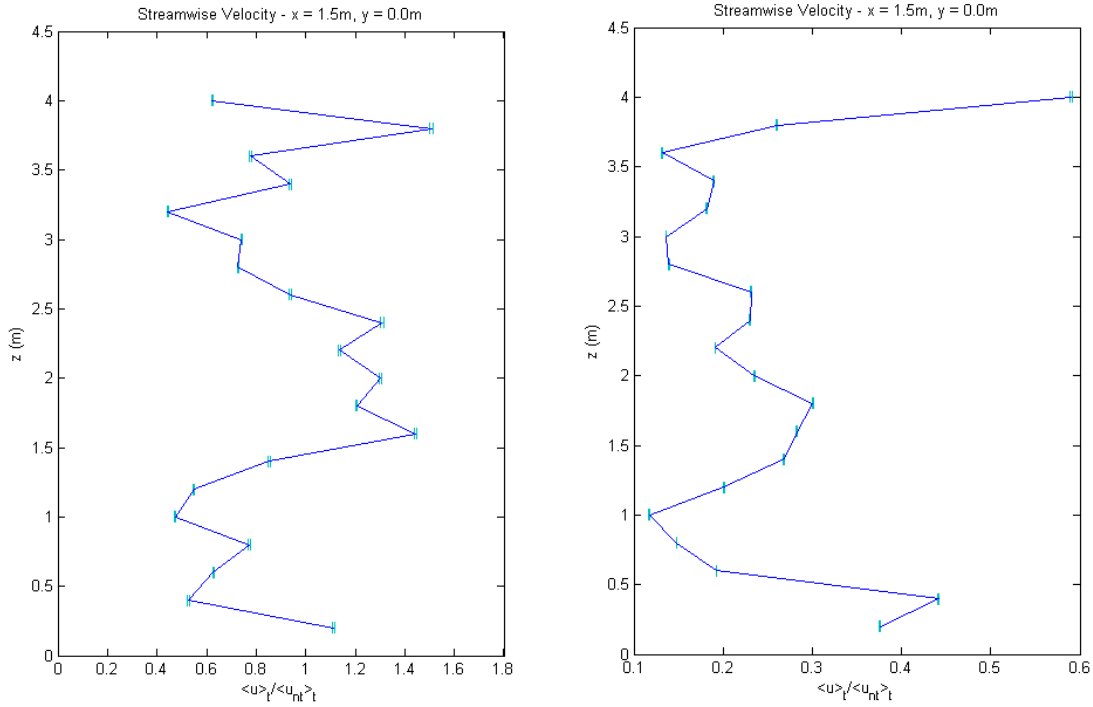

Figure C.2. – Error-bars displayed on example velocity profiles. (Left) 1 m·s-1 and (Right) 9 m·s-1 prescribed tunnel velocity

However, the actual errors involved in these estimates will include other factors. For one, the anemometers were 1D, but this does not mean that some of non-streamwise flow would not be measured. No information was provided about the calibration of the anemometers. However, the normalization approach also helps to avoid the influence of a base-state bias in the measurements. Additionally, because steady, well-behaved profiles were measured behind the tree when the data at different locations was not obtained within the same 60s interval (there was only one tower which was relocated throughout the grid), it is reasonable to suggest that drift in the measurements was minimal. Another source or error may have been deviations in between cases in the upstream tunnel flow for a particular velocity setting. The normalization technique

assumed that if the tree were removed from any experiment in Case2, 3, or 4 the velocities would be identical to those measured in Case1. In reality, owing to the fact that each experiment was performed separately with the wind tunnel being shut down between cases, this assumption will not be perfectly true. However, measured trends (such as normalized velocities slightly greater than 1 around the tree due to momentum conservation) indicated that deviations in tunnel velocities from the prescribed values did not produce large errors.

Appendix D

Issues with the Simulation of Periodic Boundary Conditions

In order to test how (W)FDS behaves with 'PERIODIC' lateral boundary conditions, 'NO_SLIP' upper and lower boundary conditions, and an initial velocity field, a case with one mesh was first simulated. The initial velocity was prescribed as 2m·s^{-1} in the x-direction. It was found that a stable condition was reached with the velocity maintained at the initially prescribe value (the small fluctuations are due to the noise that (W)FDS automatically adds to the initial velocity field).

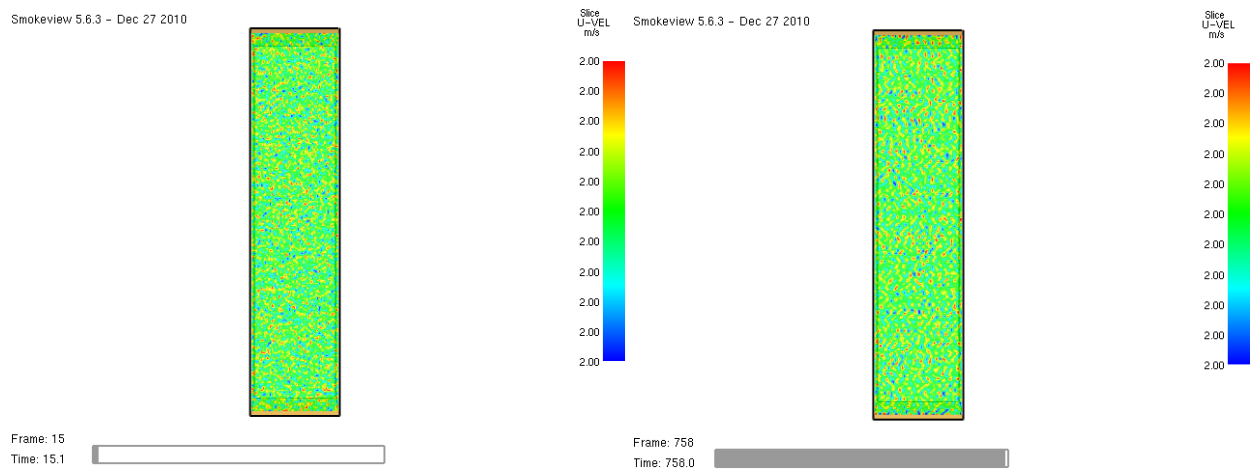Figure D.1. – Stable initialized velocity field in one mesh with periodic lateral BCs

An identical input file was then used, but utilizing two meshes instead of one. In this case, error was seen to develop at the interface between the two meshes. The periodic boundary conditions amplified this effect, and the final quasi-steady state obtained did not resemble the initially specified conditions at all.
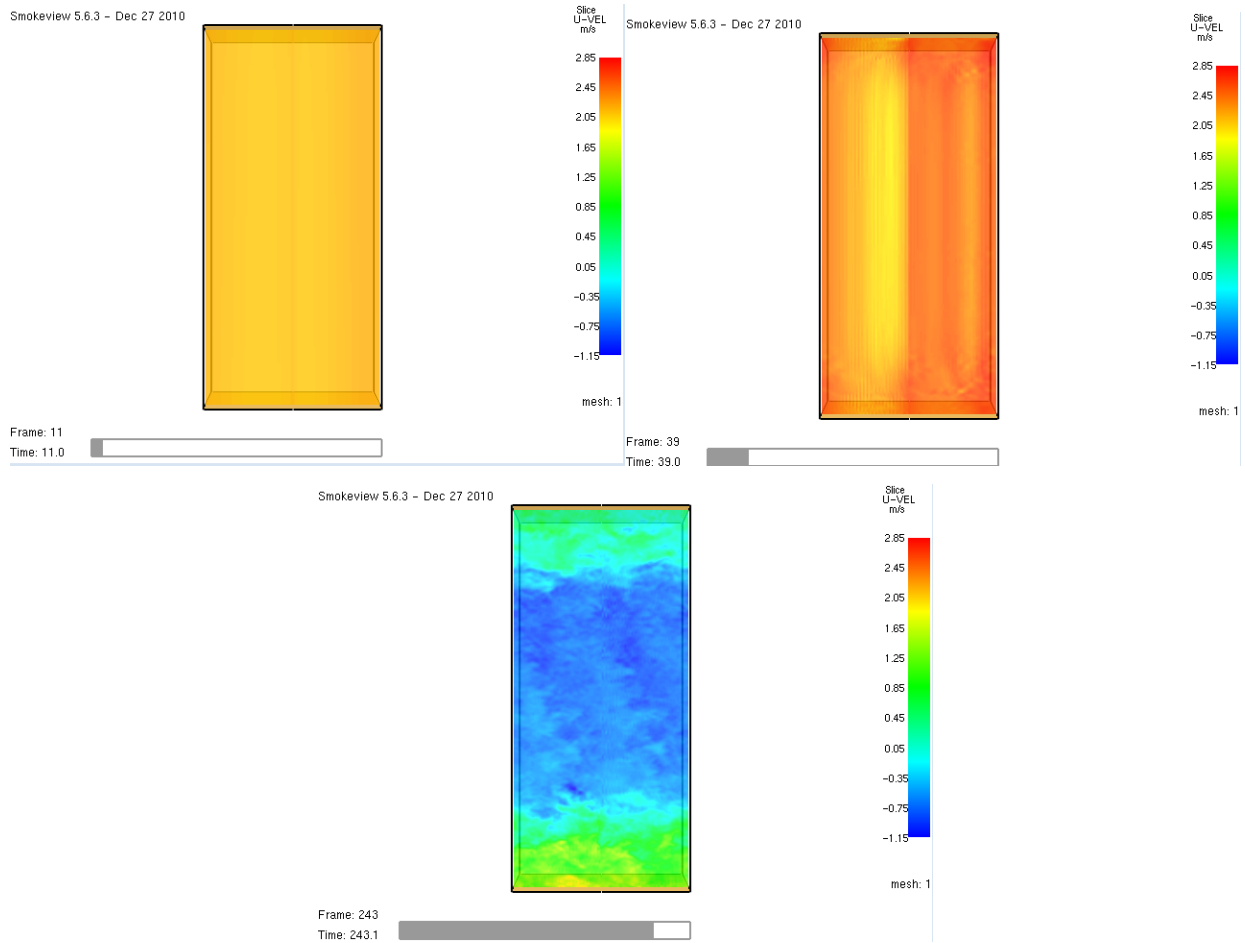
Figure D.2. – Turbulent development from initialized velocity field in two meshes with periodic lateral BCs

This scenario involved prescribing the 'VELOCITY_TOLERANCE' to $0.001 \text{m} \cdot \text{s}^{-1}$, which forces multiple iterations of the pressure solver in order to limit velocity error at mesh interfaces to this value [19]. In this example, only two pressure iterations were required to match the condition. However, decreasing the 'VELOCITY_TOLERANCE' to $0.00001 \text{m} \cdot \text{s}^{-1}$ did not alleviate the problem, and it is unclear what lower limit of velocity error (if any) would not generate this behavior. Additionally, setting a low 'VELOCITY_TOLERANCE' in a more complicated simulation will have computational costs (as the number of pressure iterations required to match the error limit increases).

Figure D.3. – The development of turbulent conditions with a 'VELOCITY_TOLERANCE' of 0.00001m·s^{-1}
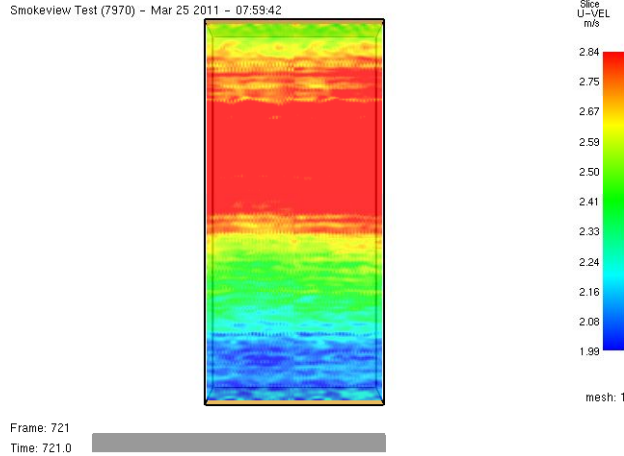
(W)FDS vs. FIRETEC Approach

Due to the unresolved complications of modeling canopy flow with periodic boundary conditions and multiple meshes in (W)FDS, the final approach used differed from the FIRETEC paper in several distinct ways [32].

Parameter	FIRETEC	(W)FDS
Domain size	200m x 150m x 615m	1050m x 150m x 216m
Grid spacing	2m x 2m horiziontal 1.5m-40m vertical stretching	2m x 2.08m x 0.9m
Lateral boundary conditions	Periodic in x Rayleigh damped in y	Periodic in y Inflow profile at x = -50m Open outflow at x = 1000m
Upper boundary condition	Rayleigh damping layer	Free-slip
Lower boundary condition	-not specified in the paper-	Werner Wengle
Initial wind profile	$u(z) = u_{2h} \frac{\log z}{\log 2h}$ throughout domain	$u(z) = u_{2h} \frac{\log z}{\log 2h}$ at inflow
Vegetation profile	Continuous in x and y, specified experimental height variation profile (a_f)	No vegetation from x = - 50m to x = 0m, specified experimental height variation profile (a_f)
Simulation time	6500s	6000s

Table D.1. – Comparison of (W)FDS and FIRETEC input parameters
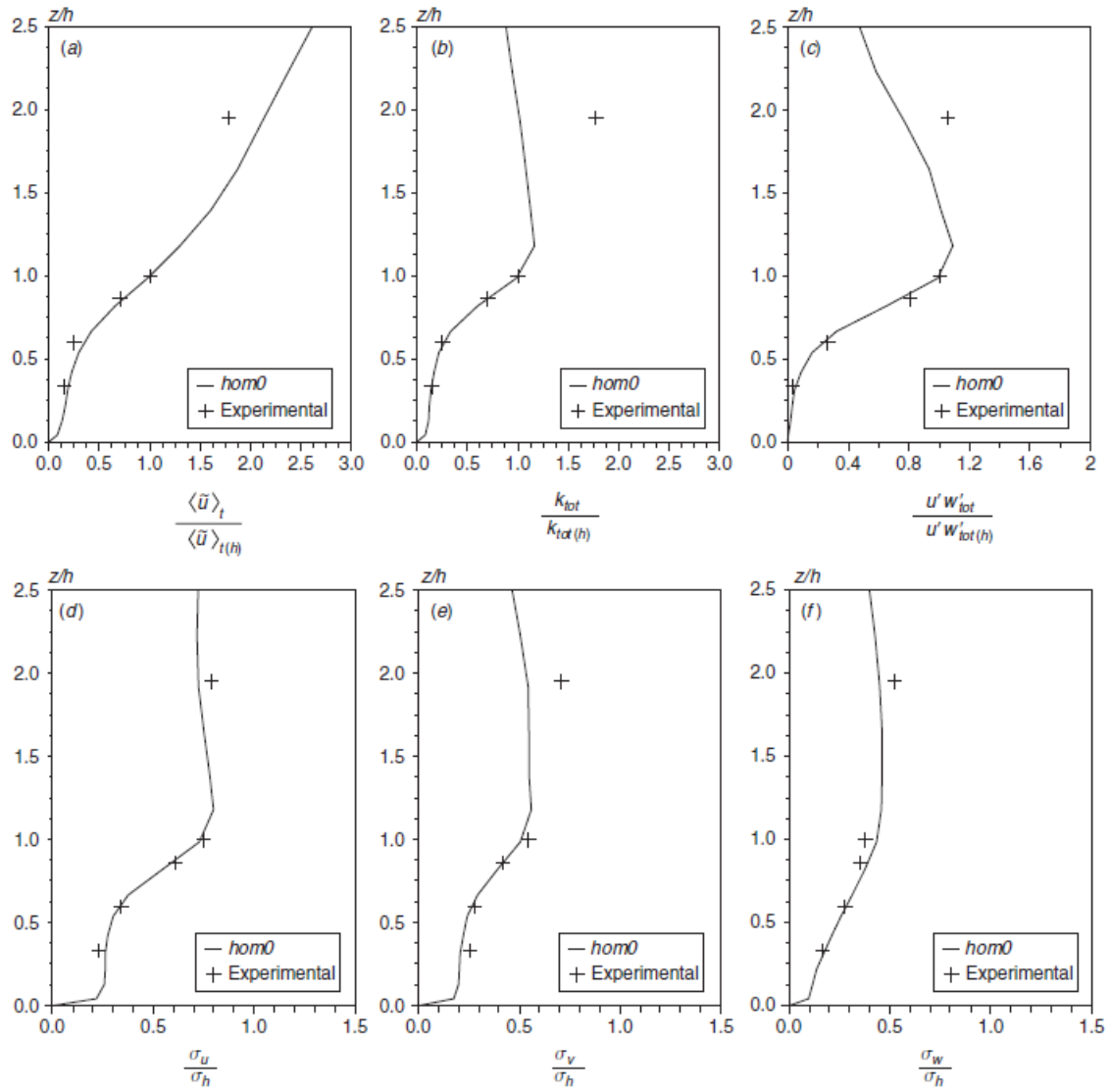
FIRETEC Simulation Results

Figure D.4. – Profiles reported from using FIRETEC to simulate flow through a forest canopy [32]

Appendix E

Grid Choice – Section 2.1

In the case of the single tree RANS and experimental comparison, the grid size was chosen by two factors. The first was that the RANS study employed a uniform grid spacing of 1m in all directions. Therefore, for comparison's sake, the same spacing was initially considered. However, it became quickly apparent that due to the nature of LES as compared with RANS, in order to more accurately capture the small scale turbulent characteristics, a finer grid would be required.

As such, a uniform spacing of 0.5 m x 0.66 m x 0.5 m was chosen. As the profiles along the centerline were primarily being studied, the slightly lower y-direction resolution was acceptable. A simulation was also conducted for a 0.25 m x 0.33 m x 0.25 m grid spacing in order to compare the sensitivity of the results.
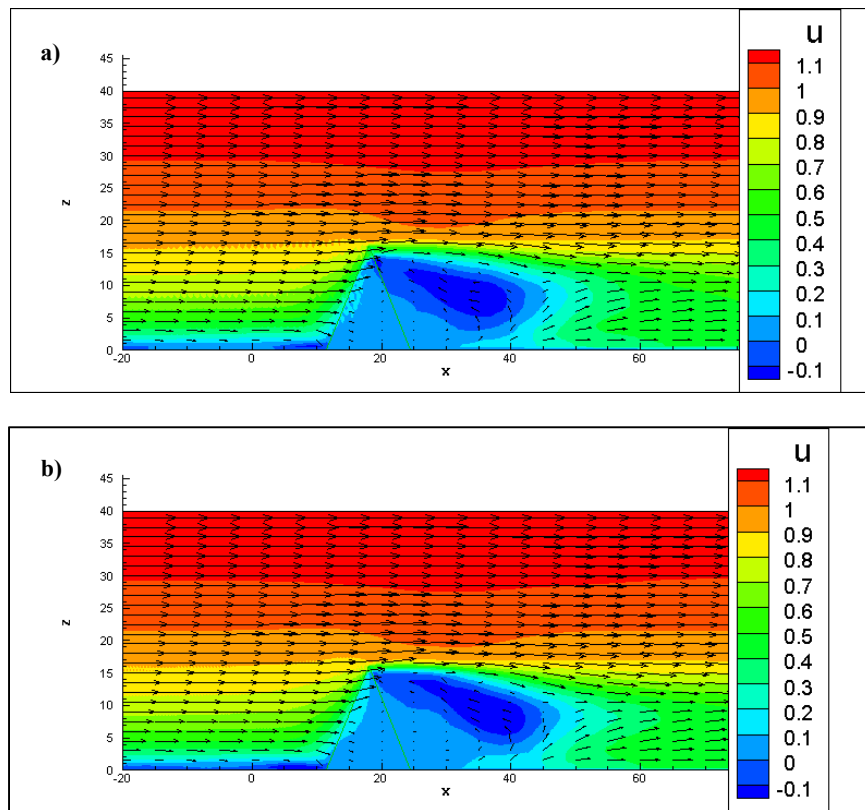

Figure E.1. – Eddy structure for **a)** 0.5 m x 0.66 m x 0.5 m grid spacing and **b)** 0.25 m x 0.33 m x 0.25 m grid spacing. Contours represent the u-velocity

As only a small change was observed in the location of the eddy, specifically as the velocity gradients became more highly resolved, the 0.25 m spacing was considered to be a reasonable

82

choice for the grid spacing. This choice was also acceptable in that the study was primarily quantitative.

Grid Choice – Section 2.2

In the case of the full canopy study, the choice of a uniform 0.1 m x 0.1 m x 0.1 m spacing was initially considered. This yielded a resolution of 40 cells along the height of the tree, which was deemed to be acceptable as only the overall shapes of the velocity profiles behind the tree were being studied. However, in order to really capture the local changes of the velocity due to the drag force as it developed within the tree, the resolution in the x-direction was increased to 0.05 m. This resolved the depth of the tree into ~64 cells at its widest point. The choice of increasing the number of these cells was supported by the fact that streamwise velocities were the only components being considered, due to the 1-dimensional nature of the measurements.
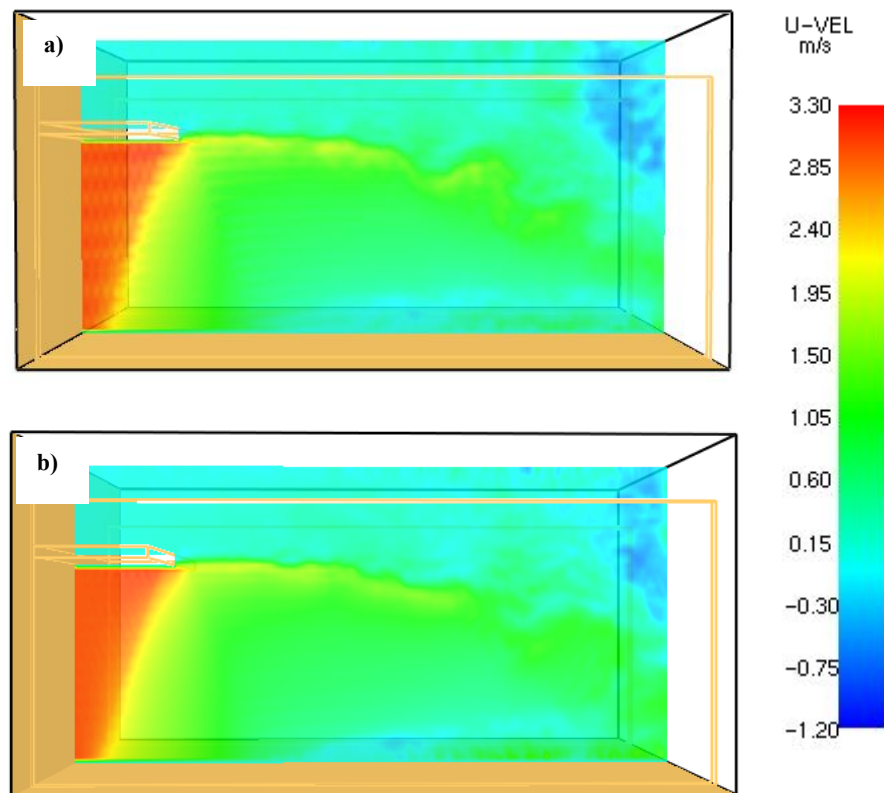

Figure E.2. – Example streamwise slices for **a)** 0.1 m uniform grid spacing and **b)** 0.05 m x 0.1 m x 0.1 m grid spacing

The slices in Fig. E.2 show that the shape of the flow behind the tree was essentially unchanged for the increase in resolution, and so an acceptable level of grid insensitivity was assumed. The choice for spacing was further confirmed in that the number of cells used to resolve the tree was comparable to the number used in the previous single tree study (where reasonable grid insensitive results were again assumed).

Grid Choice – Section 3.1

In the case of the full canopy study, the choice of grid spacing was guided by the FIRETEC simulation, with which comparisons were being made. The spacing in the horizontal direction was kept consistent with the 2 m used in the FIRETEC simulation, and the vertical spacing was decreased slightly. This was done in order to ensure that the vertical profiles within the canopy (the structure which was being studied) was well resolved. The 0.9m spacing used in (W)FDS allowed the canopy to height to be resolved over 20 cells as opposed to 12 in FIRETEC. As the results were consistent with the experiments and with FIRETEC, this spacing was deemed to be acceptable. However, in future studies, it may be of interest to reduce the resolution and study the effect on the canopy profiles. This information may be of use when it comes to understanding the lower limit of resolution, with respect to canopy height, necessary to obtain such profiles.

Appendix F

Typical Input File for the RANS/Experiment Comparison (Section 2.1)

```
&HEAD CHID='Gross5r', TITLE='Attempted comparison to the numerical simulations of wind
in/around a single tree by G.Gross 1987. CdB=5.0/
&TIME T_END = 2500.0/
&TIME T_END = 2500.0/
&MISC BAROCLINIC=.TRUE., TMPA=22.0, WIND_ONLY=.TRUE.,
TURBULENCE_MODEL='DYNAMIC SMAGORINSKY'/

&RADI RADIATION=.FALSE./


&MESH IJK=180,60,80, XB=-20,25,-30,-10,0.0,20/
&MESH IJK=180,60,80, XB=25,70,-30,-10,0.0,20/
&MESH IJK=180,60,80, XB=70,115,-30,-10,0.0,20/
&MESH IJK=180,60,80, XB=115,160,-30,-10,0.0,20/

&MESH IJK=180,60,80, XB=-20,25,-30,-10,20,40/
&MESH IJK=180,60,80, XB=25,70,-30,-10,20,40/
&MESH IJK=180,60,80, XB=70,115,-30,-10,20,40/
&MESH IJK=180,60,80, XB=115,160,-30,-10,20,40/

&MESH IJK=180,60,80, XB=-20,25,-10,10,0.0,20/
&MESH IJK=180,60,80, XB=25,70,-10,10,0.0,20/
&MESH IJK=180,60,80, XB=70,115,-10,10,0.0,20/
&MESH IJK=180,60,80, XB=115,160,-10,10,0.0,20/

&MESH IJK=180,60,80, XB=-20,25,-10,10,20,40/
&MESH IJK=180,60,80, XB=25,70,-10,10,20,40/
&MESH IJK=180,60,80, XB=70,115,-10,10,20,40/
&MESH IJK=180,60,80, XB=115,160,-10,10,20,40/

&MESH IJK=180,60,80, XB=-20,25,10,30,0.0,20/
&MESH IJK=180,60,80, XB=25,70,10,30,0.0,20/
&MESH IJK=180,60,80, XB=70,115,10,30,0.0,20/
&MESH IJK=180,60,80, XB=115,160,10,30,0.0,20/

&MESH IJK=180,60,80, XB=-20,25,10,30,20,40/
&MESH IJK=180,60,80, XB=25,70,10,30,20,40/
&MESH IJK=180,60,80, XB=70,115,10,30,20,40/
&MESH IJK=180,60,80, XB=115,160,10,30,20,40/


&PART ID='veg1', TREE=.TRUE., VEG_BULK_DENSITY=1.0, VEG_MOISTURE=0.02,
VEG_DENSITY=500. ,VEG_SV=5000.0,
        VEG_DRAG_COEFFICIENT=1, USER_DRAG_COEFFICIENT=0.5/

&TREE PART_ID='veg1', FUEL_GEOM='CONE', CROWN_BASE_HEIGHT=0.0,
      CROWN_WIDTH=13, TREE_HEIGHT=16, XYZ=18,0.0,0.0/

&SURF ID='INFLOW1', VEL=-0/
&SURF ID='INFLOW2', VEL=-0/
&SURF ID='INFLOW3', VEL=-0.132/
&SURF ID='INFLOW4', VEL=-0.225/
…CONTD…
&SURF ID='INFLOW80', VEL=-1.200/
```

```
&SURF ID='FS', FREE_SLIP=.TRUE./

&VENT MB=XMAX, SURF_ID='OPEN'/
&VENT MB=ZMAX, SURF_ID='FS'/
&VENT MB=YMIN, SURF_ID='MIRROR'/

&VENT XB=-20,-20,-30,30,0.0,0.5, SURF_ID='INFLOW1'/
&VENT XB=-20,-20,-30,30,0.5,1, SURF_ID='INFLOW2'/
&VENT XB=-20,-20,-30,30,1,1.5, SURF_ID='INFLOW3'/
&VENT XB=-20,-20,-30,30,1.5,2, SURF_ID='INFLOW4'/
…CONTD…
&VENT XB=-20,-20,-30,30,39,39.5, SURF_ID='INFLOW79'/
&VENT XB=-20,-20,-30,30,39.5,40, SURF_ID='INFLOW80'/

&TAIL/
```

Typical Input File for the BRI Simulations (Section 2.2)

```
HEAD CHID='BRI_Case2_3', TITLE='Wind tunnel test with full tree and 6 m/s flow'/
&TIME T_END=100./

&MISC BAROCLINIC=.TRUE., TMPA=22.,WIND_ONLY=.TRUE.,TURBULENCE_MODEL='DYNAMIC
SMAGORINSKY',DRAG_TOT=.TRUE. /
&RADI RADIATION=.FALSE./

&MESH IJK=240,72,60, XB=-2.0,10.0,-1.1,6.1,0.0,6.0 /

-Inflow
&SURF ID='INFLOW',VEL=-3.0 /


-Fuel
&PART ID='needles', TREE=.TRUE., VEG_BULK_DENSITY=1.27,
      VEG_DENSITY=514. ,VEG_SV=5714.0, VEG_DRAG_COEFFICIENT=0.125, DRAG_LAW='SPHERE'/
&TREE PART_ID='needles', CROWN_BASE_HEIGHT=0.0, CROWN_WIDTH=3.22, FUEL_GEOM='CONE',
      TREE_HEIGHT=4.9, XYZ=0.0,2.5,0.0/

&PART ID='small stems', TREE=.TRUE., VEG_BULK_DENSITY=0.15,
      VEG_DENSITY=514. ,VEG_SV=1333, VEG_DRAG_COEFFICIENT=0.125, DRAG_LAW='SPHERE'/
&TREE PART_ID='small stems', CROWN_BASE_HEIGHT=0.0, CROWN_WIDTH=3.22, UEL_GEOM='CONE',
      TREE_HEIGHT=4.9, XYZ=0.0,2.5,0.0/

&PART ID='large stems', TREE=.TRUE., VEG_BULK_DENSITY=0.098,VEG_DENSITY=514.,
VEG_SV=667, VEG_DRAG_COEFFICIENT=0.125, DRAG_LAW='SPHERE'/
&TREE PART_ID='large stems', CROWN_BASE_HEIGHT=0.0, CROWN_WIDTH=3.22,
FUEL_GEOM='CONE', TREE_HEIGHT=4.9, XYZ=0.0,2.5,0.0/


-BC
&VENT MB=YMIN, SURF_ID='OPEN'/
&VENT MB=YMAX, SURF_ID='OPEN'/
&VENT MB=XMAX, SURF_ID='OPEN'/
&VENT MB=ZMAX, SURF_ID='OPEN'/
&VENT XB=-2.0,-2.0,0.0,5.0,0.0,4.0, SURF_ID='INFLOW'/

-Channel
&OBST XB=-2.0,10.0,-0.2,0.0,0.0,5.0 /
&OBST XB=-2.0,10.0,5.0,5.2,0.0,5.0 /
&OBST XB=-2.0,0.0,0.0,5.0,4.0,4.2 /
```

```
&TAIL/
```

Typical Input File for the FIRETEC Comparison (Section 3)

```
&HEAD CHID='hom0', TITLE='A test of the ability of FDS LES model to replicate the work
of Pimont - U_2h=2.75, C_d=0.25'/
&TIME T_END=6000.0/

&MISC BAROCLINIC=.TRUE., TMPA=22.0, WIND_ONLY=.TRUE.,TURBULENCE_MODEL='DYNAMIC
SMAGORINSKY'/

&RADI RADIATION=.FALSE./

&MESH ID='mesh1' IJK=25,36,120, XB=-50,0,0,75,0,108/
&MESH ID='mesh2' IJK=25,36,120, XB=-50,0,75,150,0,108/
&MESH ID='mesh3' IJK=25,36,120, XB=-50,0,0,75,108,216/
&MESH ID='mesh4' IJK=25,36,120, XB=-50,0,75,150,108,216/
&MESH ID='mesh5', IJK=25,36,120, XB=0,50,0,75,0,108 /
&MESH ID='mesh6', IJK=25,36,120, XB=50,100,0,75,0,108 /
&MESH ID='mesh7', IJK=25,36,120, XB=100,150,0,75,0,108 /
&MESH ID='mesh8', IJK=25,36,120, XB=150,200,0,75,0,108 /
…CONTD…
&MESH ID='mesh82', IJK=25,36,120, XB=850,900,75,150,108,216 /
&MESH ID='mesh83', IJK=25,36,120, XB=900,950,75,150,108,216 /
&MESH ID='mesh84', IJK=25,36,120, XB=950,1000,75,150,108,216 /


&SURF ID='INFLOW1', VEL=-0.00/
&SURF ID='INFLOW2', VEL=-0.76/
&SURF ID='INFLOW3', VEL=-1.15/
…CONTD…
&SURF ID='INFLOW55', VEL=-4.08/
&SURF ID='INFLOW56', VEL=-4.11/
&SURF ID='INFLOW57', VEL=-4.11/
&SURF ID='FS', FREE_SLIP=.TRUE./

-Fuel
&PART ID='veg1', TREE=.TRUE., VEG_BULK_DENSITY=0.0085, VEG_MOISTURE=0.02,
VEG_DENSITY=514. ,VEG_SV=5714.0,
       VEG_DRAG_COEFFICIENT=0.5, USER_DRAG_COEFFICIENT=0.25/
&TREE PART_ID='veg1', FUEL_GEOM='RECTANGLE', XB=0.0,1000.0,0.0,150.0,0.0,1.8/

&PART ID='veg2', TREE=.TRUE., VEG_BULK_DENSITY=0.0103, VEG_MOISTURE=0.02,
VEG_DENSITY=514. ,VEG_SV=5714.0,
       VEG_DRAG_COEFFICIENT=0.5, USER_DRAG_COEFFICIENT=0.25/
&TREE PART_ID='veg2', FUEL_GEOM='RECTANGLE', XB=0.0,1000.0,0.0,150.0,1.8,3.6/

&PART ID='veg3', TREE=.TRUE., VEG_BULK_DENSITY=0.0139, VEG_MOISTURE=0.02,
VEG_DENSITY=514. ,VEG_SV=5714.0,
       VEG_DRAG_COEFFICIENT=0.5, USER_DRAG_COEFFICIENT=0.25/
&TREE PART_ID='veg3', FUEL_GEOM='RECTANGLE', XB=0.0,1000.0,0.0,150.0,3.6,5.4/

&PART ID='veg4', TREE=.TRUE., VEG_BULK_DENSITY=0.0198, VEG_MOISTURE=0.02,
VEG_DENSITY=514. ,VEG_SV=5714.0,
       VEG_DRAG_COEFFICIENT=0.5, USER_DRAG_COEFFICIENT=0.25/
&TREE PART_ID='veg4', FUEL_GEOM='RECTANGLE', XB=0.0,1000.0,0.0,150.0,5.4,7.2/

&PART ID='veg5', TREE=.TRUE., VEG_BULK_DENSITY=0.0252, VEG_MOISTURE=0.02,
VEG_DENSITY=514. ,VEG_SV=5714.0,
       VEG_DRAG_COEFFICIENT=0.5, USER_DRAG_COEFFICIENT=0.25/
&TREE PART_ID='veg5', FUEL_GEOM='RECTANGLE', XB=0.0,1000.0,0.0,150.0,7.2,9.0/
```

```
&PART ID='veg6', TREE=.TRUE., VEG_BULK_DENSITY=0.0273, VEG_MOISTURE=0.02,
VEG_DENSITY=514. ,VEG_SV=5714.0,
        VEG_DRAG_COEFFICIENT=0.5, USER_DRAG_COEFFICIENT=0.25/
&TREE PART_ID='veg6', FUEL_GEOM='RECTANGLE', XB=0.0,1000.0,0.0,150.0,9.0,12.6/


&PART ID='veg7', TREE=.TRUE., VEG_BULK_DENSITY=0.0247, VEG_MOISTURE=0.02,
VEG_DENSITY=514. ,VEG_SV=5714.0,
        VEG_DRAG_COEFFICIENT=0.5, USER_DRAG_COEFFICIENT=0.25/
&TREE PART_ID='veg7', FUEL_GEOM='RECTANGLE', XB=0.0,1000.0,0.0,150.0,12.6,14.4/


&PART ID='veg8', TREE=.TRUE., VEG_BULK_DENSITY=0.0175, VEG_MOISTURE=0.02,
VEG_DENSITY=514. ,VEG_SV=5714.0,
        VEG_DRAG_COEFFICIENT=0.5, USER_DRAG_COEFFICIENT=0.25/
&TREE PART_ID='veg8', FUEL_GEOM='RECTANGLE', XB=0.0,1000.0,0.0,150.0,14.4,16.2/


&PART ID='veg9', TREE=.TRUE., VEG_BULK_DENSITY=0.0062, VEG_MOISTURE=0.02,
VEG_DENSITY=514. ,VEG_SV=5714.0,
        VEG_DRAG_COEFFICIENT=0.5, USER_DRAG_COEFFICIENT=0.25/
&TREE PART_ID='veg9', FUEL_GEOM='RECTANGLE', XB=0.0,1000.0,0.0,150.0,16.2,18.0/



-BC
&VENT MB=YMAX, SURF_ID='PERIODIC'/
&VENT MB=YMIN, SURF_ID='PERIODIC'/
&VENT MB=ZMAX, SURF_ID='MIRROR'/
&VENT MB=XMAX, SURF_ID='OPEN'/

&VENT XB=-50,-50,0.0,150.0,0.0,1.8, SURF_ID='INFLOW1'/
&VENT XB=-50,-50,0.0,150.0,1.8,3.6, SURF_ID='INFLOW2'/
&VENT XB=-50,-50,0.0,150.0,3.6,5.4, SURF_ID='INFLOW3'/
…CONTD…
&VENT XB=-50,-50,0.0,150.0,205.2,212.4, SURF_ID='INFLOW56'/
&VENT XB=-50,-50,0.0,150.0,212.4,216, SURF_ID='INFLOW57'/

&TAIL/
```